Missouri S&T Library and Learning Resources

Scholars' Mine

Doctoral Dissertations | Student Theses and Dissertations

2014

Electric-drive vehicle emulation using advanced test bench

Poria Fajri

Follow this and additional works at: https://scholarsmine.mst.edu/doctoral_dissertations

 Part of the Electrical and Computer Engineering Commons

Department: Electrical and Computer Engineering

Recommended Citation

Fajri, Poria, "Electric-drive vehicle emulation using advanced test bench" (2014). *Doctoral Dissertations*. 2575.
https://scholarsmine.mst.edu/doctoral_dissertations/2575

This thesis is brought to you by Scholars' Mine, a service of the Missouri S&T Library and Learning Resources. This work is protected by U. S. Copyright Law. Unauthorized use including reproduction for redistribution requires the permission of the copyright holder. For more information, please contact scholarsmine@mst.edu.

ELECTRIC-DRIVE VEHICLE EMULATION USING ADVANCED TEST BENCH

by

PORIA FAJRI

A DISSERTATION

Presented to the Faculty of the Graduate School of the

MISSOURI UNIVERSITY OF SCIENCE AND TECHNOLOGY

In Partial Fulfillment of the Requirements for the Degree

DOCTOR OF PHILOSOPHY

In

ELECTRICAL ENGINEERING

2014

Approved by

Mehdi Ferdowsi, Advisor

Jonathan W. Kimball

Mariesa L. Crow

Maciej J. Zawodniok

Susan L. Murray

© 2014
Poria Fajri
All Rights Reserved

PUBLICATION DISSERTATION OPTION

This dissertation consists of the following three articles that have been submitted for publication as follows:

Pages 17-54 have been submitted to the *IEEE Transactions on Energy Conversion*.

Pages 55-85 have been submitted to the *IEEE Transactions on Vehicular Technology*.

Pages 86-114 have been submitted to the *IEEE Vehicular Technology Magazine*.

ABSTRACT

Vehicle electrification is considered to be the most promising approach toward addressing the concerns on climate change, sustainability, and rapid depletion of fossil fuel resources. As a result electric-drive vehicle (EDV) technology is becoming the subject of many research studies, from academia and research laboratories to automotive industries and their suppliers. However, a crucial step toward the success of EDV implementation is developing test platforms that closely emulate the behavior of these vehicles.

In this dissertation, a new approach for emulating an EDV system on a motor/dynamometer test bench is investigated. Two different methods of emulation are discussed which are based on predefined drive cycle and unpredictable driving behavior. MATLAB/Simulink is used to model the test bench and simulations are carried out for each case. Experimental test bench results are also presented to validate hardware-in-the-loop (HIL) real-time performance for each method.

Furthermore, to provide a more realistic approach towards EDV emulation a braking system suitable for motor/dynamometer architecture is proposed. The proposed brake controller represents a very close model of an actual EDV braking system and takes into account both regenerative and friction braking limitations.

Finally, the challenges and restrictions of using a full scale test bench are outlined. To overcome these limitations, the development of an educational small scale hybrid electric vehicle (HEV) learning module is discussed which provides an ideal test platform to simulate and study both electric and HEV powertrains.

ACKNOWLEDGEMENTS

I would like to offer my gratitude to my advisor, Dr. Mehdi Ferdowsi, for his continuous support, patience, and encouragement throughout my graduate studies. It goes without saying that this work could not have been completed without his guidance.

I would also like to thank my committee members, Dr. Jonathan Kimball, Dr. Mariesa Crow, Dr. Maciej Zawodniok, and Dr. Susan Murray for serving on my doctoral committee and for all their valuable guidance, assistance and time.

A special thanks to my parents, Hassan and Hengameh for their encouragement and unconditional love and support. Words cannot express how grateful I am for all the sacrifices that they have made on my behalf. I could not have asked for better parents.

At the end I would like to express my appreciation to my beloved wife, Neda, for her love, support and understanding. I am forever grateful for finding such a compatible partner in life.

Support for this research was partially provided by the U.S. Department of Energy under grant DE-EE0002012.

TABLE OF CONTENTS

LIST OF ILLUSTRATIONS

Page

PAPER II

PAPER III

LIST OF TABLES

Page

1. INTRODUCTION

The deteriorating air quality, global warming issues, and depleting petroleum resources are becoming serious threats to modern life [1]. The demand for oil has significantly increased and is projected to increase even more in the near future. Furthermore, due to increasing oil usage, anxiety regarding its scarcity in the near future is also growing.

In recent decades, the highly developed automotive industry and the increasingly large number of automobiles in use around the world have caused the oil consumption of the transportation sector to grow at a higher rate than any other sector. This increase has mainly come from rising demands for personal conventional internal combustion engine (ICE) powered vehicles. Therefore transportation, in particular, accounts for a major share of oil consumption and is accounted as a serious threat to oil resources. Figure 1.1 shows the increasing trend in the transportation sector share in the global oil demand.

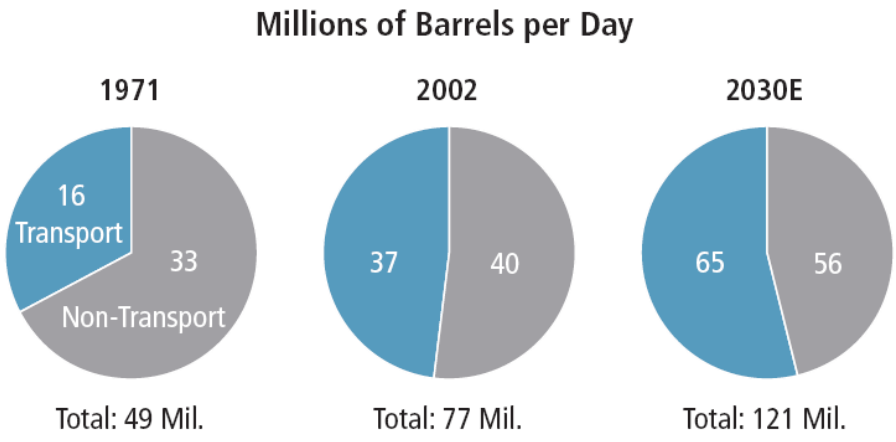

Figure 1.1. Transportation sector share in the global oil demand [2].

Limitation of fossil fuels as well as the high consumption rate of this energy for transportation have stimulated the aggressive development of cleaner and more efficient vehicles. In addition to economic and political complications that transportation oil consumption poses, environmental concerns have also had tremendous influence on the motivation to transition to transportation electrification. As a result, technologies that show the potential for decreasing energy use and air pollution are being evaluated. At the same time, research and development related to transportation have emphasized on higher efficiency and cleaner vehicles.

One advancement in the field of transportation is electric-drive vehicle (EDV) technology, a logical evolution of today's conventional vehicle that is powered by one or more electric motors. Although the market share is still insignificant today, it is recognized that EDVs are the most promising vehicle solutions for the foreseeable future [1]. Due to their fuel economy improvement they provide a solution to significantly reduce the oil dependencies of the transportation sector. These vehicles are projected to replace conventional vehicles in the near future [1]. Therefore, it is of great importance to both conduct research and also educate a new generation of engineers in this field. To meet this challenge, an increasing number of engineering schools have initiated academic programs in advanced energy and EDV technologies at the undergraduate and graduate levels [1].

There are different methods to develop and study EDVs, each with their own advantages and disadvantages. In this dissertation, after briefly discussing the different ways to study EDVs, emulation of electric-drive propulsion systems using a motor/dynamometer test bench is discussed. In paper one, detailed analysis and

challenges of developing such a platform are presented and a new approach for emulating road load conditions for an EDV system on a test bench is proposed.

Paper two, overcomes some of the limitations of the existing motor/dynamometer setup by integrating an accurate model of EDV regenerative and friction braking into the developed test bench control system. The new model not only provides a comprehensive and more realistic approach towards emulating EDV performance on a test bench, but can further be used in efficiency and energy consumption analysis studies related to these vehicles.

Finally, in paper three the development of an educational small-scale hybrid electric vehicle (HEV) setup is discussed that is inclusive of all the major components of a real HEV powertrain. The developed test bench can be used in institutes of higher education to complement theoretical coursework and to serve as an HEV research platform.

1.1. DIFFERENT WAYS TO STUDY EDV IMPLEMENTATION

In addition to books that provide narrative descriptions of these vehicles and their components, there are mainly three other methods to develop and study EDV implementation. These are; full system simulation based on software packages [3]-[8], hardware-in-the-loop (HIL) simulation using a test bench [9]-[15], and real vehicle test. The advantages of system software simulation are; good flexibility, low cost, and short simulation period. However, an EDV is a very complex system that is difficult to accurately model or describe and usually the simulations carried out are a mere approximation of the real system. Therefore, in most cases verification and validation of

the simulation results should be proved by other methods. On the other hand, the advantage of a real vehicle test is that it provides good reliability and a realistic evaluation of the vehicle under study. Yet, this approach presents some drawbacks which cannot be ignored. This method often leads to a dedicated system that is very expensive, rigid, and difficult to test and adjust. Thus, as a combination of advantages of two approaches above, the HIL test bench is drawing more and more attention [16]. It combines both physical and simulated elements of a system by substituting a model of the physical system inside the control loop. This method of emulation is essential for fast powertrain design and is considered a necessary tool in the study and implementation of EDVs [17].

HIL is a technique for performing system-level tests in a quick and cost-effective manner [18]. This method of simulation is particularly useful when a complex system cannot be tested easily in its operational environment. In the HIL simulation, part of the system is simulated and part is real hardware. Usually one or several hardware devices of the system are used instead of their simulated models. To ensure accurate results, all dynamic models of the rest of the system are required. Additionally, all significant interactions that exist within the system under evaluation should be considered. This type of simulation adds real measures compared to pure simulation methods and reduces the cost and the required infrastructure needed for pure hardware implementation.

The HIL concept can be applied to a wide variety of vehicle system studies including EDV systems. In recent years, HIL has been used increasingly in test bench evaluation of these vehicles and is considered as an effective approach for simulating EDV systems. This method of vehicle emulation is considered to be a low cost and

flexible approach which enables vehicle designers to analyze powertrain performance and energy consumption in early development stages. Additionally, it allows researchers to evaluate and study electric-drive performance and develop new control strategies in academic environments.

1.2. VEHICLE DYNAMICS

In order to model the dynamic behavior of a vehicle on a test bench, knowledge of physical aspects of the vehicle and test platform and the dynamic equation governing them is required. Resistive forces opposing vehicle movement include rolling resistance of the tires, aerodynamic drag, and hill climbing or grading resistance. Rolling resistance and aerodynamic drag forces are opposing forces in nature and tend to reduce the speed of the vehicle. Whereas grading resistance force can either reduce or help increase the speed of the vehicle depending on the slope angle that the vehicle is traveling on. Figure 1.2 shows some of the forces applied to the vehicle climbing a grade.

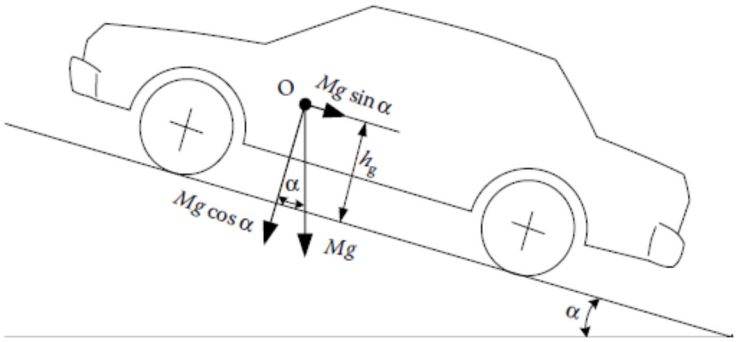

Figure 1.2. Forces applied to a vehicle climbing a grade [17].

For a vehicle with a mass of m the total resistive forces on a road can be calculated from [19]:

$$F_R = F_r + F_w + F_g = mgf_r \cos\alpha + \frac{1}{2}\rho_a C_D A_f (V + V_W)^2 + mg \sin\alpha \quad (1)$$

where F_r is the rolling resistance, F_w is the aerodynamic drag, F_g is the grading resistance, fr is the rolling resistance coefficient, α is the ground slope angle, V is the vehicle speed in m/s, C_D is the aerodynamic drag coefficient that characterizes the shape of the vehicle's body, V_w is the wind speed on the vehicle's moving direction, A_f is the frontal area of the vehicle, and ρ is the mass density of air.

The dynamic equation of a vehicle with regards to the second law of motion and taking into account the resistive forces can be expressed as:

$$F_D - F_R = Ma \quad (2)$$

where F_D is the driving force and F_R is the resistive force. In an EDV, the driving force is produced by the electric motor.

In the rotational context, the equivalent vehicle dynamic equation can be expressed as [19]:

$$T_w - T_R = J_{ew} \times \left(\frac{d\omega_w}{dt}\right) \quad (3)$$

where ω_w is the rotational speed of the wheels and T_w and T_R are the electric motor and total resistive torques calculated at the wheels. The two expressions are actually

equivalent, with the difference that expression (2) is in the linear context and expression (3) is the rotational version of the second law [20]. The equivalence can be easily seen by considering a linear system with a force operating directly on a mass, or a torque acting on an equivalent rotational mass with a rotational inertia of J_{ew}. J_{ew} is the equivalent rotational inertia of the vehicle calculated at the wheels. This term relates to the amount of flywheel rotational inertia that would be sufficient for emulating the vehicle inertia effect on a test bench [21]. From (3) it is obvious that vehicle moment of inertia is one of the crucial properties when emulating vehicle performance on a test bench. Considering vehicle inertia when testing transient performance, provides insight into how different components of powertrain can be expected to behave in situations where the vehicle is experiencing sudden acceleration or deceleration. The reasons for acquiring inertia measurements are numerous. Most importantly, automotive manufacturers require inertia properties for use in their vehicle handling and stability analysis and also in brake dynamometer testing [22]. Vehicle moment of inertia is also extensively used in computer models and simulations of existing vehicles and most importantly in the development stages of new vehicle design [23].

The moment of inertia for any object can be calculated, if enough is known about the distribution of its masses. However, actual calculation of the inertial properties of a vehicle is a complex process which requires accurate weight and dimension measurements of different components. As an alternative way, the moment of inertia of a vehicle is more practically measured by testing. Test facilities have been designed and built to measure moment of inertia properties of light vehicles [23]-[25]. While test facilities tend to provide reliable and accurate results, still this method of measurement

often requires a dedicated system that is very expensive and not easily accessible. On the other hand, practical tests using these facilities are done on the final prototype which implies that this method cannot be used to calculate vehicle inertia during the first stages of vehicle design.

1.3. TEST BENCH DYNAMICS

The hardware of an EDV test bench consists of a dynamometer coupled to an electric motor that serves as the drive motor (DM) [19]. Typically a test bench has one large flywheel attached to it in order to simulate the effect of vehicle inertia. An example of such test system is shown in Figure 1.3.

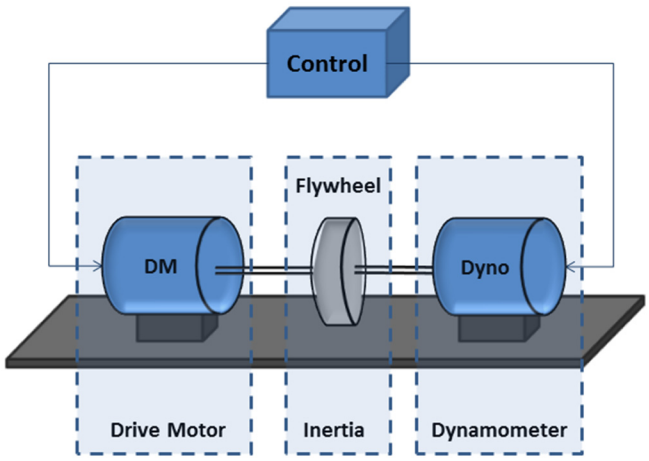

Figure 1.3. Typical EDV test bench.

A dynamometer is an energy-absorbing device capable of applying a controllable load in which the load is varied under computer control to simulate driving scenarios. In an electric dynamometer, this resistive load is produced by an electric motor and is

applied as a torque or a rotating force. In this case, the dynamometer resistive torque is applied to oppose the motion of the DM and simulates vehicle resistive forces, while the flywheel provides a fixed inertial mass to emulate vehicle inertia.

The dynamics of a test bench for EDV emulation should include the dynamics of the following three main components: the dynamometer, the vehicle DM, and the flywheel. The equivalent dynamic equation for a test bench with these three components can be expressed as:

$$T_{DM} - T_{Dyno} - \left(B_{DM} + B_{Dyno}\right)\omega_m = J_{total} \times \left(\frac{d\,\omega_m}{dt}\right) \tag{4}$$

where ω_m is the motor rotational speed, T_{DM} and T_{Dyno} are the DM and dynamometer motor torque, respectively. J_{total} is the total rotating inertia of all the rotating components of the system, which includes the rotating inertia of the DM, dynamometer, flywheel, and the coupling. In addition, B_{DM} and B_{Dyno} are the viscous coefficients of the DM and the dynamometer which represent friction losses of the test platform.

A properly designed test bench for EDV emulation can decrease the development time and result in more thorough tests at a cost that may be significantly less than the cost of using traditional system test methods. However, the development of such test platform itself can be a complex process since it needs a real-time simulation model capable of controlling both electric motors at the same time for different driving scenarios [26].

1.4. CHALLENGES OF EDV EMULATION USING ADVANCED TEST BENCH

One of the most difficult tasks in developing a HIL platform for EDV emulation is creating a suitable control system that can synthetically generate input signals to the

system under test at each time interval [26]. Ranges of literature have focused on emulating EDV dynamic load characteristics by control of electric dynamometers and different control strategies have been proposed [27]-[32]. However, in most cases, accurate knowledge of the dynamic characteristics of all components must be known and the accuracy of the results is highly dependent on the transfer function and dynamics of the system. Also, in some cases the overall inertia effect of a vehicle due to its mass is not taken into account and only the inertia of rotating parts such as the electric motor, gears and wheels, which account for only a portion of the total vehicle inertia, have been taken into consideration. Therefore, it is of importance to find a way to estimate the inertia of a vehicle and emulate the effect of vehicle linear inertia using simple test bench configurations. Additionally, vehicle emulation with a real driver and undefined driving profile has rarely been discussed, and it is always assumed that a predefined drive cycle is to be simulated. In this case the driver behavior is not taken into account and the test bench is designed to simulate only a few standard drive cycles.

In this dissertation a new approach based on equivalent vehicle rotational inertia calculations is discussed which takes into account the dynamic torque variations imposed on the EDV due to vehicle inertia effect. To address the issue of incorporating the driver behavior, two different cases are studied in this dissertation, and a control strategy is designed for each case; one using a predetermined speed profile, where the speed at each instance is known and given as a drive cycle. The other, using a driver model, where the demanded speed is obtained through pedal control.

Another challenge is eliminating the flywheel from the test bench. Although using a flywheel to simulate vehicle inertia tends to generate more accurate results in the final

implementation, however, it is not preferred in many laboratory environments [19]. This is due to several facts such as safety, and the fact that a flywheel with the same equivalent inertia as a vehicle can induce additional mechanical stress on the coupling and motor shafts. Also, different vehicles will require different amounts of inertia, whereas flywheel disks are in discrete steps and there is a limitation on the maximum inertia that can be obtained. Therefore, by eliminating the flywheel, the challenge of emulating the rotational inertia effect of the vehicle by using only the electric dynamometer should be addressed. In this dissertation, this was achieved by incorporating the dynamics of the flywheel into the controller and controlling the dynamometer to emulate both the rotational inertia effect of the flywheel and the resistive vehicle forces simultaneously.

Furthermore, to provide a realistic approach to EDV emulation on a test bench, all characteristics of the vehicle should be considered. A key feature of EDVs is their regenerative braking capability which allows the electric motor to operate as a generator alongside friction braking and absorb excess energy while the vehicle is decelerating [33]. Although the interaction between regenerative and friction braking has been studied in the literature [34]-[37], however, an EDV motor/dynamometer HIL test bench that incorporates a realistic braking model has never been considered. Part two of this dissertation tackles the challenge of integrating EDV braking into a control system of the test bench to provide an even more accurate approach to EDV emulation.

Part three of this dissertation is dedicated to the development of an educational small scale HEV setup as an alternative approach to overcome the restrictions of other available methods of studying HEVs. Some of the restrictions of practical methods such as real vehicle tests and HIL simulations for both electric and hybrid vehicles are that

they require expensive and dedicated systems [38]. Moreover, appropriate safety precautions should be taken when operating with these systems. On the other hand, these platforms can only be used to study a specific architecture of HEVs and lack the flexibility of being reconfigurable. Hence they do not provide a complete platform to study all different configurations of HEVs. Also, due to restrictions on using an ICE in most indoor environments, HIL simulation platforms for HEVs often model the ICE using an electric motor and so the ICE which is one of the main components of a HEV is absent from the test platform [38].

To ensure a practical hands-on laboratory experience that is safe, affordable, and at the same time consists of all the major components available in a real HEV powertrain, the idea of small scale HEV setup is proposed in this dissertation and the development process is explained in detail in the third paper. This test bench features the flexibility to switch between different HEV architectures and is intended to serve as a test platform to familiarize and educate on different aspects of electric and hybrid vehicles. The developed test bench can also be used in institutes of higher education to complement theoretical coursework and carry out research related to HEVs. Some of the research topics that can be studied on the test bench include design optimization of HEVs, implementation of different control strategies, battery management systems [39], battery SOC estimation [40], fuel consumption minimization and many other research challenges encountered in real-world HEVs.

REFERENCES

[1] M. Ehsani, Y. Gao, S. E. Gay, and A. Emadi, *Modern Electric, Hybrid Electric, and Fuel Cell Vehicles: Fundamentals, Theory, and Design*. Boca Raton, FL: CRC, Dec. 2004.

[2] A. Raskin and S. Shah. *The emergence of hybrid vehicles*. Alliance Bernstein, Research on Strategic Change (2006).

[3] K. L. Butler, M. Ehsani, and P. Kamath, "A Matlab-based modeling and simulation package for electric and hybrid electric vehicle design," *IEEE Trans. Veh. Technol.*, vol. 48, no. 6, pp. 1770-1778, Nov. 1999.

[4] K. B. Wipke, M. R. Cuddy, and S. D. Burch, "ADVISOR 2.1: A user-friendly advanced powertrain simulation using a combined backward/forward approach," *IEEE Trans. Veh. Technol.*, vol. 48, no. 6, pp. 1751-1761, Nov. 1999.

[5] B. Ganji, A. Z. Kouzani, and H. M. Trinh, "Drive cycle analysis of the performance of hybrid electric vehicles," in *Proc. International Conference on Life System Modeling and Simulation*. China, Sep. 17-20, 2010, pp. 434-444

[6] D. W. Gao, C. Mi, and A. Emadi, "Modeling and simulation of electric and hybrid vehicles," *Proc. IEEE*, vol. 95, no. 4, pp. 729-745, Apr. 2007.

[7] B. Auert, C. Cheny, B. Raison, and A. Berthon, "Software tool for the simulation of the electromechanical behavior of a hybrid vehicle," in *Proc. Electric Vehicle Symp. 15*, Brussels, Belgium, Oct. 1998.

[8] J. Huo, X. Guo, "Modeling and simulation of hybrid electric vehicles using HEVSIM and ADVISOR," in *Proc. IEEE Vehicle Power and Propulsion Conference (VPPC'08)*, Harbin, China, Sep. 3-5, 2008, pp. 1-5.

[9] G. Lo Bianco, G. Pede, A. Puccetti, and E. Rossi, "Vehicle Testing in ENEA Drive-train Test Facility," *SAE Technical Paper 2001-01-0961*, 2001, doi:10.4271/2001-01-0961.

[10] P. Baracos, G. Murere, C. Rabbath, and J. Wensi, "Enabling PC-Based HIL Simulation for Automotive Applications," in *Proc. 2001 International Electric Machines and Drives Conference (IEMDC)*, Cambridge, June 17-20, 2001, pp. 721-729.

[11] S. Raman, N. Sivashankar, W. Milam, W. Stuart, and S. Nabi, "Design and implementation of HIL simulators for powertrain control system software development," in *Proc.1999 American Control Conference*, vol. 1, June 1999, pp. 709-713.

[12] K. Athanasas, I. Dear, "Validation of complex vehicle systems of prototype vehicle," *IEEE Trans. Veh. Technol.*, Vol. 53, no. 6, November 2004, pp. 1835-1846.

[13] X. Xi-ming, X. Liang-fei, H. Bin, L. Xi-hao, O. Ming-gao, "Real time simulation of SHEV powertrain system," *Journal of System Simulation*, vol. 16, 2004. pp. 1467-1471.

[14] C. Dufour, J. Belanger, S. Abourida, "Using Real-Time Simulation in hybrid electric drive and power electronics development: process, problems and solutions," *SAE Technical Paper 2006-01-0114*, 2006, doi:10.4271/2006-01-0114.

[15] S. G. Semenov, "Automation of Hardware-in-the-Loop and In-the-Vehicle testing and validation for Hybrid Electric Vehicles at Ford," *SAE Technical Paper 2006-01-1448*, 2006, doi:10.4271/2006-01-1448.

[16] Z. Hui, L. Cheng, and Z. Guojiang, "Design of a Versatile Test Bench for Hybrid Electric Vehicles," in *Proc. IEEE Vehicle Power and Propulsion Conference (VPPC'08)*, Harbin, China, Sep. 3-5, 2008, pp. 1-4.

[17] R. M. Schupbach and J. C. Balda, "A versatile laboratory test bench for developing powertrains of electric vehicles," in *Proc. IEEE 56th Vehicular Technology Conference*, vol. 3, 2002, pp. 1666-1670.

[18] S. C. Oh and A. Emadi, "Test and simulation of axial flux-motor characteristics for hybrid electric vehicles," *IEEE Trans. Veh. Technol.*, vol. 53, no. 3, pp. 912-919, 2004.

[19] P. Fajri, R. Ahmadi, and M. Ferdowsi, "Test Bench for Emulating Electric Drive Vehicle System Using Equivalent Vehicle Rotational Inertia," in *Proc. Power and Energy Conference at Illinois (PECI)*, Champaign, IL, Feb. 22-23, 2013, pp. 83-87.

[20] H. Zha and Z. J. Zong, "Emulating Electric Vehicle's Mechanical Inertia Using an Electric Dynamometer," in *Proc. IEEE International Conference on Measuring Technology and Mechatronics Automation(ICMTMA)*, Changsha City, March 13-14, 2010, pp. 100-103.

[21] P. Fajri, R. Ahmadi, and M. Ferdowsi, "Equivalent Vehicle Rotational Inertia Used for Electric Vehicle Test Bench Dynamic Studies," in *Proc. 38th IEEE Industrial Electronics Society Annual Conference*, Montreal, Canada, Oct. 25-28, 2012, pp. 4115-4120.

[22] J. K. Thompson, A. Marks, and D. Rhode, "Inertia Simulation in Brake Dynamometer Testing," *SAE Technical Paper 2002-01-2601,* 2002, doi:10.4271/2002-01-2601.

[23] D. A. Andreatta, G. J. Heydinger, R. A. Bixel and D. A. Coovert, "Inertia Measurements of Large Military Vehicles," *SAE Technical Paper 2001-01-0792*, 2001, doi:10.4271/2001-01-0792.

[24] G. J. Heydinger, N. J. Durisek, D. A. Coovert, D. A. Guenther, and S. J. Novak, "The Design of a Vehicle Inertia Measurement Facility," *SAE Technical Paper 950309,* 1995, doi:10.4271/950309.

[25] G. J. Heydinger, N. J. Durisek, D. A. Coovert, R. D. Lawrence, J. A. Nowjack, and D. A. Guenther, "An Overview of a Vehicle Inertia Measurement Facility," *27th International Symposium on Automotive Technology and Automation*, Germany, Oct. 31 –Nov. 4, 1994, Paper No. 94SF034.

[26] P. Fajri, R. Ahmadi, and M. Ferdowsi, "Control Approach Based on Equivalent Vehicle Rotational Inertia Suitable for Motor-Dynamometer Test Bench Emulation of Electric Vehicles," in *Proc. IEEE International Electric Machines and Drives Conference (IEMDC)*, Chicago, IL, May 12-15, 2013, pp. 1155-1159.

[27] R. M. Schupbach and J. C. Balda, "A versatile laboratory test bench for developing powertrains of electric vehicles," in *Proc. IEEE 56th Vehicular Technology Conference*, vol. 3, 2002, pp. 1666-1670.

[28] S. C. Oh, "Evaluation of motor characteristics for hybrid electric vehicles using the Hardware in-the-Loop concept," *IEEE Trans. Veh. Technol.*, vol. 54, no. 3, pp. 817-824, May 2005.

[29] J. M. Timmermans, J. Van Mierlo, P. Lataire, F. Van Mulders, and Z. McCaffree, "Test platform for hybrid electric power systems: Development of a HIL test platform," in *Proc. Eur. Conf. Power Electron. Appl.*, Aalborg, Denmark, Sep. 2-5, 2007, pp. 1-7.

[30] D. Winkler and C. Gühmann, "Hardware-in-the-loop simulation of a hybrid electric vehicle using Modelica/Dymola," in *Proc. 22nd Int. Battery, Hybrid Fuel Cell Elect. Vehicle Symp. Exhib.*, Yokohama, Japan, 2006, pp. 1054-1063.

[31] A. Bouscayrol, W. Lhomme, P. Delarue, B. Lemaire-Semail, S. Aksas, "Hardware-in-the-loop simulation of electric vehicle traction systems using Energetic Macroscopic Representation," in *Proc. 32nd IEEE Industrial Electronics Society Annual Conference (IECON)*, Paris, Nov. 6-10, 2006, pp. 5319-5324.

[32] Y. Zhu, H. Hu, G. Xu, and Z. Zhao, "Hardware-in-the-loop simulation of pure electric vehicle control system," in *Proc. Int. Asia Conf. Informatics in Control, Automation, and Robotics* , Bangkok, Thailand, Feb. 1-2, 2009, pp. 254-258.

[33] P. Fajri, V. A. K. Prabhala, N. Lotfi, M. Ferdowsi, and P. Shamsi, "Emulating Electric Vehicle Regenerative and Friction Braking Effect Using a Hardware-in-the-Loop (HIL) Motor/Dynamometer Test Bench," in *Proc. 40th IEEE Industrial Electronics Society Annual Conference*, Oct. 29- Nov.1, 2014, Dallas, TX.

[34] M. J. Yang, H. L. Jhou, B. Y. Ma, and K. K. Shyu, "A cost-effective method of electric brake with energy regeneration for electric vehicles," *IEEE Trans. Ind. Electron*., vol. 56, no. 6, pp. 2203–2212, Jun. 2009

[35] Z. Ling and T. Lan, "Braking force distribution research in electric vehicle regenerative braking strategy," in *Proc. IEEE Computational Intelligence and Design (ISCID),* Hangzhou, China, Oct. 28-29, 2012, pp. 98-101.

[36] J. Ko, S. Ko, I. Kim, D. Hyun, and H. Kim, "Co-operative Control for Regenerative Braking and Friction Braking to Increase Energy Recovery without Wheel Lock," *Int. J. Automot. Technol.*, vol. 15, no. 2, pp. 253-262, 2014.

[37] D. Kim and H. Kim, "Vehicle stability control with regenerative braking and brake force distribution for a four-wheel drive hybrid electric vehicle," *Proceedings of the Institution of Mechanical Engineers, Part D: Journal of Automobile Engineering*, vol. 220, no. 6, pp. 683–693, 2006.

[38] P. Fajri, N. Lotfi, M. Ferdowsi, and R. G. Landers, "Development of an Educational Small Scale Hybrid Electric Vehicle (HEV) Setup," in *Proc. IEEE International Electric Vehicle Conference (IEVC)*, Santa Clara, CA, Oct. 23-25, 2013, pp. 1-6.

[39] N. Lotfi, P. Fajri, S. Novosad, J. Savage, R. G. Landers, and M. Ferdowsi "Development of an Experimental Testbed for Research in Li-Ion Battery Management Systems," *Energies*, vol. 6, no. 10, pp. 5231-5258, 2013.

[40] N. Lotfi and R.G. Landers, "Robust nonlinear observer for state of charge estimation of Li-ion batteries," *5th Annual Dynamic Systems and Control Conference*, Ft. Lauderdale, FL, Oct. 17-19, 2012, pp. 641-648.

PAPER

I. Emulating On-Road Operating Conditions for Electric-Drive Propulsion Systems

***Abstract*—** This paper provides a new approach for emulating road load conditions for an electric-drive vehicle (EDV) system on a test bench setup consisting of a drive motor (DM) connected to a dynamometer. Two different methods of EDV emulation are discussed, which are based on a predefined drive cycle and unpredictable driving behavior. The effect of total vehicle inertia is considered for both scenarios, and a control scheme is developed for each case based on equivalent vehicle rotational inertia. This method of EDV emulation not only takes into account all of the stress imposed on the DM due to vehicle inertia effect, but also allows electric vehicle emulation for any standard drive cycle, as well as undefined driving scenarios. Simulations are conducted for each case using a MATLAB/Simulink test bench model, and the results are validated using ADVISOR, a well-proven software package, to confirm the effectiveness of the proposed method. To investigate hardware-in-the-loop (HIL) real-time performance, each method is applied to the experimental test platform, and the accuracy of the experimental results is compared to the results obtained from simulation.

I. INTRODUCTION

Emulating an electric-drive vehicle (EDV) by means of an electric motor/dynamometer test bench is a timely research topic that has received increased attention in recent years. It is considered a low-cost and flexible approach that enables vehicle designers to evaluate and analyze powertrain performance and energy consumption in the early development stages of EDV design. Additionally, it allows researchers to evaluate and study electric-drive performance and develop new control strategies in academic environments.

There are mainly three primary methods by which to develop and study EDV implementation: system simulation based on software [1]-[6], hardware-in-the-loop (HIL) simulation with a test bench [7]-[13], and real vehicle testing. The advantages of system software simulation include flexibility, low cost, and time effectiveness; however, software simulation provides no guarantee that the real-time performance constraints can be met. Therefore, in most cases, the simulation results should be verified and validated using other methods. The main advantage of real vehicle testing is good fidelity; however, this method often leads to a dedicated system that is very expensive, rigid, and difficult to test and adjust. As a combination of the advantages of these two approaches, HIL simulation using a test bench is drawing increasingly more attention.

A properly designed HIL test bench for EDV emulation can decrease the development time and result in more thorough tests at a cost that may be significantly less than the cost of using traditional system test methods. However, the development of such a test platform itself can be a complex process because it requires a real-time

simulation model capable of controlling the drive motor (DM) and the dynamometer electric motor simultaneously under different driving scenarios.

A number of articles in the literature have focused on EDV emulation studies, proposing different test benches with different emulation capabilities [14]-[20]. However, in most cases, the effect of vehicle inertia is either absent or replaced with only the rotational inertia of rotating parts, such as the electric motor and wheels, which account for only a portion of the total vehicle inertia. Additionally, vehicle emulation with a real driver and undefined driving profile has rarely been discussed, and it is always assumed that a predefined drive cycle is to be simulated.

This paper describes a method for emulating the EDV behavior on a motor/dynamometer test bench that is based on equivalent vehicle rotational inertia calculations. Two different cases are studied, and a control strategy is designed for each case; one using a predetermined speed profile, where the speed at each instance is known and given as a drive cycle. The other using a driver model, where the demanded speed is obtained through pedal control.

The remainder of this paper is organized as follows. In Section II, a brief description of the forces acting on a vehicle and the importance of the vehicle inertia force for test bench studies is discussed. The term vehicle equivalent rotational inertia is introduced in Section III, and an expression for the equivalent rotational inertia of a vehicle is derived analytically. In Section IV, vehicle and test bench dynamics are discussed, and a suitable test bench structure for emulating EDV is presented. A Matlab/Simulink test bench simulation model is developed in Section V, and two cases of EDV emulation are studied in detail. In Section VI, simulation results are validated using

a different vehicle simulator software. The experimental test bench configuration is presented in Section VII, and the results of HIL real-time performance for both operating modes, followed by a comparison between the simulation and experimental results, are discussed in Section VIII. Finally, in Section IX, conclusions are drawn.

II. ACTING FORCES ON A VEHICLE

In order to better understand a vehicle's moment of inertia, all forces applied to a moving vehicle should be known. The dynamic equation of a vehicle with regards to the second law of motion and under consideration of the resistive forces can be expressed as

$$F_D = F_R + Ma \tag{1}$$

where M is the vehicle mass, and F_D and F_R denote the driving and resistive forces, respectively. The total forces acting upon a vehicle can be divided into two terms. The first term represents all of the resistive forces opposing the vehicle's motion and is given by

$$F_R = F_r + F_w + F_g = Mgf_r \cos\alpha + \frac{1}{2}\rho_a C_D A_f (V + V_W)^2 + Mg \sin\alpha \tag{2}$$

where F_r is the rolling resistance, F_w is the aerodynamic drag, F_g is the grading resistance, fr is the rolling resistance coefficient, α is the ground slope angle, V is the vehicle speed in m/s, C_D is the aerodynamic drag coefficient that characterizes the shape of the vehicle's body, V_w is the wind speed on the vehicle's moving direction, A_f is the frontal area of the vehicle, and ρ is the mass density of air. The second term in (1) is

caused by the vehicle's mass and acceleration and represents vehicle inertia. It is also highly dependent on the vehicle's rate of change of speed or acceleration/deceleration. In the transient performance evaluation of a vehicle powertrain, most of the stress on the driving force arises from this term, as shown in Figures 1 and 2, where the two forces acting on a typical vehicle are plotted against each other for the Urban Dynamometer Driving Schedule (UDDS) and the Highway Fuel Economy Test (HWFET).

Clearly, the resistive force acting on the vehicle is relatively less than the acceleration force in both cases. In addition, the acceleration force shows fast transient changes, especially when a sudden change in vehicle speed is detected, whereas the resistive force has very little or no transient changes. Since most of the stress on a vehicle arises from a change in the speed of its moving mass, the effect of vehicle inertia for test bench studies should be considered carefully.

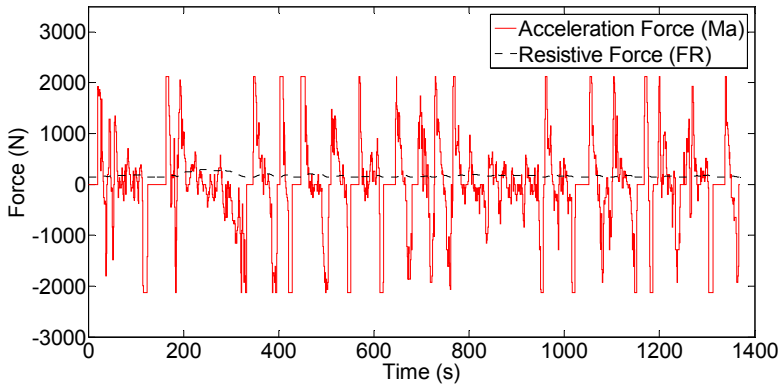

Figure 1. Resistive and acceleration forces of a typical vehicle for the UDDS cycle.

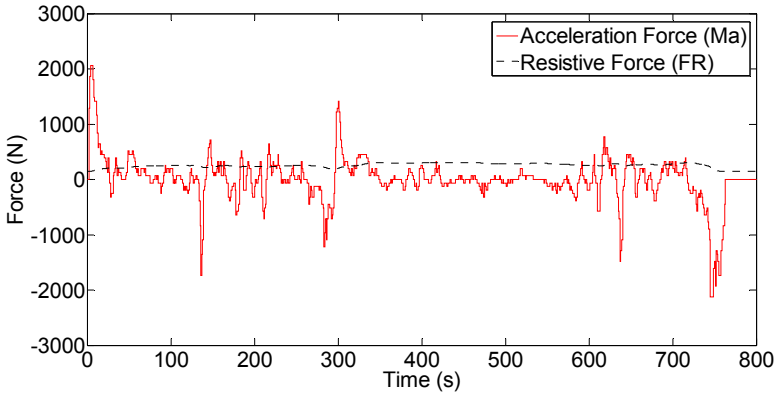

Figure 2. Resistive and acceleration forces of a typical vehicle for the HWFET cycle.

III. VEHICLE EQUIVALENT ROTATIONAL INERTIA

In many test bench platforms, the challenge is to determine how much flywheel inertia is needed to emulate vehicle inertia based on the vehicle's specifications and weight. In order to determine how much flywheel inertia is sufficient to simulate a vehicle's weight on a test bench and map vehicle's linear inertia to a rotational inertia, the term *equivalent rotational inertia* is introduced. For an EDV test bench, this equivalent inertia relates to the amount of flywheel rotational inertia that would be sufficient for emulating the vehicle inertia effect while rotating at the same speed as the vehicle's electric motor. In this section, the equivalent rotational inertia of a vehicle is analytically calculated using the expression for kinetic energy in the translational and rotational contexts.

The total kinetic energy stored in a moving vehicle is a combination of its translational kinetic energy and its rotational kinetic energy

$$E = \frac{1}{2}mv^2 + \frac{1}{2}J{\omega_w}^2 \tag{3}$$

where m is the vehicle's true static mass, v is the vehicle's linear velocity in m/s, ω_w is the rotational velocity of tires in rad/s, and J is the rotational inertia of all rotating components calculated at the wheel. This energy can be expressed as a non-rotating energy of some equivalent mass such that the kinetic energy of this equivalent mass equals the total energy at the same speed

$$\frac{1}{2}m_e v^2 = \frac{1}{2}mv^2 + \frac{1}{2}J{\omega_w}^2 \tag{4}$$

where m_e is the equivalent mass and is defined as the mass increase due to the angular moments of the rotating components of the vehicle. Substituting the rotational velocity in (4) with the vehicle's linear velocity yields

$$m_e = m + J(\frac{1}{r_d})^2 \tag{5}$$

where r_d is the vehicle's wheel radius, which defines the ratio between the rotational velocity of the wheels and the vehicle's linear velocity. In order to calculate m_e, one must first calculate J and since the rotational inertia of all rotating components in a vehicle equals the sum of the rotational inertia of each component, all rotating parts must be considered. However, it should be taken into account that these calculations are impossible without knowing the weight, form, and dimensions of each rotating component. Another approach to calculating m_e is discussed in [21] and used extensively

in the literature [22]-[26]. In this approach, the equivalent mass increase caused by the angular moments of all rotating components in a vehicle is calculated using a rotational inertia factor, which is

$$m_e = \delta \times m \tag{6}$$

where δ is the rotational inertia factor or mass factor and is given by

$$\delta = 1 + \frac{I_W}{Mr_d^2} + \frac{i_0^2 i_g^2 I_P}{Mr_d^2} \tag{7}$$

where I_w and I_p denote the total angular inertial moments of the wheels and rotating components associated with the power plant, respectively, and i_g and i_o are the gear ratios of the transmission and the final drive, respectively.

Calculation of the mass factor, δ, requires knowledge of the values of the mass moments of inertia of all rotating parts. If these values are not known, the rotational inertia factor for a passenger car can be estimated using the following empirical relation

$$\delta = 1 + \delta_1 + \delta_2 i_0^2 i_g^2 \tag{8}$$

where δ_1 represents the second term on the right-hand side of (7), with a reasonable estimate value of 0.04, and δ_2 represents the effect of the power-plant-associated rotating parts, with a reasonable estimate value of 0.0025 [21]. Given these estimates and considering the product of the transmission and final drive gear ratio as the total gear ratio, (8) can be simplified to the following equation

$$\delta = 1 + 0.04 + 0.0025G^2 \tag{9}$$

These calculations yield the equivalent mass (m_e) of the entire car, rotating bits and non-rotating bits, as a function of its static mass (m) and total gear ratio (G). The 0.04 term in (9) accounts for the effects of the wheels, and $0.0025G^2$ accounts for the rest of the drive train.

After having calculated the equivalent mass of the vehicle, the equivalent rotational inertia of the vehicle can be calculated by taking into account the expression for kinetic energy in the rotational context, as well as the fact that the expression for kinetic energy in both the rotational and linear contexts is similar and that the two definitions are equivalent

$$\frac{1}{2} m_e v^2 = \frac{1}{2} J_{ew} {\omega_w}^2 \tag{10}$$

where J_{ew} is the equivalent rotational inertia of the vehicle calculated at the wheels and can be expressed as

$$J_{ew} = m_e \frac{v^2}{{\omega_w}^2} \tag{11}$$

Since the vehicle's speed is directly proportional to the rotational velocity of the wheels by r_d, the equivalent rotational inertia at the wheels can be written as

$$J_{ew} = m_e {r_d}^2 \tag{12}$$

Note that this equivalent rotational inertia is calculated at the wheels. However, considering an EDV, the rotational velocity of the motor is related to the rotational velocity of the tires by *G*. Hence, one can easily calculate the equivalent rotational inertia on the motor side from (10) by substituting J_{ew} with J_{em}, ω_w with ω_m and taking into account that $\omega_m = \omega_w / G$. This yields

$$J_{em} = \frac{m_e {r_d}^2}{G^2} \tag{13}$$

where J_{em} is the equivalent rotational inertia of a vehicle with an equivalent mass of m_e calculated on the motor side.

IV. Vehicle Dynamics and Test Bench Structure

Modeling the dynamic behavior of an EDV on a test bench requires knowledge of physical aspects of the vehicle and test platform and the dynamic equation governing them. The dynamic equation of a vehicle in the rotational context can be expressed as

$$T_w - T_R = J_{ew} \times \left(\frac{d\omega_w}{dt}\right) \tag{14}$$

where T_w and T_R are the DM and total resistive torques calculated at the wheels. J_{ew} is the equivalent rotational inertia of the vehicle calculated at the wheels and is given by (12).

An HIL test bench system consisting of a dynamometer, a DM and a flywheel is

considered an effective way to emulate the EDV behavior. Dynamometers are widely used in HIL implementations for emulating mechanical loads and evaluating the performance of electrical machines [27]-[31]. A dynamometer is an energy-absorbing device capable of applying a controlled load that varies under computer control to simulate different load scenarios. Electromechanical dynamometers are specialized types of adjustable-load drives that are best suited for automotive testing because of their responsiveness and power/torque capacity at high speeds. In a typical EDV test bench, both motors are coupled together and share a common shaft to which a large flywheel is attached. Figure 3 depicts an example of such a test system.

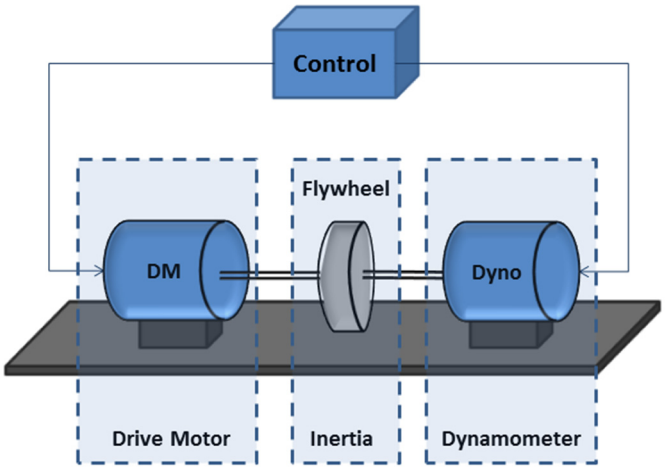

Figure 3. Typical EDV test bench with flywheel.

With this configuration, the dynamometer electric motor is used only for absorbing power and simulating the vehicle's resistive forces, while the flywheel provides a fixed inertial mass and is utilized to simulate vehicle inertia. Use of a flywheel is a good candidate for emulating vehicle's inertia effect because the magnitude of the acting torque on the flywheel is proportional to the rate of change of its rotational speed.

Although using a flywheel to simulate vehicle inertia tends to generate more accurate results in the final implementation, it is not preferred in many laboratory environments, mainly because of safety concerns. Another disadvantage of using a flywheel is the fact that each type of vehicle requires a different inertia and, hence, a different flywheel size, whereas flywheel disks come in discrete steps, and there is often a compromise among the number of disks, the smallest possible increment in inertia, and the maximum range of inertia that can be simulated [32]. Additionally, using a large flywheel with the same equivalent inertia as a vehicle can occupy a large space, and the weight of such mass can place a great deal of stress on the coupling and motor shafts. As an alternative, the flywheel can be eliminated by controlling the dynamometer to emulate both the rotational inertia effect of the flywheel and the resistive vehicle forces simultaneously. This provides a much safer environment for emulating EDVs and is more suitable in academic and industrial laboratories. The equivalent dynamic equation for a test bench with no flywheel can be expressed as

$$\begin{aligned} T_{DM} - T_{Dyno} - \left(B_{DM} + B_{Dyno}\right)\omega_m &= J_{total} \times \left(\frac{d\,\omega_m}{dt}\right) \\ &= \left(J_{DM} + J_{coupling} + J_{Dyno}\right) \times \left(\frac{d\,\omega_m}{dt}\right) \end{aligned} \tag{15}$$

where ω_m is the motor rotational speed, $J_{coupling}$ is the rotating inertia of the coupling, T_{DM} and J_{DM} are the torque and rotating inertia of the DM, and T_{Dyno} and J_{Dyno} are the torque and rotating inertia of the dynamometer motor, respectively. In addition, B_{DM} and B_{Dyno} are the viscous coefficients of the DM and the dynamometer which represent friction losses of the test platform.

V. TEST BENCH SIMULATION MODEL

One of the most significant elements in the development of an EDV test bench is the design of its control system, which must be capable of controlling both the DM and the dynamometer electric motor simultaneously under different driving scenarios. In this case, the aim is not only to follow the drive cycle profile but to control both motors in such a way that the contribution of torque from the dynamometer resembles the resistive forces acting on the actual vehicle, while simultaneously, the torque generated by the DM closely matches the DM torque of a real vehicle under different scenarios.

In this section, the investigation of two different modes of EDV emulation and the design of a control strategy for each case is discussed; one uses a predetermined speed profile, or drive cycle, in which the resistive torque values are calculated for each step. The other uses a driver model in which the desired speed is calculated based on torque command input.

A. Case 1: Drive-Cycle Mode

A.1 Control Strategy

This case is used for simulating the EDV behavior on a predetermined drive cycle, where the speed at each instance is known and given as a drive cycle, allowing the required resistive torque value to be calculated from the speed profile. In this configuration, the reference for the vehicle's translational speed is obtained from a predetermined drive cycle and translated into a required rotational speed, which is then given to the DM through a PI controller that ensures accurate speed tracking. The required dynamometer resistive torque is calculated directly from the speed trace using

the test bench and vehicle dynamic equations at each instance. Figure 4 depicts a block diagram view of such a system.

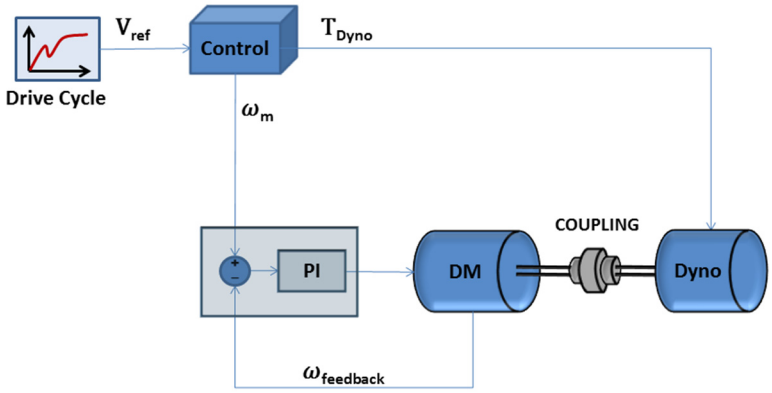

Figure 4. Block diagram representation of the drive-cycle mode

The dynamometer resistive torque can be obtained by substituting T_w from (14) into (15) and taking into account that (T_{DM}=T_w/ηG), where η is the overall efficiency of the vehicle drive train to be emulated. This yields

$$\frac{\left(J_{ew}\left(\frac{d\omega_w}{dt}\right)+T_R\right)}{\eta G}-T_{Dyno}-\left(B_{DM}+B_{Dyno}\right)\omega_m = \left(J_{DM}+J_{coupling}+J_{Dyno}\right)\times\left(\frac{d\omega_m}{dt}\right) \quad (16)$$

Considering that motor speed is related to wheel speed by (ω_w=ω_m/G), (16) can be written as

$$\frac{J_{ew}}{\eta G^2}\left(\frac{d\omega_m}{dt}\right)+\frac{T_R}{\eta G}-T_{Dyno}-\left(B_{DM}+B_{Dyno}\right)\omega_m = \left(J_{DM}+J_{coupling}+J_{Dyno}\right)\times\left(\frac{d\omega_m}{dt}\right) \quad (17)$$

As a consequence, T_{Dyno} is given by

$$T_{Dyno}=\frac{T_R}{\eta G}-\left(B_{DM}+B_{Dyno}\right)\omega_m+\left(\frac{J_{ew}}{\eta G^2}-J_{DM}-J_{coupling}-J_{Dyno}\right)\times\left(\frac{d\omega_m}{dt}\right) \quad (18)$$

In this approach, it is assumed that the trace is always met and, hence, that the derivative of speed at each operating point can be mathematically computed from the drive cycle instead of the actual motor speed. In order to accomplish this in a real test bench, the DM and the dynamometer must both be capable of following the speed and torque profiles with minimum error and delay. If these requirements are met, this method allows the test bench to accurately simulate the dynamic changes of the vehicle for a certain driving schedule. The main drawback of this method is that, because the torque signal is calculated from the speed profile, the speed profile must always be known and given as a drive cycle, allowing the required resistive torque signal to be calculated. Therefore, this method cannot be used to simulate the behavior of an EDV for an unknown drive cycle.

A.2 Modeling and Simulation

This method was modeled and simulated in the Matlab/Simulink environment. In order to model the exact components of the experimental test bench, a simulation model

of a permanent magnet synchronous motor (PMSM) and a DC motor were used to model the DM and the electric dynamometer, respectively. A mechanical shaft model has been also used to simulate mechanical coupling between the two electric machines. In this model, the controller block is responsible for calculating the speed and resistive torque and synchronously controlling the motors to produce opposing torques. Figure 5 shows the simulation circuit used in Simulink to model the test bench system.

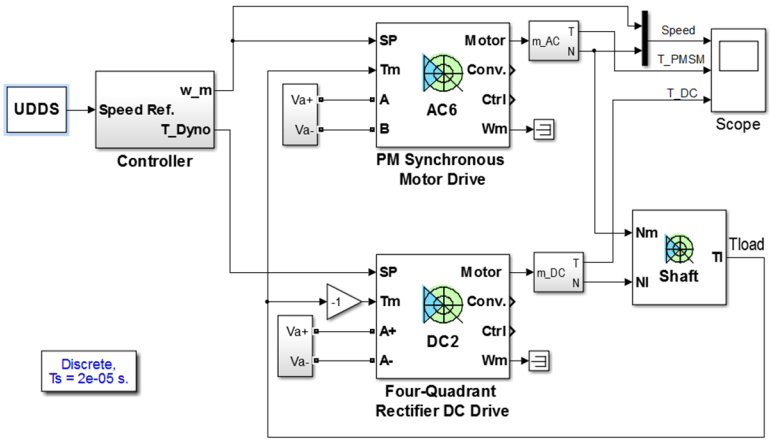

Figure 5. Test bench simulation model of the drive cycle mode.

In this model, the PMSM block resembles the DM of an EDV, while the DC motor acts as the electric dynamometer. Both PMSM and DC motor blocks consist of all the necessary sub-circuits for motor drive and speed/torque control. The controller block receives the speed reference from the driving schedule and converts the vehicle's linear speed into the rotational speed of the motor, which is used as a reference speed for the PMSM. For this mode of operation, the PMSM is speed controlled; its controller receives the difference between the reference and actual speed and generates the desired torque signal. On the other hand, the dynamometer is torque controlled; it receives its torque

reference directly from the controller block, which calculates the resistive torque from (18). Figure 6 shows the control block circuit configuration.

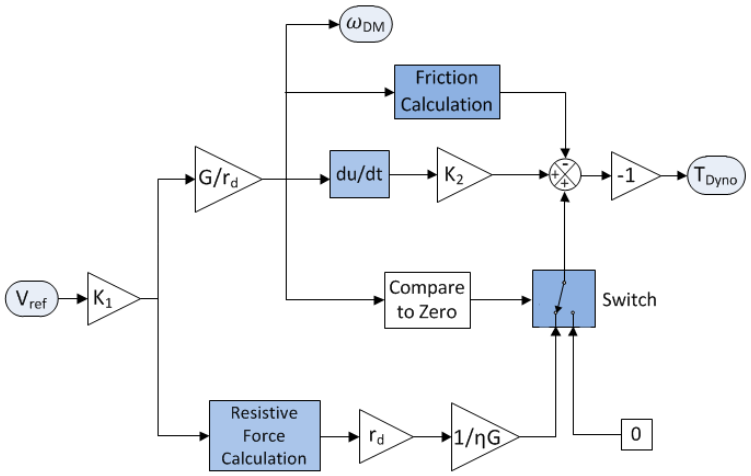

Figure 6. Control block for the drive-cycle mode of operation.

K_1 is a constant for converting the translational speed of the vehicle in mile/h to m/s and K_2 is a constant whose value depends on the inertia of the motors and their coupling as well as the vehicle equivalent rotational inertia. The function of the switch after the comparison block in the control unit is to prevent the DC motor from applying a resistive torque when the speed is zero. This insures that when there is no speed, the calculated resistive torque is forced to zero, thus preventing either motor from producing any torque. The reason for this is that the vehicle's dynamic equation always includes a resistive torque (rolling resistance), even when the vehicle is stationary. So even if the speed command is zero, the calculated resistive torque will still have a negative value equal to the rolling resistance torque. On the other hand, because the DM is speed controlled, it is forced to produce a positive torque in order to oppose the resistive torque

and maintain the speed at zero. This results in an inaccurate balance of energy compared to an actual EDV, where the produced torque of the DM is zero when the vehicle is stationary.

In order to investigate the effectiveness of the drive-cycle method, a simulation was carried out in Matlab/Simulink using the simulation model shown in Figure 5. The vehicle and test bench parameters used for this simulation are presented in Table I, and the simulation results are presented in Figure 7 for the duration of one UDDS cycle.

Table I

Vehicle and Test Bench Specifications

Parameter	**Value**
Vehicle mass (m)	400 kg
Air Density(ρ_a)	1.22 kg/m^3
Aerodynamic drag coefficient (C_d)	0.19
Frontal area (A_f)	1.6 m^2
Rolling resistance coefficient (fr)	0.01
Wheel radius (r_d)	0.28 m
Alpha (α)	0
Overall gear ratio (G)	2.3
DM inertia (J_{DM})	0.016 kgm^2
Dynamometer motor inertia (J_{Dyno})	0.019 kgm^2
Coupling inertia ($J_{coupling}$)	0.003 kgm^2
Equivalent Vehicle Rotational Inertia (J_{ew})	33.029 kgm^2
Vehicle drive train overall efficiency (η)	90 %
DM viscous coefficient (B_{DM})	0.0086 N.m/(rad/s)
Dynamometer viscous coefficient (B_{Dyno})	0.0133 N.m/(rad/s)

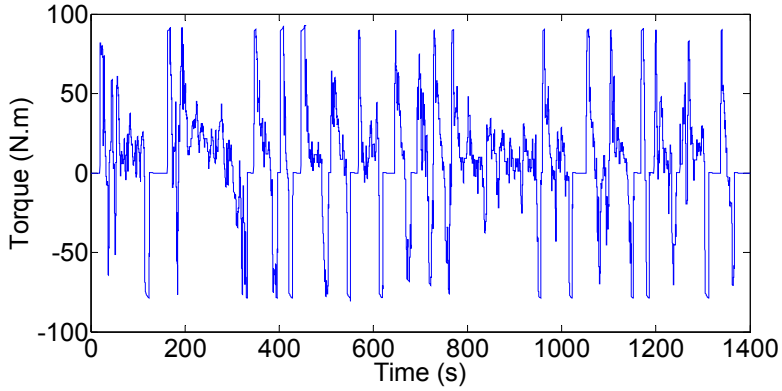

(a)

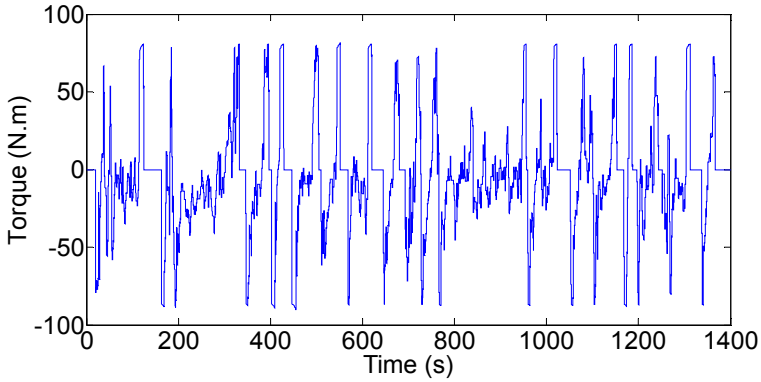

(b)

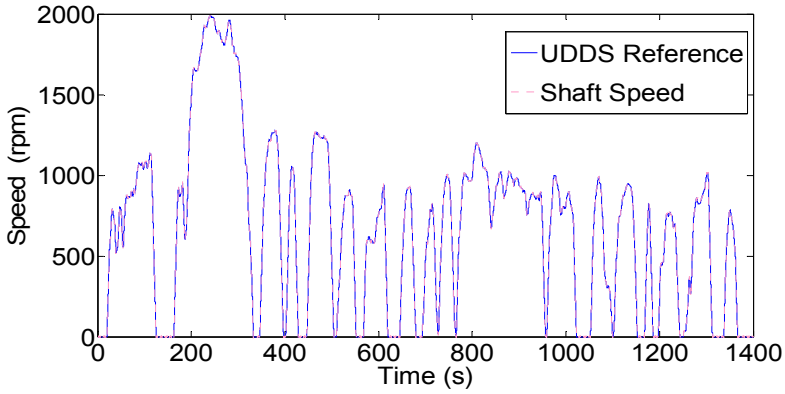

(c)

Figure 7. Simulation results for the drive-cycle mode. (a) PMSM torque. (b) DC motor torque. (c) Reference speed and actual shaft rotational speed.

Figure 7(c) indicates that the vehicle followed the UDDS cycle with minimum errors. As expected, the resistive torque generated by the DC motor was found to be opposing the applied torque with the same deviations and almost the same amplitude. The results also indicated that when the speed increased, the PMSM provided a positive torque, while a decrease in speed resulted in a negative torque. The maximum torque required to complete this cycle was found to be approximately 92 N.m for this vehicle.

B. Case 2: Driver Mode

B.1 Control Strategy

In order to simulate the behavior of an EDV on a test bench for an unknown drive cycle, a different mode of operation is investigated. This method is useful when the behavior of the vehicle is analyzed directly from the torque command given by the driver. In this case, the input reference signal is a varying torque signal that is applied directly to the DM, with the aim of producing the resistive torque such as to obtain the exact speed profile of a real vehicle. For this case, the DM is torque controlled, and the dynamometer is speed controlled. A block diagram implementation of such a system is presented in Figure 8.

The desired vehicle speed can be derived from the equivalent vehicle dynamic equation in the rotational context given in (14) by replacing T_w with $\eta G T_{DM}$. This yields

$$\omega_w = \frac{1}{J_{ew}} \int (\eta G T_{DM} - T_R)\, dt \tag{19}$$

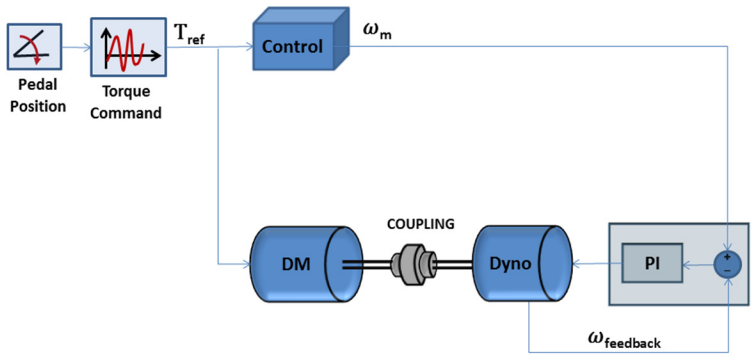

Figure 8. Block diagram representation of the driver mode.

Taking into account the relationship between the rotational velocity of the motor and tires, the desired motor speed can be calculated as

$$\omega_m = \frac{G}{J_{ew}} \int (\eta G T_{DM} - T_R)\, dt \tag{20}$$

The calculated motor speed then is used as a command to the dynamometer, which is operated in speed control mode. With this approach, actual vehicle driving conditions can be achieved as a result of the interaction between the dynamometer and the DM.

B.2 Modeling and Simulation

For this mode of operation, the same simulation model presented in Figure 5 was used, with the difference being that this time, the PMSM was torque controlled and the dynamometer was speed controlled. The PMSM receives its torque reference from the driver pedal position, and the control block generates a speed command that is fed to the DC motor, which is responsible for maintaining the overall speed equal to the calculated

speed. The simulation circuit used in Simulink to implement this method is shown in Figure 9. The control block circuit configuration for this method is also shown in Figure 10. Once again, the function of the switch block in the control unit is to insure the correct balance of energy by eliminating the rolling resistance term, thereby preventing the dynamometer from applying a resistive torque when the speed is zero.

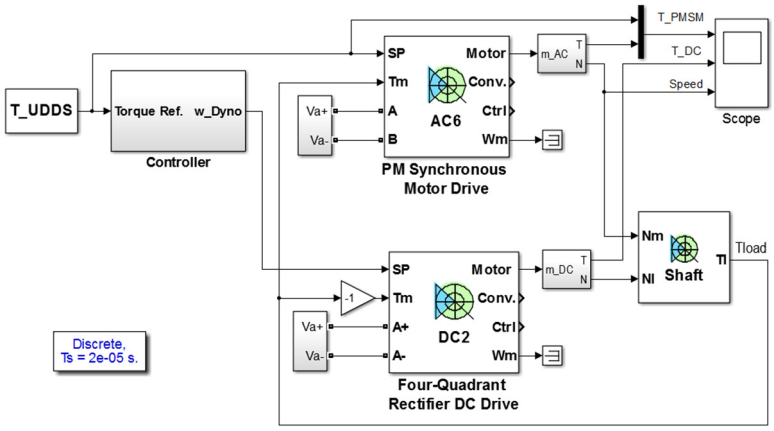

Figure 9. Test bench simulation model for the driver mode.

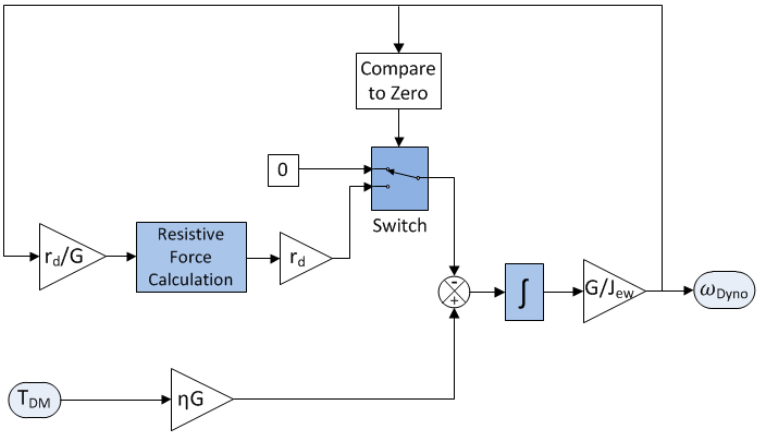

Figure 10. Control block for the driver mode of operation.

In order to validate and compare the results of this method with those obtained using the previous method, the torque input reference was reconstructed using the same torque values obtained from the drive-cycle method given in Figure 7(a). The simulation was carried out for one UDDS cycle using the test bench model shown in Figure 9 with the same vehicle and test bench parameters as provided in Table I. Figure 11 shows the plots obtained for this case.

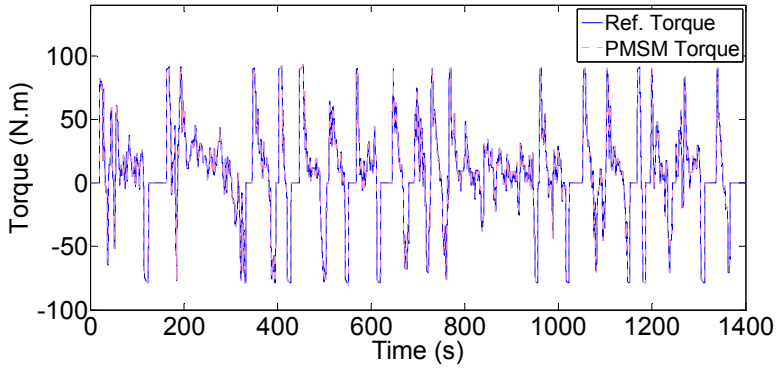

(a)

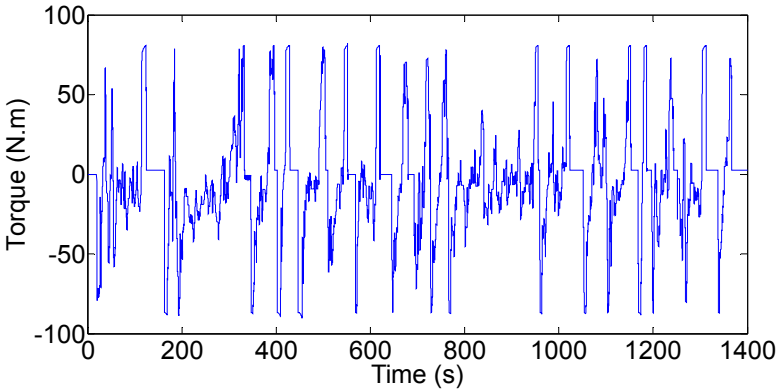

(b)

Figure 11. Simulation results for the driver mode. (a) PMSM reference and actual torque. (b) DC motor torque. (c) Actual shaft rotational speed.

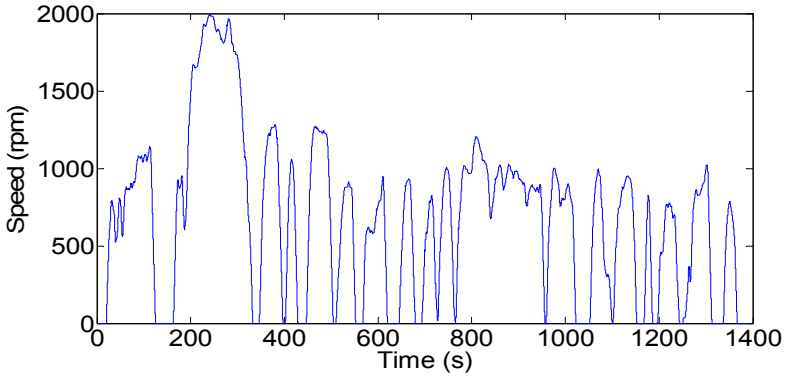

(c)

Figure 11. Simulation results for the driver mode. (a) PMSM reference and actual torque. (b) DC motor torque. (c) Actual shaft rotational speed. (cont.)

Comparing Figure 11(c) to the UDDS reference motor speed in Figure 7(c) shows that the actual system speed obtained from this simulation is the same as the equivalent motor speed profile of the UDDS cycle. This implies that if the torque profile in Figure 7(a) is applied to this model, the resulting vehicle speed will be the same as the UDDS speed profile. Comparing Figures 7(b) and 11(b) also reveals that the resistive torque produced by the dynamometer for both methods is the same. This indicates a duality between these two systems; one emulates the vehicle's resistive forces from the speed profile as input, and the other produces a similar speed profile from the same torque reference as input.

VI. SIMULATION MODEL COMPARISON

In most cases, the results obtained from one method of simulation should be validated by other known methods to verify the effectiveness and correctness of the results. To validate the results obtained from the Matlab/Simulink simulation model, a

vehicle with the same vehicle specifications as those provided in Table I was designed and simulated in ADvanced VehIcle SimulatOR (ADVISOR) [33], [34]. The results of the DM torque obtained from ADVISOR were compared to the results of the torque generated by the DM of the simulation model. Figure 12 shows the comparison between the ADVISOR-simulated DM torque and the respective PMSM torque measurements shown in Figure 7(a) and obtained from the Matlab/Simulink model.

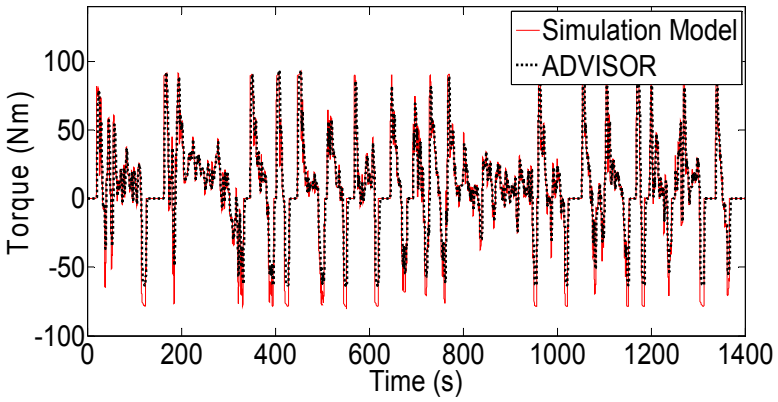

Figure 12. DM torque comparison between ADVISOR and the Matlab/Simulink model.

Figure 12 indicates that the torque measurements produced by ADVISOR and Matlab/Simulink closely follow the same path. Slight mismatches exist, however, due to the limitations imposed by ADVISOR on motor and powertrain control. Also, noticeable differences exist in the negative torque values where the electric motor absorbs energy and the vehicle applies regenerative braking [35]. This is due to the fact that in a real vehicle operating in regenerative braking mode, only part of the energy can be absorbed by the electric motor, and the rest is wasted through mechanical brakes. As a result,

ADVISOR sets braking limitations, which is not the case for the proposed test bench model because no mechanical brakes are present.

VII. Experimental Test Bench

Figure 13 shows the experimental test platform used in this paper, and Figure 14 shows the overall block diagram of the hardware system. The architecture is based on real-time simulation and execution of the HIL system and consists of two motors on a common shaft. The experimental arrangement consists of a 15 kW, 6-pole PMSM representing the DM, which is connected to a 15 kW DC machine acting as the dynamometer to emulate road load and vehicle inertia.

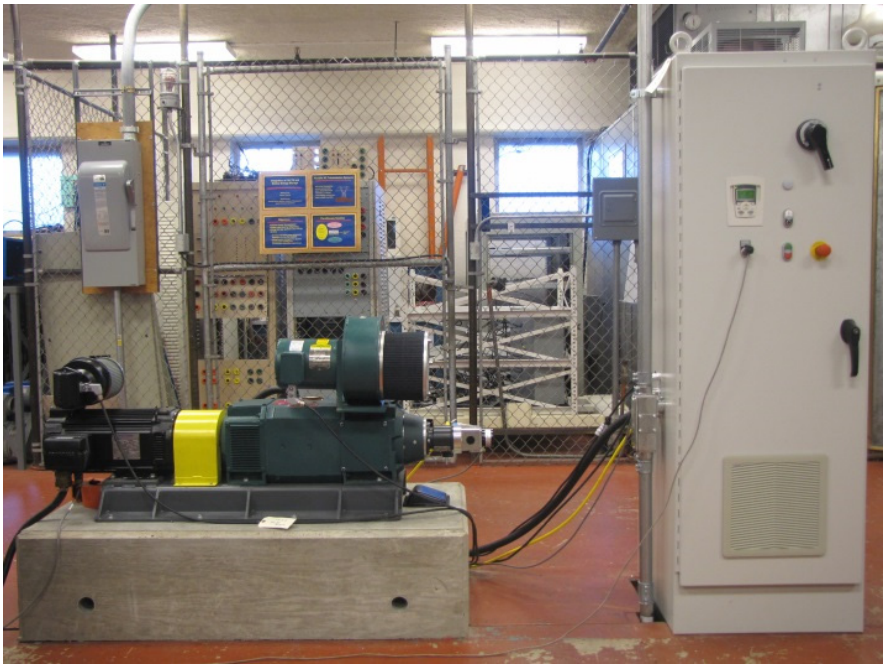

Figure 13. Experimental test platform.

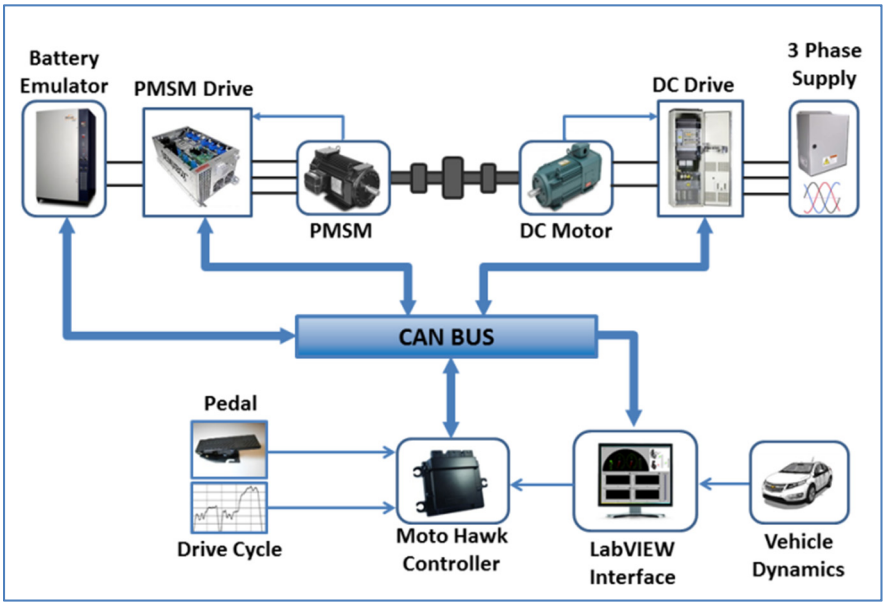

Figure 14. Block diagram of the test system.

The need for real-time communication is satisfied by means of a Controller Area Network (CAN) bus. The experimental test platform uses CANopen protocol to integrate all of the elements and assure synchronous distribution of reference speed and torque commands, as well as to read back the actual speed and torque. With the CAN bus data rate set at 500 Kbps, a 10ms update rate is achieved to command and monitor all variables.

System supervisory control is achieved by MotoHawk, a controls system application development tool based on the MPC5553 processor that offers fast development cycle times and high flexibility. It allows the designer to build the vehicle model, directly implement any system control created in Matlab/Simulink using embedded control modules, and perform real-time simulation modeling. To emulate on-road operating conditions for the PMSM, speed and torque commands are calculated from the mathematical model of vehicle dynamics, road load, and equivalent vehicle

rotational inertia. The MotoHawk controller then changes the operating point of the dynamometer and DM continuously via CAN and sends synchronous speed and torque signals to the two drives at each instance, allowing exact interaction between the DM and the dynamometer to ensure accurate simulation results.

LabVIEW is used as a graphical user interface (GUI) that allows the user to define the mode of operation between driver and drive-cycle modes at the start of simulation and also to determine the configuration of the vehicle to be simulated. Using LabVIEW, real-time system monitoring is also achieved through a National Instruments™ CAN-board (NI-CAN) connected to the CAN bus.

A Bitrode model FTF battery emulator with full regenerative capability is used as a high-power DC source for the PMSM drive. The Bitrode battery emulator is controlled via CAN to represent real vehicle batteries, allowing the PMSM drive to operate in regenerative mode for better control and more accurate speed tracking.

VIII. Experimental Results

To verify the overall performance of the system and validate the effectiveness of the implemented control approach, two experiments were conducted using the test platform shown in Figure 13. The experimental tests were performed with the following two aims: 1) to validate that the test bench could indeed meet real-time performance constraints using this approach and 2) to compare the accuracy of the experimental results with the results obtained from simulation. Consequently, the vehicle parameters chosen in LabVIEW were the same as those provided in Table I. The first test was performed in drive-cycle mode using the UDDS drive cycle. The second test was

executed in driver mode, and for comparison purposes, the PMSM torque results obtained from the first test were used as the torque reference input instead of a driver-generated torque command. The experimental results for both modes of operation are illustrated in Figures 15 through 18.

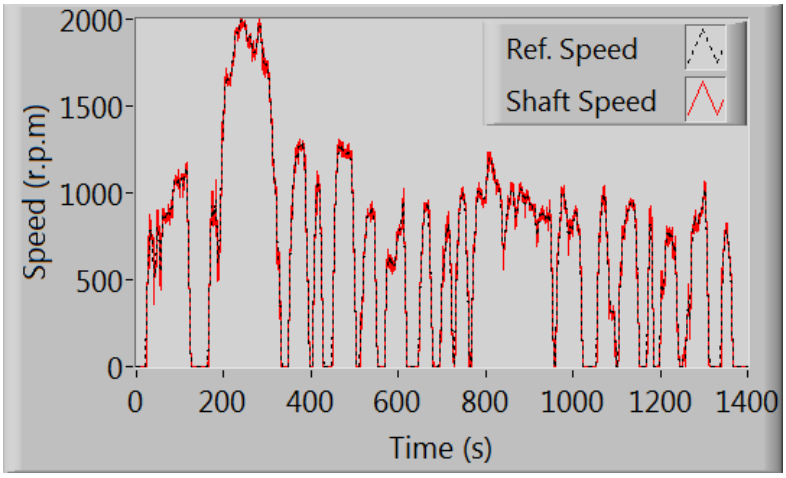

Figure 15. Experimental results of reference and actual speed for drive-cycle mode of operation.

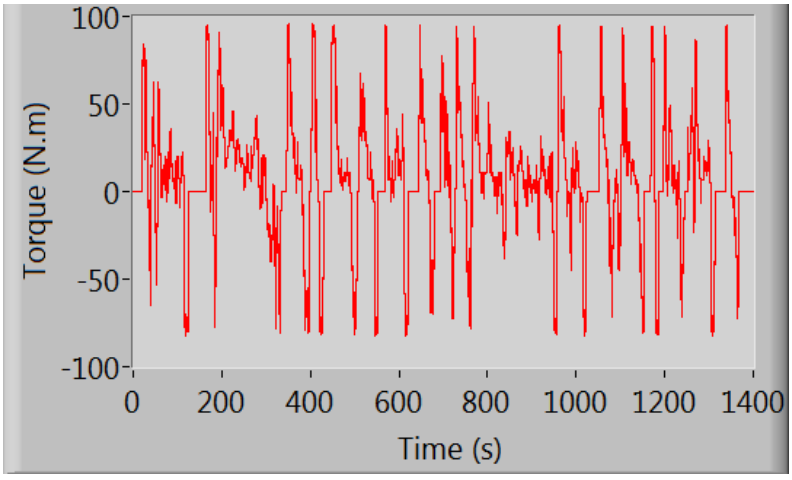

Figure 16. Experimental results of PMSM torque for drive-cycle mode of operation.

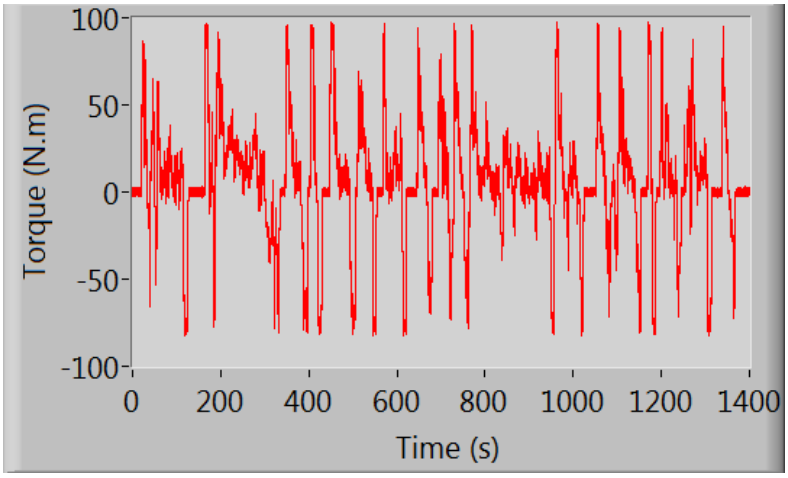

Figure 17. Experimental results of PMSM torque for driver mode of operation.

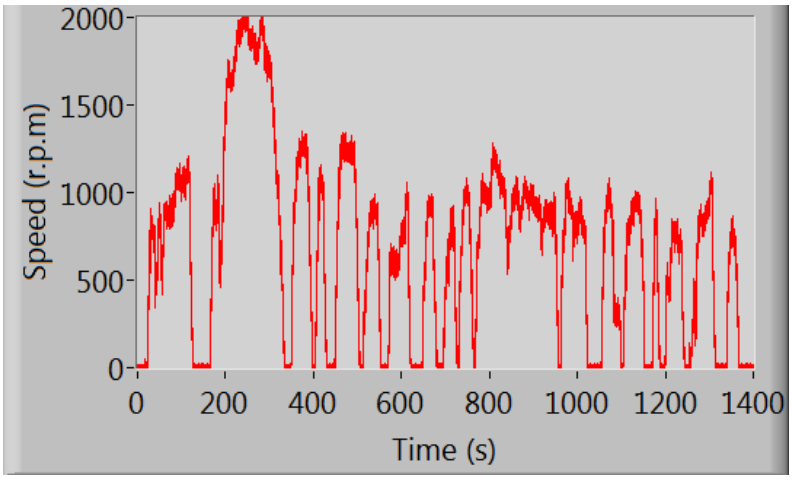

Figure 18. Experimental results of actual speed for driver mode of operation.

Figure 15 shows the reference and actual shaft speed for a complete drive cycle under test bench operation in drive-cycle mode. Clearly, the speed command is followed throughout the driving cycle, with only minor deviations. Figure 16 shows the actual torque generated by the PMSM to cancel the DC motor resistive force and maintain the speed equal to the desired reference speed. The PMSM torque obtained from Figure 16 also was used as a reference torque for the second experiment. Figure 17 shows the

actual PMSM output torque measured for the driver mode of operation, and Figure 18 shows the resulting shaft speed.

Comparing Figure 15 with Figure 18 and Figure 16 with Figure 17 reveals that the overall profile of the resulting shaft speed and PMSM torque were almost the same under both operating modes. Although the system seemed to follow both the speed and torque commands for both cases, it must be noted that the smallest mismatch between the actual speed and generated torque with respect to time can lead to simulation conditions that do not adequately represent on-road operation. Therefore, in order to more precisely determine the accuracy of the results, the experimental waveforms were compared with those obtained from simulation by plotting the difference between the experimental and simulation results versus the simulation results. Linear curve fitting was used to illustrate the similarity between the experimental and simulation results. The slope and offset of the fitted linear curve served as a good indicator of how closely the experimental results matched the respective simulation results.

The analysis method employed was based on the fact that for an ideal case in which the experimental and simulation results match exactly, the plot of the experimental results versus the simulation results would be a straight line with a slope of one. Similarly, the plot of the difference between the experimental and simulation results versus the simulation results would be a straight line with a slope and offset of zero [36]. Figures 19 and 20 show the analysis used to indicate the difference between the experimental and simulation results of PMSM torque and shaft speed for both modes of operation. The results of this analysis for each case also are summarized in Table II.

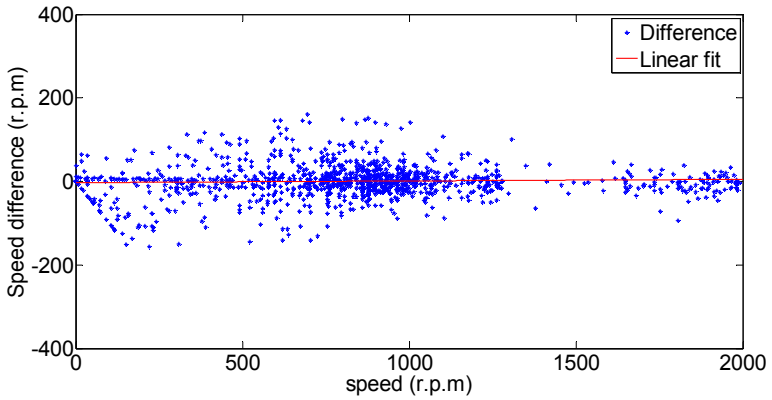

(a)

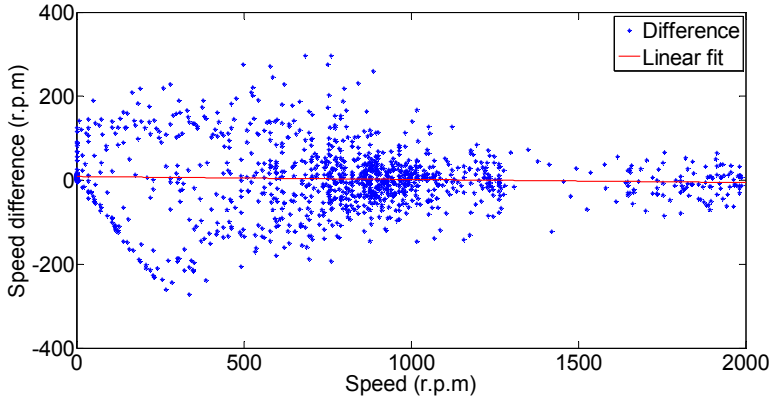

(b)

Figure 19. Experimental and simulation data differences for motor speed. (a) Drive-cycle mode. (b) Driver mode.

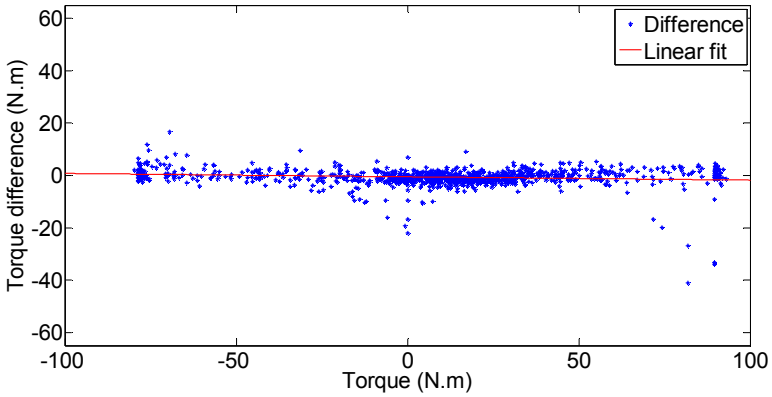

(a)

Figure 20. Experimental and simulation data differences for PMSM torque. (a) Drive-cycle mode. (b) Driver mode.

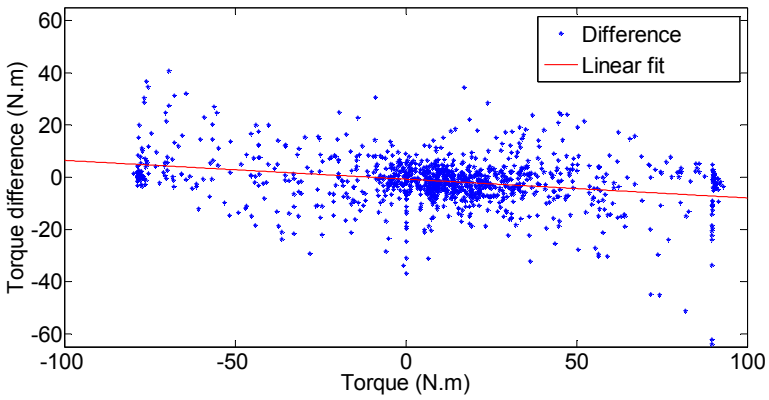

(b)

Figure 20. Experimental and simulation data differences for PMSM torque. (a) Drive-cycle mode. (b) Driver mode. (cont.)

Figures 19 and 20 indicate that the simulation and experimental results matched very closely under both modes of operation. The linear fit for the speed and PMSM torque of each case shows a very small slope and offset, indicating a very small difference between the simulation and experimental results. However, the results provided in Table II indicate that the experimental results obtained from the test bench more closely matched their respective simulation results for the drive-cycle mode of operation. Most of the difference between the experimental and simulation results for the driver mode occurred because under this mode of operation, the reference torque is extracted from the drive-cycle mode, which itself contains small deviations from its simulation results. Based on these results, the overall effectiveness of the control approach is validated, and this method of EDV emulation can be considered a flexible and accurate approach applicable to different vehicles with different specifications using an HIL motor/dynamometer setup.

Table II

Analysis of Differences Between Experimental and Simulation Results

Parameter	**Mode of operation**	**Linear Fit y=mx+c**
Motor speed	Drive-cycle mode	m= 0.004 c= -2.6
	Driver mode	m= -0.007 c= 8.6
PMSM torque	Drive-cycle mode	m=-0.013 c=-0.51
	Driver mode	m=-0.072 c=-0.73

IX. CONCLUSION

A new approach for emulating the behavior of EDVs was proposed based on equivalent vehicle rotational inertia. The method used to properly map the linear inertia of a vehicle to an equivalent rotational inertia was described in detail, and an expression for the equivalent rotational inertia of a vehicle was derived analytically. Using this expression, two different methods by which to emulate the behavior of EVDs on a test bench consisting of a motor/dynamometer set were investigated, and a control approach was developed for each case. Each control approach was simulated using the test bench simulation model, and the accuracy of the results was validated using the ADVISOR software. Moreover, each method was applied to the experimental test platform, and the results were compared to the simulation results to verify the effectiveness of this approach for conducting HIL real-time simulations.

REFERENCES

[1] K. L. Butler, M. Ehsani, and P. Kamath, "A Matlab-based modeling and simulation package for electric and hybrid electric vehicle design," *IEEE Trans. Veh. Technol.*, vol. 48, no. 6, pp. 1770-1778, Nov. 1999.

[2] K. B. Wipke, M. R. Cuddy, and S. D. Burch, "ADVISOR 2.1: A user-friendly advanced powertrain simulation using a combined backward/forward approach," *IEEE Trans. Veh. Technol.*, vol. 48, no. 6, pp. 1751-1761, Nov. 1999.

[3] B. Ganji, A. Z. Kouzani, and H. M. Trinh. "Drive cycle analysis of the performance of hybrid electric vehicles," In *Life system modeling and intelligent computing*, pp. 434-444. Springer Berlin Heidelberg, 2010.

[4] D. W. Gao, C. Mi, and A. Emadi, "Modeling and simulation of electric and hybrid vehicles," *Proc. IEEE*, vol. 95, no. 4, pp. 729-745, Apr. 2007.

[5] B. Auert, C. Cheny, B. Raison, and A. Berthon, "Software tool for the simulation of the electromechanical behavior of a hybrid vehicle," in *Proc. Electric Vehicle Symp. 15*, Brussels, Belgium, Oct. 1998.

[6] J. Huo, X. Guo, "Modeling and simulation of hybrid electric vehicles using HEVSIM and ADVISOR," in *Proc. IEEE Vehicle Power and Propulsion Conference (VPPC'08)*, Harbin, China, Sep. 3-5, 2008, pp. 1-5.

[7] G. Lo Bianco, G. Pede, A. Puccetti, and E. Rossi, "Vehicle Testing in ENEA Drive-train Test Facility," *SAE Technical Paper 2001-01-0961*, 2001, doi:10.4271/2001-01-0961.

[8] P. Baracos, G. Murere, C. Rabbath, and J. Wensi, "Enabling PC-Based HIL Simulation for Automotive Applications," in *Proc. 2001 International Electric Machines and Drives Conference (IEMDC)*, Cambridge, June 17-20, 2001, pp. 721-729.

[9] S. Raman, N. Sivashankar, W. Milam, W. Stuart, and S. Nabi, "Design and implementation of HIL simulators for powertrain control system software development," in *Proc.1999 American Control Conference*, vol. 1, June 1999, pp. 709-713.

[10] K. Athanasas, I. Dear, "Validation of complex vehicle systems of prototype vehicle," *IEEE Trans. Veh. Technol.*, Vol. 53, no. 6, November 2004, pp. 1835-1846.

[11] X. Xi-ming, X. Liang-fei, H. Bin, L. Xi-hao, O. Ming-gao, "Real time simulation of SHEV powertrain system," *Journal of System Simulation*, vol. 16, 2004. pp. 1467-1471.

[12] C. Dufour, J. Belanger, S. Abourida, "Using Real-Time Simulation in hybrid electric drive and power electronics development: process, problems and solutions," *SAE Technical Paper 2006-01-0114*, 2006, doi:10.4271/2006-01-0114.

[13] S. G. Semenov, "Automation of Hardware-in-the-Loop and In-the-Vehicle testing and validation for Hybrid Electric Vehicles at Ford," *SAE Technical Paper 2006-01-1448*, 2006, doi:10.4271/2006-01-1448.

[14] R. M. Schupbach and J. C. Balda, "A versatile laboratory test bench for developing powertrains of electric vehicles," in *Proc. IEEE 56th Vehicular Technology Conference*, vol. 3, 2002, pp. 1666-1670.

[15] Z. Hui, L. Cheng, and Z. Guojiang, "Design of a Versatile Test Bench for Hybrid Electric Vehicles," in *Proc. IEEE Vehicle Power and Propulsion Conference (VPPC'08)*, Harbin, China, Sep. 3-5, 2008, pp. 1-4.

[16] S. C. Oh, "Evaluation of motor characteristics for hybrid electric vehicles using the Hardware in-the-Loop concept," *IEEE Trans. Veh. Technol.*, vol. 54, no. 3, pp. 817-824, May 2005.

[17] J. M. Timmermans, J. Van Mierlo, P. Lataire, F. Van Mulders, and Z. McCaffree, "Test platform for hybrid electric power systems: Development of a HIL test platform," in *Proc. Eur. Conf. Power Electron. Appl.*, Aalborg, Denmark, Sep. 2-5, 2007, pp. 1-7.

[18] D. Winkler and C. Gühmann, "Hardware-in-the-loop simulation of a hybrid electric vehicle using Modelica/Dymola," in *Proc. 22nd Int. Battery, Hybrid Fuel Cell Elect. Vehicle Symp. Exhib.*, Yokohama, Japan, 2006, pp. 1054-1063.

[19] A. Bouscayrol, W. Lhomme, P. Delarue, B. Lemaire-Semail, S. Aksas, "Hardware-in-the-loop simulation of electric vehicle traction systems using Energetic Macroscopic Representation", in *Proc. 32nd IEEE Industrial Electronics Society Annual Conference (IECON)*, Paris, Nov. 6-10, 2006, pp. 5319-5324.

[20] Y. Zhu, H. Hu, G. Xu, and Z. Zhao, "Hardware-in-the-loop simulation of pure electric vehicle control system," in *Proc. Int. Asia Conf. Informatics in Control, Automation, and Robotics* , Bangkok, Thailand, Feb. 1-2, 2009, pp. 254-258.

[21] M. Ehsani, Y. Gao, S. E. Gay, and A. Emadi, *Modern Electric, Hybrid Electric, and Fuel Cell Vehicles: Fundamentals, Theory, and Design*. Boca Raton, FL: CRC, Dec. 2004.

[22] M. Ehsani, K. M. Rahman, and H. A. Toliyat, "Propulsion system design of electric and hybrid vehicles," *IEEE Trans. Ind. Electron.* , vol. 44, no. 1, pp. 19-27, Feb. 1997.

[23] F. J. Pérez-Pinal, C. Nunez, R. Alvarez, and M. Gallegos, "Step by step design procedure of an Independent-Wheeled Small EV applying EVLS," in *Proc. 32nd IEEE Industrial Electronics Society Annual Conference (IECON)*, Paris, Nov. 6-10, 2006, pp. 1176-1181.

[24] M. van Wieringen, M. Bernacki, and R. Pop-Iliev, "Design and development of a plug in by wire(less) hydrogen internal combustion engine extended range electric vehicle," in *Proc. IEEE Veh. Power Propulsion Conf.*, 2008, pp. 1-8.

[25] W. Gao, "Performance comparison of a fuel cell-battery hybrid powertrain and a fuel cell-ultra capacitor hybrid power train," *IEEE Trans. Veh. Technol.*, vol. 54, no. 3, pp. 846-855, May 2005.

[26] A. H. Niasar, H. Moghbelli, and A. Vahedi, "Design methodology of drive train for a series–parallel hybrid electric vehicle (SP-HEV) and its power flow control strategy," in *Proc. Int. Conf. Elect. Mach. Drives*, 2005, pp. 1549-1554.

[27] C.R. Hewson, G.M. Asher, M. Summer, "Dynamometer control for emulation of mechanical loads", *IEEE Trans. Ind. Appl.*, vol. 2, pp. 1511-1518, Oct. 1998.

[28] E. R. Collins and Y. Huang, "A programmable dynamometer for testing rotating machinery using a three-phase induction machine," *IEEE Trans. Energy Convers.*, vol. 9, no. 3, pp. 521-527, Sep. 1994.

[29] Z. H. Akpolat, G. M. Asher, and J. C. Clare, "Experimental dynamometer emulation of nonlinear mechanical loads," *IEEE Trans. Ind. Appl.*, vol. 35, pp. 1367-1373, Nov.-Dec. 1999.

[30] Z. H. Hakan, G. M. Asher, and J. C. Clare, "Dynamic emulation of mechanical loads using a vector-controlled induction motor-generator set," *IEEE Trans. Ind. Electron.*, vol. 46, no.2, pp. 370-379, Apr. 1999.

[31] J. Arellano-Padilla, G. M. Asher, and M. Sumner, "Control of an dynamometer for dynamic emulation of mechanical loads with stiff and flexible shafts," *IEEE Trans. Ind. Electron.*, vol. 53, no. 4, pp. 1250-1260, Jun. 2006

[32] H. Zha and Z. J. Zong, "Emulating Electric Vehicle's Mechanical Inertia Using an Electric Dynamometer," in *Proc. IEEE International Conference on Measuring Technology and Mechatronics Automation(ICMTMA)*, Changsha City, March 13-14, 2010, pp. 100-103.

[33] K. B. Wipke, M. R. Cuddy, and S. D. Burch, "ADVISOR 2.1: A user-friendly advanced powertrain simulation using a combined backward/forward approach," *IEEE Trans. Veh. Technol.*, vol. 48, pp. 1751-1761, Nov. 1999

[34] T. Markel, A. Brooker, T. Hendricks, V. Johnson, K. Kelly, B. Kramer, M. O'Keefe, S. Sprik, and K. Wipke, "ADVISOR: A systems analysis tool for advanced vehicle modeling," *J. Power Sources*, vol. 110, no. 2, pp. 255-266, Aug. 2002

[35] H. Yeo and H. Kim, "Hardware In the Loop Simulation of Regenerative Braking for a Hybrid Electric Vehicle," *Journal of Automobile Engineering*, vol. 216, no. 11, pp. 855-864, 2002.

[36] F. U. Syed, M. L. Kuang, J. Czubay, and H. Ying, "Derivation and experimental validation of a power-split hybrid electric vehicle model," *IEEE Trans. Veh. Technol.*, vol. 55, no. 6, pp. 1731-1747, Nov. 2006.

II EV Braking Emulation Using a Hardware-in-the-Loop (HIL) Motor/Dynamometer Test Bench

***Abstract*—** This paper provides a new approach for emulating electric vehicle (EV) braking performance on a motor/dynamometer test bench. The brake force distribution between regenerative braking and friction braking of both the front and rear axles are discussed in detail. A brake controller is designed, which represents a very close model of an actual EV braking system and takes into account both regenerative and friction braking limitations. The proposed brake controller is then integrated into the controller of an EV Hardware-in-the-Loop (HIL) test bench, and its performance is validated in real-time. The effect of adding the brake model is further investigated by comparing the experimental HIL energy consumption results to those obtained from ADvanced VehIcle SimulatOR (ADVISOR).

I. INTRODUCTION

Energy crisis, global warming, and environmental pollution have forced the developed countries to focus more progressively on a new generation of clean transportation. Electric vehicle (EV) technology, as a viable solution to clean transportation, is becoming the leading developmental trend of most major automotive companies. At the same time, a lot of research is made towards the design and control of EV powertrain components to maximize performance, efficiency, and to extend the driving range of these vehicles. Research and advancement of this cutting edge technology and the need to obtain accurate predictions of powertrain performance,

without the implications associated with manufacturing, has led to the use of Hardware-in-the-loop (HIL) simulations. This method of emulation is considered a necessary tool in the study and implementation of EVs and allows for accurate verification and testing of developed control and energy management strategies.

An EV HIL test bench setup is typically composed of the vehicle drive motor (DM), which is coupled to a dynamometer through a shaft. A dynamometer is an adjustable load-drive capable of applying a controlled load in the form of torque or rotating force. Dynamometers are widely used in HIL implementations and are suited for automotive testing because of their responsiveness and power/torque capacity at high speeds. A number of articles in the literature have focused on EV emulation using HIL setups [1], [2]. Some works have focused on the comparison of different motors and energy analysis for electric drive vehicle concepts. Others have focused on evaluation of electric motor performance for different drive cycles [3], [4].

One of the most significant elements in the development of an EV test bench is controlling both the DM and the dynamometer electric motor simultaneously under different driving scenarios, thus providing an accurate model of the actual vehicle under study. Furthermore, to accurately emulate the behavior of an EV on a test bench and provide a realistic model, all characteristics of the vehicle should be considered. One inherent feature of EVs is regenerative braking [5]-[7]. This capability allows the electric motor to operate as a generator alongside friction braking and absorb excess energy while the vehicle is decelerating. Regenerative braking is an effective approach that improves vehicle efficiency, especially in heavy stop and go traffic [8]. The amount of energy

returned to the battery through regenerative braking can substantially extend the vehicle driving range [5].

The effect of vehicle braking and brake force distribution between regenerative and friction braking has been thoroughly studied in the literature and different simulation models have been proposed [7], [9]-[15]. Some experimental work have also been conducted on vehicle braking emulation using hardware setups [16]-[20]. However, in most cases either an actual vehicle is used to test the braking performance or in the case of using a test bench, only the braking performance of the vehicle is studied and a realistic representation of vehicle dynamics is not considered. As a result, modeling EV braking system on a motor/dynamometer HIL test bench that also incorporates vehicle dynamics has never been considered before. Therefore, to provide a more realistic approach towards EV emulation, a need to integrate an accurate model of EV regenerative and friction braking into a HIL test bench control system is of great importance.

This paper extends the authors' previous research in [21] and [22] on emulating on-road operating conditions for EVs using a HIL motor/dynamometer setup. In the previous work, the behavior of an EV was emulated by calculating the resistive forces of an actual vehicle and controlling the motor/dynamometer set to represent an accurate model of EV performance for different scenarios. The current study provides a new approach for modeling and integration of EV braking system on the existing motor/dynamometer setup while taking into account the limitations imposed by friction and regenerative braking. The new model not only provides a comprehensive and more realistic approach towards emulating EV performance on a motor/dynamometer test

bench, but can further be used in efficiency and energy consumption analysis studies related to these vehicles. The brake dynamic emulation is achieved by controlling the DM to follow the required drive cycle profile while taking into account its regenerative braking capabilities and controlling the dynamometer motor to emulate both the friction braking effect as well as the resistive forces acting on the actual vehicle.

This paper is organized as follows. In Section II, EV braking forces are explained. In Section III, the fundamentals of EV brake system design are discussed. Brake force distribution between the front and rear axles followed by proper distribution of brake force between the electric motor and friction braking is also explained in this Section. In Section IV, the HIL motor/dynamometer test bench structure for emulating EV performance is presented which is also used to implement the proposed braking model. A braking model is developed in Section V. The developed model is integrated into the controller of the existing HIL setup in Section VI and experimental results are presented in Section VII to validate its effectiveness. In Section VIII a case study is presented to highlight the importance of considering braking on vehicle energy analysis for HIL test bench studies. Finally, in Section IX, conclusions are drawn.

II. EV BRAKING FORCES

The total braking force of an EV is made up of two terms; regenerative braking force of the electric motor, and friction braking force of the wheels. Regenerative braking is a key feature of EVs that allows the vehicle to recover significant amounts of energy during braking and store it in the energy storage system for future use. This inherent advantage is considered an effective method to improve the driving range [5], [10].

Energy recovery through regenerative braking is accomplished by controlling the electric motor to operate as a generator and converting the kinetic or potential energy of the vehicle's mass into electric energy [23]. In this case, only the driven axle is effective during regenerative braking.

During most heavy braking situations the required braking force to decelerate, or stop the vehicle, is much greater than the resistive force produced by the electric motor. As a result, the majority of the braking energy must be absorbed by the friction brake system [24]. Therefore, in order to allow brake energy recovery while ensuring braking performance, both regenerative and friction braking have to coexist together

III. BRAKE FORCE DISTRIBUTION

One of the most important concerns affecting vehicle safety is the braking performance. The two fundamental design considerations for EV braking system are: (1) To quickly reduce the vehicle speed by applying sufficient braking force while maintaining the stability and controllability of the vehicle direction, and (2) To maximize the ability to recover as much braking energy as possible to improve the overall vehicle efficiency and therefore, extend the driving range. The former requires proper brake force distribution between the front and rear axles, while the latter requires a proper distribution of brake force between the electric motor and the friction braking system.

Advancement and development of new braking mechanisms such as electromechanical brakes (EMB) [25]-[27] have made it possible to implement and control brake force distribution. This braking system is also considered to be essential in the development of regenerative braking control for electric and hybrid electric vehicles

[28]. The EMB technology uses an electric motor to generate braking force and oppose to hydraulic brakes it allows accurate brake force control on each wheel [29], [30].

A. Brake Force Distribution Between Front and Rear Axles

In order to achieve the shortest braking distance while ensuring maximum braking stability of the vehicle under various road conditions, proper allocation of the total braking force between the front and rear axles is essential. Not complying with this requirement will result in either the front or the rear wheels to lock sooner than expected and may lead to loss of stability or directional control. In the case where the rear wheels lock first, the vehicle will be prone to directional instability and a slight lateral movement of the rear end of the vehicle will result in swinging and eventually loss of vehicle control. On the other hand, the lockup of the front wheels does not cause directional instability but results in a loss of directional control which may be regained by partial release of the brakes [23].

In order for the front and rear wheels to obtain their maximum braking force and lock simultaneously under various road conditions, braking theory and design principles emphasize on distribution of total brake force between rear and front wheels in accordance with a nonlinear hyperbolic curve referred to as the ideal braking force distribution curve or *I* curve. The ideal braking force distribution curve can be calculated by considering the load transfer from the rear axle to the front axle during braking. Based on the vehicle body specifications this distribution is given by [31], [32]

$$F_{bf} = \frac{-\sqrt{m^2 g^2 {L_a}^2 - 4mgh_g L F_{br}} - 2F_{br}h_g + mgL_a}{2h_g} \tag{1}$$

where m is the vehicle mass, L is the vehicle wheel base, h_g is the gravity center height of the vehicle, L_a is the length from the vehicle's center of gravity to the front axle, and F_{bf} and F_{br} are the braking forces acting on the front and rear wheels, respectively.

The resulting I curve is depicted in Figure 1 for a typical vehicle. If the brake force distribution between the front and rear axle follows the ideal distribution curve, the front and rear wheels will be locked simultaneously and maximum brake performance and stability of the vehicle is achieved. If the ratio of the braking force is above the ideal curve, the rear wheels will be locked earlier than the front wheels. Otherwise, if the operating point falls below the ideal distribution curve, the front wheels will be locked prior to the rear wheels.

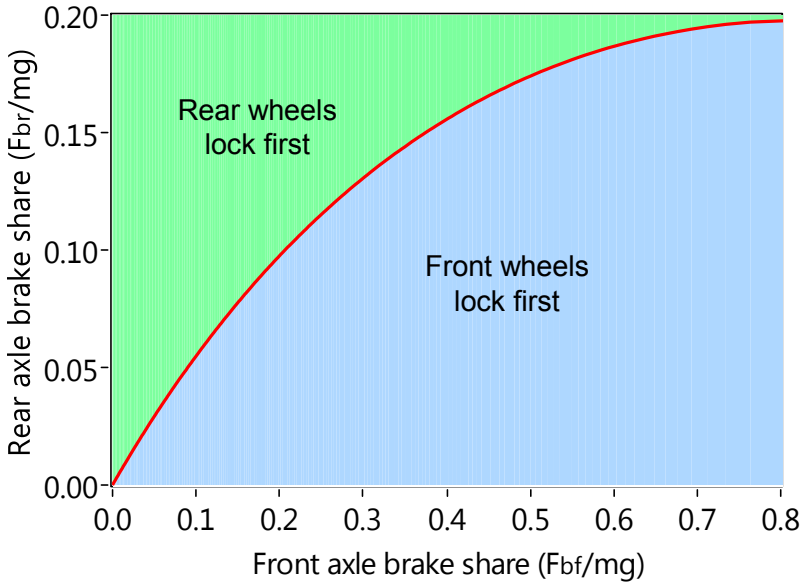

Figure 1. Ideal brake force distribution curve on the front and rear axles of a typical vehicle.

B. Brake Force Distribution Between Regenerative and Friction Braking

Another concern for the EV brake system design is proper allocation of brake force between the friction brakes and the regenerative braking of the electric motor. In practice, regenerative braking should be applied to recapture as much energy as possible without compromising the vehicle stability and controllability. As far as EV driving and braking operations are concerned, the most important issue is safety [33]. Therefore, brake force control strategy and coordination of motor resistive torque with friction braking force plays an important role in both brake energy recovery and vehicle stability. Taking into account motor limitations and the fact that only the driven axle is effective during regenerative braking, the brake controller is responsible for balancing the regenerative and friction braking force. The brake controller is designed to maximize regenerative braking and to minimize the amount of kinetic energy lost to heat and friction.

When coordinating EV braking and calculating regenerative braking share, two main limitations should be considered. The first limitation is the maximum regenerative braking capability which is usually determined by the braking torque capability of the electric motor while operating as a generator [11]. This limitation affects maximum energy recovery during harsh deceleration of the vehicle. The other limitation which plays an important role particularly when considering efficiency and energy consumption is the inability of the electric motor to charge the vehicle battery at low speeds. During deceleration, regenerative braking employs the back electromotive force (EMF) of the motor which can be considered as a voltage source to recharge the battery [19]. However, at low speeds due to the insufficient back EMF voltage generated by the electric motor,

the regenerative braking process is no longer effective. The low speed threshold depends on the type and specifications of the electric motor and the energy storage used within the vehicle. Although operating in regenerative mode at speeds below this threshold the electric motor is still capable of applying a resistive torque to slow down the vehicle, however, it is not capable of harvesting this energy. Hence, current is drawn from the energy storage resulting in further depletion of the vehicle energy storage system.

To more clearly analyze the effect of motor regenerative braking at low speeds an experiment was performed using a motor/dynamometer set. In this test the electric motor resembling the DM of the vehicle was connected to a bi-directional DC source and operated as a generator to emulate regenerative braking effect of a vehicle during deceleration. The DM was controlled to linearly reduce the shaft speed from 1750 rpm to a full stop. At the same time the dynamometer was controlled to provide a fixed torque of 50 Nm to represent the resistive forces acting on a vehicle as well as the inertial force of a moving vehicle during deceleration. It should be noted that calculating vehicle resistive forces is a more complex process discussed in section IV and cannot be considered constant for different speeds. However for the sake of simplicity this test was executed assuming a constant resistive force to show the DM regenerative braking capability during low speed operation. The results of this experiment are shown in Figures 2 and 3.

It can be seen that while the dynamometer is controlled to produce a constant torque, the DM reduces the shaft speed from 1750 rpm by producing an opposing torque. Figure 3 shows that during this period the DM DC current is negative until point A, indicating that current is being pushed back into the energy source. The shaft speed at point A is almost 200 rpm. However, at speeds below point A positive current is drawn

from the energy storage to resist the dynamometer torque and bring the shaft speed to zero. Assuming a fixed DC bus voltage throughout the simulation, the area below positive values of current (area B), represents energy loss during regenerative braking. This indicates that below a certain speed, regenerative braking is not capable of energy harvesting and can have a negative impact on the overall efficiency of the vehicle.

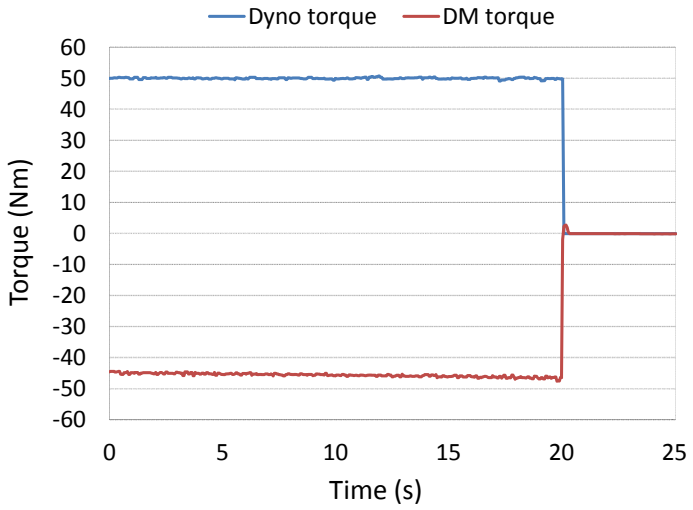

Figure 2. Experimental results of DM and dynamometer generated torque.

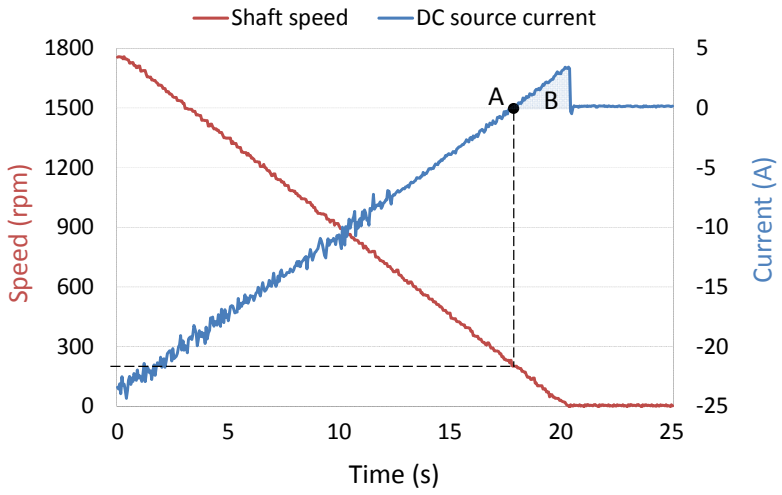

Figure 3. Experimental results of shaft speed and DC source current variation.

Although the energy loss during regenerative braking is small compared to the energy gained prior to point A, however, when longer driving times with frequent braking at lower speeds are considered, it would have a significant impact on energy consumption and range of the vehicle. As a result, in an actual EV, when the wheel speed is lower than a given threshold, braking is completely performed by the friction brakes and the electric motor is controlled to produce no braking force. The boundaries for maximum regenerative braking capability and low speed operation are shown in Figure 4.

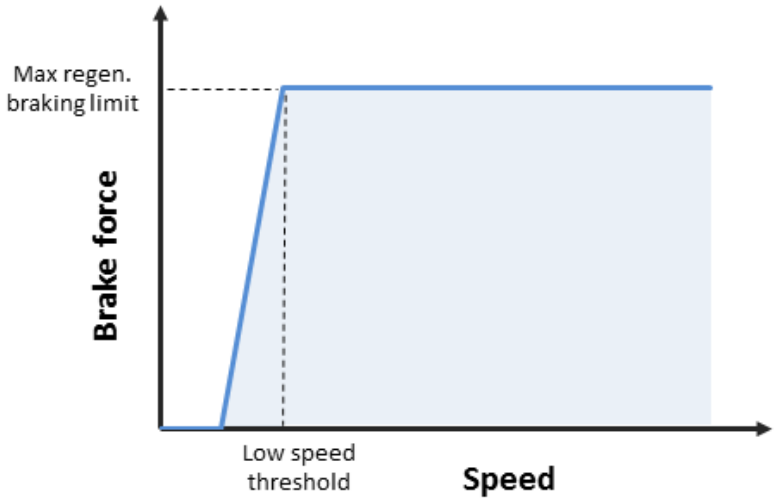

Figure 4. Boundaries for regenerative braking capability.

IV. Previous Motor/Dynamometer Test Bench Structure and its Limitations

Figure 5 shows the block diagram representation of the test platform used in [21] to emulate EV performance on a predetermined drive cycle. The architecture is based on real-time simulation and consists of two motors on a common shaft. The controller block

diagram for this setup is depicted in Figure 6 and is also used in this paper to implement the brake controller.

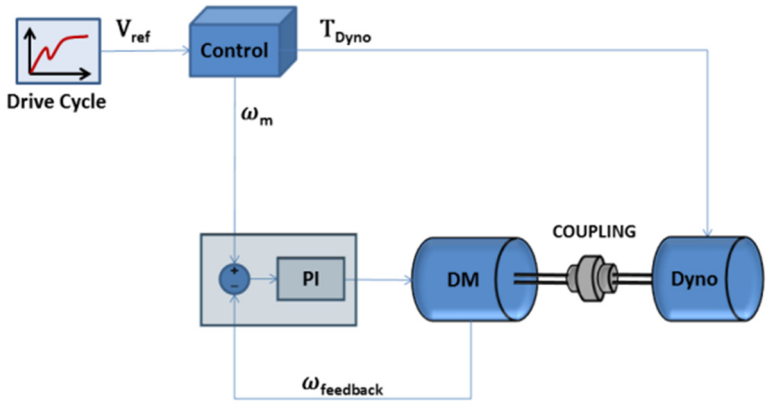

Figure 5. Block diagram representation of the EV test bench [21].

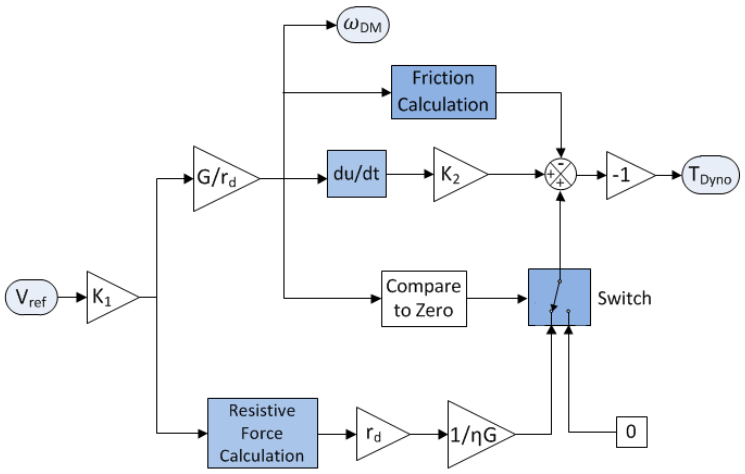

Figure 6. Controller block for the EV test bench.

In this configuration, the reference for the vehicle's translational speed is obtained from a predetermined drive cycle and is translated into a required rotational speed, which

is then given to the DM through a PI controller that ensures accurate speed tracking. The required dynamometer resistive torque (T_{Dyno}) is calculated directly from the speed trace using the test bench and the vehicle dynamic equations at each instance and is given by [21]

$$T_{Dyno} = \frac{T_R}{\eta G} - \left(B_{DM} + B_{Dyno}\right)\omega_m + \left(\frac{J_{ew}}{\eta G^2} - J_{rotation}\right) \times \left(\frac{d\,\omega_m}{dt}\right) \tag{2}$$

where ω_m is the motor rotational speed, G and η are the total gear ratio and overall efficiency of the vehicle drive train to be emulated, $J_{rotation}$ is the rotating inertia of all the rotating components of the system, which includes the rotating inertia of the DM, dynamometer, and the coupling. In addition, B_{DM} and B_{Dyno} are the viscous coefficients of the DM and the dynamometer which represent friction losses. T_R is the total resistive torque calculated at the wheels, and is calculated from the resistive forces acting on the vehicle [22]. Knowing the vehicle specifications T_R is given by

$$T_R = \frac{mgf_r \cos\alpha + \frac{1}{2}\rho_a C_D A_f (V + V_W)^2 + mg \sin\alpha}{r_d} \tag{3}$$

where m is the vehicle mass, fr is the rolling resistance coefficient, α is the ground slope angle, V is the vehicle speed in m/s, C_D is the aerodynamic drag coefficient that characterizes the shape of the vehicle's body, V_w is the wind speed on the vehicle's moving direction, A_f is the frontal area of the vehicle, and ρ_a is the mass density of air. Also, r_d is the vehicle's wheel radius, which also defines the ratio between the rotational velocity of the wheels and the vehicle's linear velocity.

J_{ew} is the equivalent rotational inertia of the vehicle, which is discussed in detail in [34]. This term corresponds to the amount of flywheel inertia that has the same stored energy as a moving vehicle with a known mass when rotating at the same rotational speed as the vehicle's electric motor and is given by

$$J_{ew} = (1 + 0.04 + 0.0025G^2) \times m \times {r_d}^2 \quad (4)$$

The experimental motor/dynamometer test platform used both in [21] and in this paper is shown in Figure 7. The experimental arrangement consists of a 15 kW, 6-pole permanent magnet synchronous motor (PMSM), which represents the DM. The PMSM shaft is connected to a 15 kW DC machine fed by a 4-quadrant chopper acting as the dynamometer to emulate road load, vehicle inertia, and friction braking force.

The PMSM drive is connected to a high power bi-directional DC sources with full regenerative capability allowing it to transferring back energy to the energy storage during regenerative braking. LabVIEW software is used to perform real-time simulation by building the vehicle model and executing the commands in real time using an on-board PC processor. To emulate on-road operation conditions for the DM, speed and torque commands are calculated from mathematical models of vehicle dynamics, road load, and vehicle inertia effects according to the drive cycle profile. The controller then changes the operating point of the dynamometer and the DM continuously and sends synchronous speed and torque signals to the two drives at each instance allowing exact interaction between them.

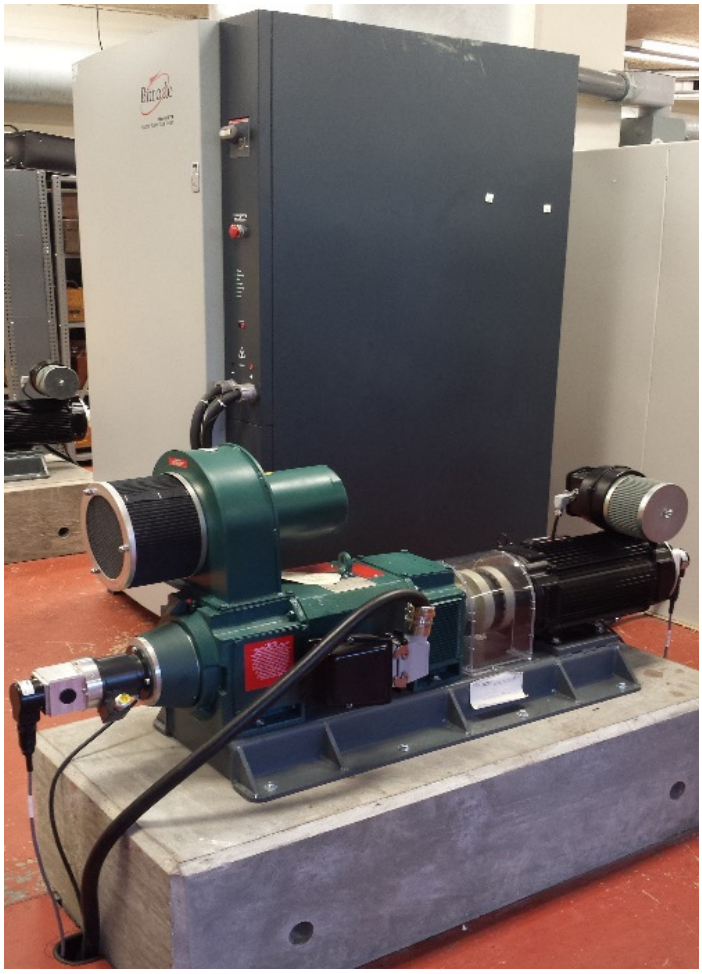

Figure 7. Motor/dynamometer experimental setup.

V. DECISION LOGIC OF BRAKE CONTROLLER

In order to accurately emulate EV braking performance on a motor/dynamometer HIL setup, first the braking control strategy should be defined so that it represents a very close model of an actual EV braking system. In this paper, a front wheel-drive configuration is considered. As a result the braking forces on the front axle consist of motor regenerative braking as well as front wheel friction brakes, while the rear axle braking force only consists of rear wheel friction brakes.

Since the EV HIL setup under study is designed to follow a standard drive cycle, the required DM torque can be calculated from the vehicle and test bench dynamic equations at each instance [22]. Based on the control model of Figure 6, the desired DM torque to ensure accurate speed tracking is given by

$$T_{DM} = \frac{J_{ew}}{\eta G^2}\left(\frac{d\omega_m}{dt}\right) + \frac{T_R}{\eta G} \tag{5}$$

The calculated DM torque from (5) is used as an input reference to the brake controller. As long as this torque is positive, the brake controller is inactive. As soon as the calculated DM torque is negative the brake controller calculates the required braking torque on the front and rear axles according to the ideal braking curve distribution. It should be noted that the brake torque distribution follows the same trend as the brake force distribution given in (1) and brake torque and force are related to each other by vehicle wheel radius. As long as the front axle's share is within the motor capabilities and the motor speed is above the low speed threshold, the front axle's share of the braking force is met solely by the DM. At speeds below the threshold, the brake controller gradually decreases the regenerative braking share of the DM and at the same time, increases the friction braking share of the front wheels. A flowchart representation of the brake controller is shown in Figure 8.

VI. INTEGRATION OF THE BRAKING CONTROL STRATEGY INTO HIL SETUP

The proposed controller for the motor/dynamometer test bench platform shown in Figure 7 does not take into account the effect of friction braking. In this model, it is

assumed that the only means of deceleration is the regenerative braking force of the DM. Also, there are no limitations on the regenerative braking capabilities of the DM. In order to consider the effect of friction brakes and present a comprehensive EV emulation controller suitable for any motor/dynamometer test bench, the brake controller of Figure 8 is integrated into the previous EV HIL controller shown in Figure 6.

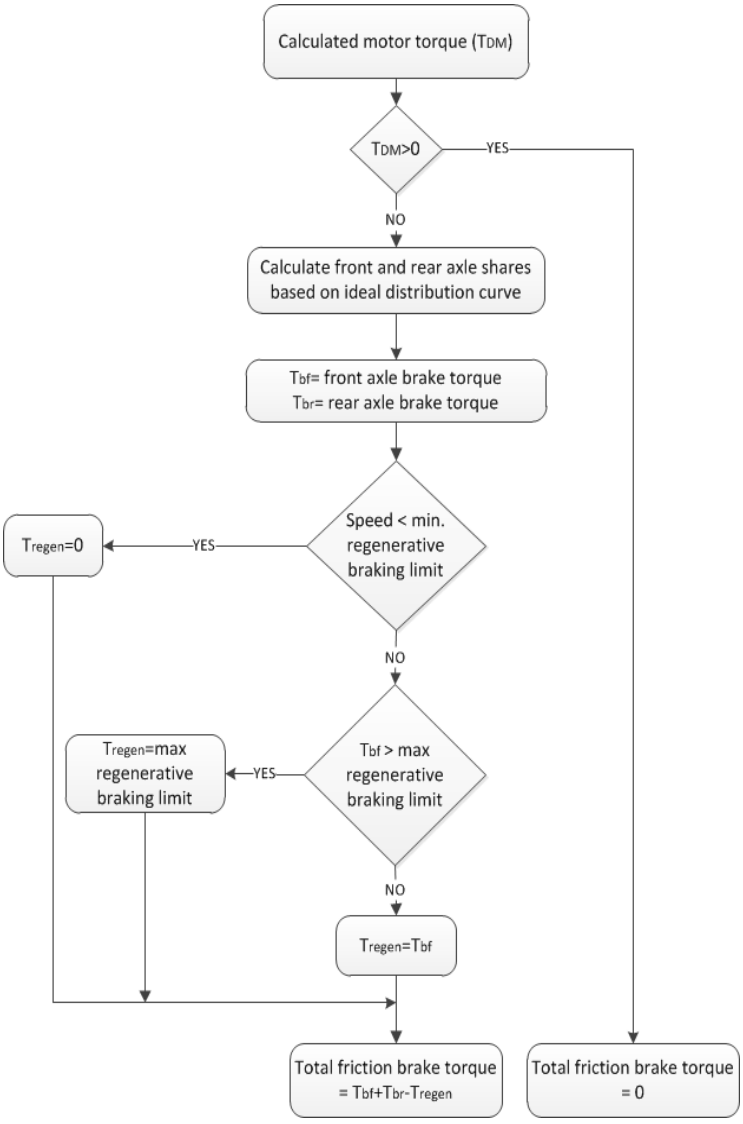

Figure 8. Flow chart representation of the brake controller.

This is achieved by subtracting the total friction braking term, calculated by the brake controller, from the original dynamometer torque reference. The reason for this is that during deceleration and in regenerative braking mode, the DM is providing opposing torque to reduce the shaft speed, which is proportional to vehicle speed. At the same time, the dynamometer is controlled to provide a torque in positive alignment with the shaft rotational direction, hence, emulating the available kinetic energy of the vehicle and assisting vehicle movement. As a result, since friction brake force is also considered as a resistive force opposing vehicle movement, friction braking effect can be realized by subtracting the calculated friction braking torque from the torque produced by the dynamometer during deceleration. Therefore, after the brake controller calculates the required friction braking on the rear and front axles with regards to the ideal braking curve and motor regenerative braking capabilities, the sum of the front and rear axle friction braking is subtracted from the original dynamometer torque command. The complete motor/dynamometer controller block diagram containing the brake controller block is shown in Figure 9.

VII. EXPERIMENTAL RESULTS AND VALIDATION

To verify the overall performance of the system and validate the effectiveness of the implemented control approach, two experiments were conducted using the HIL experimental setup of Figure 7. The vehicle and test bench parameters used for both tests are presented in Table I. Each test was performed for the duration of 510 seconds of the Urban Dynamometer Driving Schedule (UDDS).

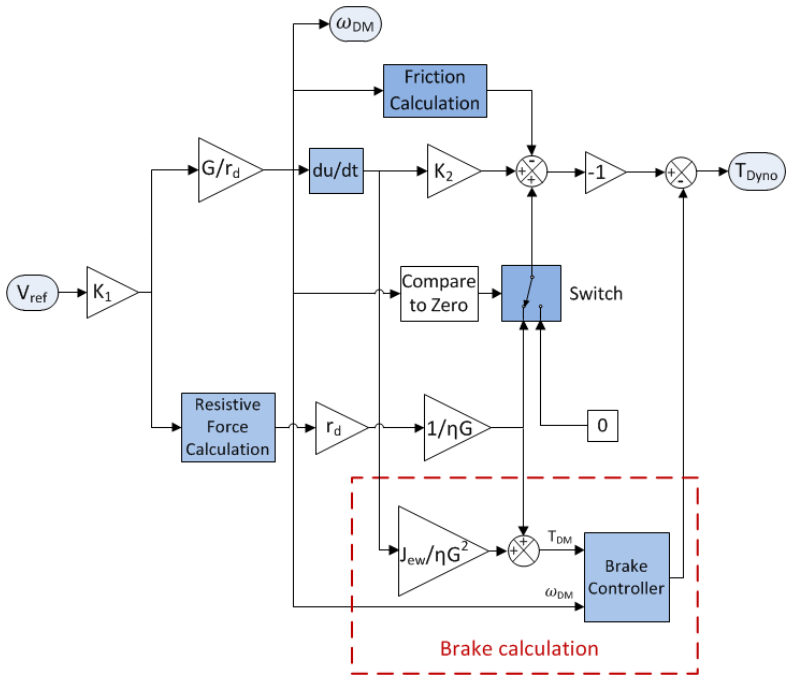

Figure 9. Modified control block for the EV test bench.

Table I

Vehicle and Test Bench Specifications

Parameter	**Value**
Vehicle mass (m)	600 kg
Air density(ρ_a)	1.22 kg/m^3
Aerodynamic drag coefficient (C_d)	0.19
Frontal area (A_f)	1.6 m^2
Rolling resistance coefficient (fr)	0.01
Wheel radius (r_d)	0.28 m
Overall gear ratio (G)	2.6
Inertia of all the rotating components ($J_{rotation}$)	0.038 kgm^2
Equivalent Vehicle Rotational Inertia (J_{ew})	33.029 kgm^2
Vehicle drive train overall efficiency (η)	95 %
DM viscous coefficient (B_{DM})	0.0086 N.m/(rad/s)
Dynamometer viscous coefficient (B_{Dyno})	0.0133 N.m/(rad/s)
Distance from center of gravity to the front axle (L_a)	0.95 m
Gravity center height (h_g)	0.5 m
Wheel base (L)	2.2 m

The first test was performed using the original control model of Figure 6 without taking into account the friction braking effect. The results for this case are illustrated in Figure 10. The second test was executed considering the brake distribution between regenerative braking and friction braking of the front and rear axles and using the modified control block diagram of Figure 9. For this case, the maximum regenerative braking limit was assumed to be -50 Nm and the motor low speed limit was chosen to be 200 rpm based on the DM specifications. The experimental results for this case are illustrated in Figure 11.

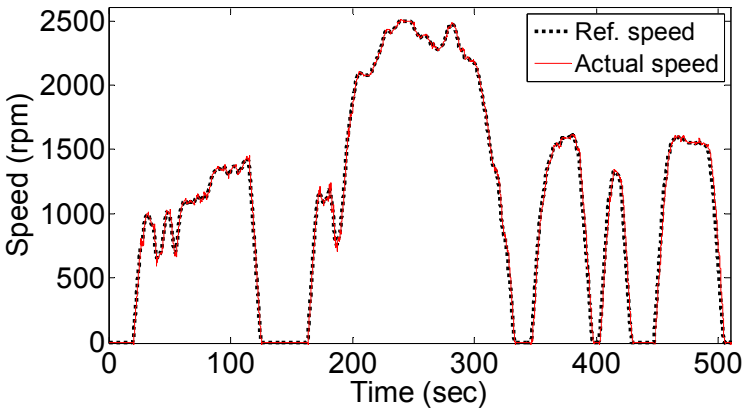

(a)

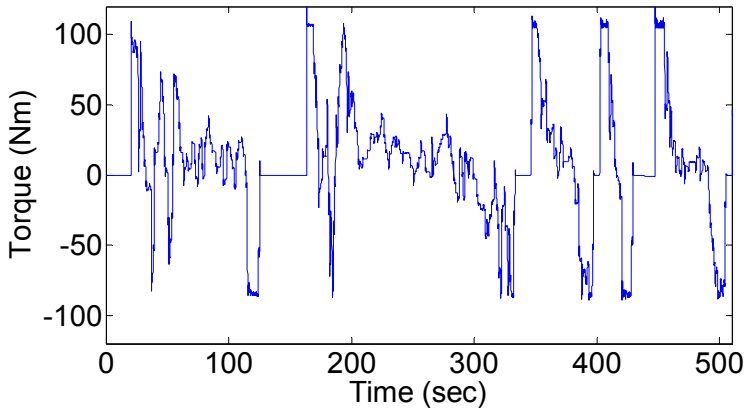

(b)

Figure 10. Experimental results without the brake controller (a) Reference and actual DM speed (b) DM torque.

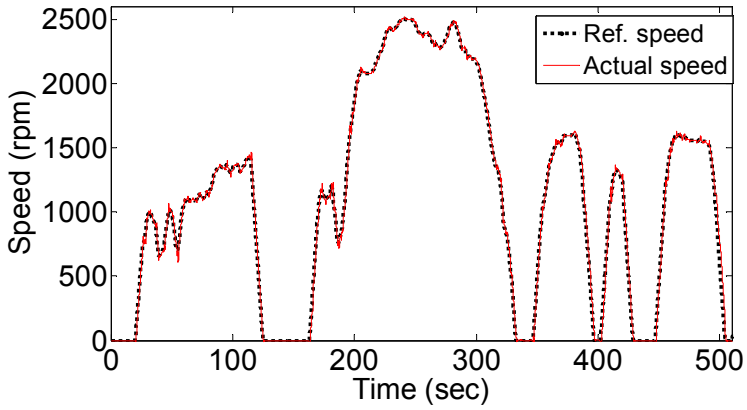

(a)

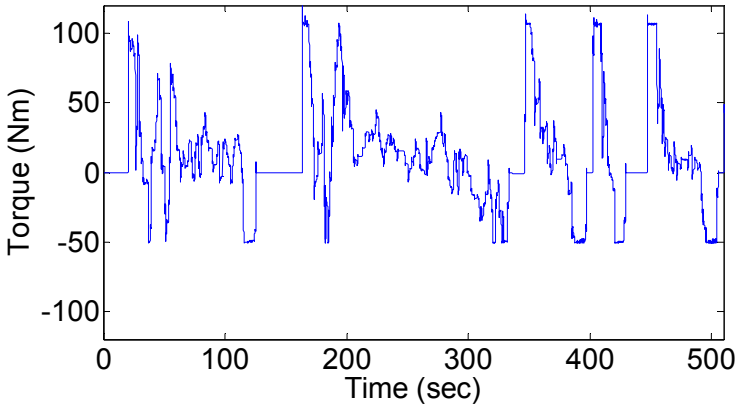

(b)

Figure 11. Experimental results with the implemented brake controller (a) Reference and actual DM speed (b) DM torque.

Comparing the results from Figures 10(a) and 11(a), it can be seen that for both cases the vehicle follows the drive cycle precisely and only minor speed variations from the reference speed exist for both cases. From Figure 10(b), it is concluded that the required maximum DM regenerative torque to meet the drive cycle deceleration needs is approximately -86 Nm for this vehicle. However, as seen in Figure 11(b), it is clear that due to the presence of the brake controller, the distribution of friction braking and

regenerative braking is controlled such that the motor regenerative braking torque is limited to the preset value of -50 Nm. Also, since the shaft speed is the result of the interaction between the DM and the dynamometer torque, a lower DM torque indicates that the dynamometer share of positive torque is also reduced to compensate for the effect of friction braking while the vehicle is decelerating.

The DM regenerative braking torque and total friction braking share of both axles are also shown in Figures 12 and 13. These results show the effectiveness of the brake controller in accurately allocating the required brake power between friction and regenerative braking. It is also observed that while the DM regenerative torque is limited to -50 Nm, for values more than this limit, total friction brake torque is used to meet the drive cycle deceleration needs. The friction braking share of each axle is also shown in Figures. 14 and 15.

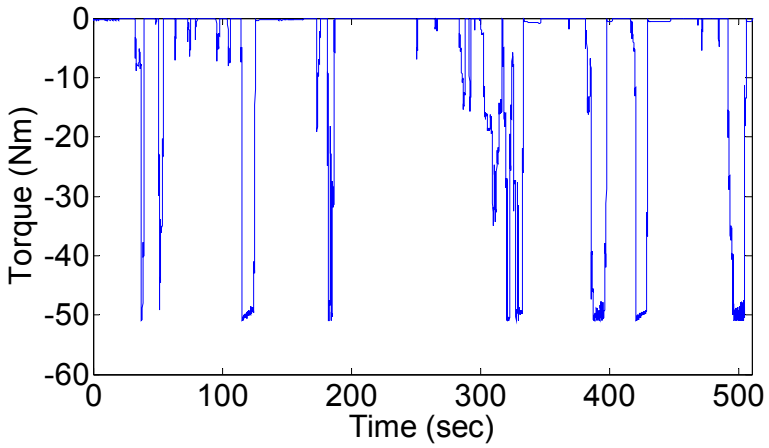

Figure 12. DM regenerative braking share.

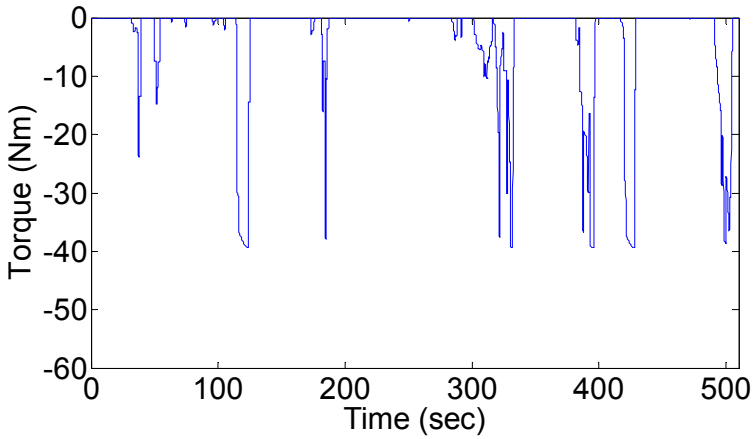

Figure 13. Total friction braking share.

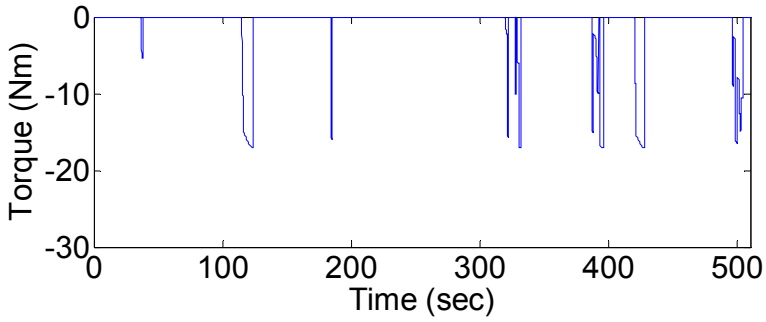

Figure 14. Front axle share of friction brake.

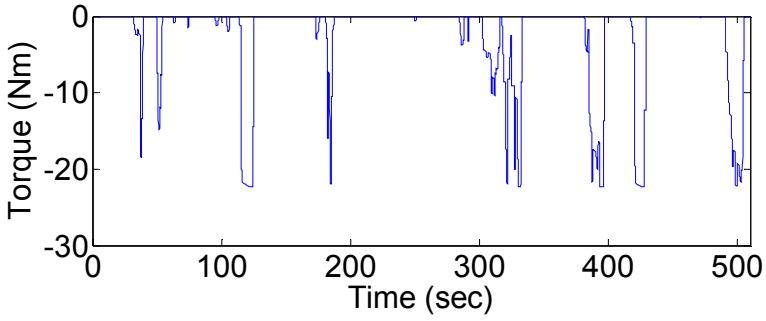

Figure 15. Rear axle share of friction brake.

A closer look into the results of Figures. 12 through 15 reveals that for values below the regenerative limit, the front axle's friction braking share is zero and all the braking requirement of the front axle is met by regenerative braking. However, as soon as the regenerative braking torque exceeds its higher limit, the front axle friction braking is used to assist with the deceleration process and meet vehicle's braking requirements. It is also noted from Figures. 14 and 15 that the front axle's share of friction braking is slightly lower than the rear axle's share due to the regenerative braking effect of the DM on the front axle.

VIII. Case Study Showing the Importance of Considering Braking on Energy Consumption

To further analyze the effect of considering braking on energy consumption, two cases of EV emulation discussed in section VII were compared to the results obtained from the ADvanced VehIcle SimulatOR (ADVISOR) [35], [36]. For this comparison a full UDDS drive cycle was considered and once again the vehicle and test bench parameters were assumed to be the same as those given in Table I. Given the significant advantage of ADVISOR in using MATLAB/Simulink environment, and the flexibility of changing the parameters, the ADVISOR vehicle and regenerative braking parameters were chosen to closely resemble those used in the experimental setup.

To measure the energy consumption for each experimental case, current and voltage measurements from the DC source connected to the PMSM were recorded in real time. The final results of energy consumed, recovered, and lost to friction braking throughout the drive cycle are presented in Table II for each case.

Table II

Energy Results for the UDDS Drive Cycle

CASE / ENERGY DISTRIBUTION	**Experimental**		**Simulation**
	Case I	Case II	Case III
	Without brake modeling	With brake modeling	ADVISOR
Consumed (Wh)	856.3	852.5	851.1
Recovered through Regen. braking (Wh)	-226.2	-145.1	-139.2
Net consumption (Wh)	630.1	707.4	711.9
Lost to Friction (Wh)	0	-90.1	-94.5

The total energy consumed from the source is calculated by integrating the positive values of power over the full drive cycle. The consumed energy represents the required energy to propel the vehicle and does not take into account the energy recovered from regenerative braking. Similarly the energy recovered through regenerative braking was calculated from integration of the negative values of power over the complete drive cycle. Also, the energy lost to friction for the case with the braking model was calculated from the real-time brake torque command given to the dynamometer with respect to vehicle speed.

Comparing the results of consumed energy reveals that the ADVISOR simulation result is closer to the result obtained from the experimental case with brake modeling. On the other hand, the consumed energy for the case with no braking is relatively higher compared to the other two cases. This difference is mainly due to the extra current being

drawn from the source during low speed regenerative braking discussed in section III (b) which adds up to the total consumption. As for energy recovered through regenerative braking, it is clear that the regenerative braking energy obtained from the experimental case with the brake model is once again very close to the result obtained from ADVISOR. For both these cases the recovered energy is almost 17% of their total consumed energy. However, as expected, the total energy recovered during braking for the case without the brake model (case I) is significantly higher and accounts for almost 26% of its consumed energy. This is due to the fact that in the absence of friction braking, the DM is the only means of reducing the speed. As such it is sometimes forced to generate very high regenerative braking force to fulfil the deceleration requirements of the drive cycle, resulting in more energy recovery. It should be noted that although in the case of not considering braking, more energy can be recovered, but since the brake force distribution requirements are not considered, the simulation is far from realistic. The high regenerative braking energy recovery for case I can also be justified from the results of energy lost to friction. Considering that the energy lost to friction is no longer available for recovery, the results show no friction losses in the absence of a braking model while a relatively high friction loss is recorded for the other two cases.

In Table II the net energy consumption is calculated from the difference between the absolute values of consumed energy and the recovered energy from regenerative braking. This value corresponds to the total energy required to complete the drive cycle while also considering the energy recovered through regenerative braking. The net energy consumption is a crucial parameter when estimating the range of an EV with respect to its energy storage capacity. Comparing the results of the net consumption obtained from

ADVISOR with each experimental case shows an error of 11.5% for case I and 0.6 % for case II. This notable difference indicates that by implementing a braking model that represents a close model of an actual EV braking system, very accurate HIL test bench results could be achieved. Whereas not considering braking could result in significant errors that can lead to unrealistic results. This can also be concluded by comparing the results of other parameters from Table II between the experimental cases and the results obtained from ADVISOR.

IX. CONCLUSION

A new approach for emulating EV braking performance on a motor/dynamometer test bench was proposed. This was achieved by introducing a brake controller which takes into account brake force distribution between regenerative and friction braking. To validate the effectiveness of this approach, experiments with and without the brake controller were conducted using a motor/dynamometer HIL experimental setup. The experimental results confirmed the desired operation of the brake controller in distributing the required brake force between regenerative and friction braking without impairing the overall system performance. The results also indicated that when considering a front wheel-drive EV configuration, the front axle's share of friction braking can be lower than the rear axle's share due to DM regenerative braking capability. It was also concluded that from the perspective of energy consumption, considering braking limitations provides a more realistic approach towards EV emulation on a motor/dynamometer setup and allows for a more accurate assessment of EV performance.

REFERENCES

[1] S. Jeschke, H. Hirsch, M. Koppers, and D. Schramm, "HIL Simulation of electric vehicles in different usage scenarios," in *Proc. IEEE Electric Vehicle Conference (IEVC)*, Greenville, March 4-8, 2012, pp. 1-8.

[2] R. M. Schupbach and J. C. Balda, "A versatile laboratory test bench for developing powertrains of electric vehicles," *IEEE 55th Vehicular Technology Conference,* 2002, pp. 1666-1670.

[3] C. Oh, "Evaluation of motor characteristics for hybrid electric vehicles using the Hardware in-the-Loop concept," *IEEE Trans. Veh. Technol.*, vol. 54, no. 3, pp. 817-824, May 2005.

[4] S. Oh and A. Emadi, "Test and simulation of axial flux motor characteristics for hybrid electric vehicles," *IEEE Trans. Veh. Technol.*, vol. 53, no. 3, pp. 912-919, May 2004.

[5] X. Nian, F. Peng ; H. Zhang, "Regenerative Braking System of Electric Vehicle Driven by Brushless DC Motor," *IEEE Trans. Ind. Electron.*, vol. 61, no. 10, pp. 5798-5808, Jan. 2014.

[6] D. Kim, S. Hwang, and H. Kim, "Vehicle Stability Enhancement of Four-Wheel-Drive Hybrid Electric Vehicle Using Rear Motor Control," *IEEE Trans. Veh. Technol.*, vol. 57, no. 2, pp. 727-735, 2008.

[7] F. Wyczalek, and T. Wang, "Regenerative Braking Concepts for Electric Vehicles - A Primer, " *SAE Technical Paper* 920648, 1992, doi:10.4271/920648.

[8] H. Yeo, D. Kim, S. Hwang, and H. Kim, "Regenerative braking algorithm for a HEV with CVT ratio control during deceleration," In *Proc. of SAE CVT Congress*. 2004.

[9] B. Cao, Z. Bai, and W. Zhang, "Research on control for regenerative braking of electric vehicle," in *Proc. IEEE International Conference on Vehicular Electronics and Safety*, Shaan'xi, China, Oct. 14-16, 2005, pp. 92-97.

[10] J. Guo, J. Wang, and B. Cao, "Regenerative braking strategy for electric vehicles," in *Proc. IEEE Intelligent Vehicles Symposium*, Xi'an , China, June 3-5, 2009, pp. 864-868.

[11] L. Chu, L. Yao, J. Chen, L. Chao, and J. Guo, "Integrative braking control system for electric vehicles," in *Proc. IEEE Vehicle Power and Propulsion Conference (VPPC)*, Chicago, IL, Sep. 6-9, 2011, pp. 1-5.

[12] Z. Ling and T. Lan, "Braking force distribution research in electric vehicle regenerative braking strategy," in *Proc. IEEE Computational Intelligence and Design (ISCID),* Hangzhou, China, Oct. 28-29, 2012, pp. 98-101.

[13] G. Jinfang, W. Lifang, L. Chenglin, Z. Junzhi, and Y. Xiaowei, “The coordinated control of motor regenerative braking torques defined by accelerator pedal and brake pedal of electric vehicle,” in *Proc. IEEE Vehicle Power and Propulsion Conference (VPPC)*, Seoul, South Korea, Oct. 9-12, 2012, pp. 119-123.

[14] J. Ko, S. Ko, I. Kim, D. Hyun, and H. Kim, “Co-operative Control for Regenerative Braking and Friction Braking to Increase Energy Recovery without Wheel Lock,” *Int. J. Automot. Technol.*, vol. 15, no. 2, pp. 253-262, 2014.

[15] D. Kim and H. Kim, “Vehicle stability control with regenerative braking and brake force distribution for a four-wheel drive hybrid electric vehicle,” *Proceedings of the Institution of Mechanical Engineers, Part D: Journal of Automobile Engineering*, vol. 220, no. 6, pp. 683-693, 2006.

[16] J. Ko, J. Kim, G. Lee, S. Byun, D. Hyun, and H. Kim, “Development of a co-operative control algorithm during regenerative braking for a fuel cell electric vehicle,” in *Proc. IEEE Vehicle Power and Propulsion Conference (VPPC)*, Chicago, IL, Sep. 6-9, 2011, pp. 1-6.

[17] H. Fujimoto, S. Harada, Y. Goto, and D. Kawano, "Field and bench test evaluation of range extension control system for electric vehicles based on front and rear driving-braking force distributions." in *Proc. IEEE Power Electronics Conference (IPEC)*, Hiroshima, Japan, May 18-21, 2014, pp. 1671-1678.

[18] J. Ko, S. Ko, H. Son, B. Yoo, J. Cheon, and H. Kim, “Development of Brake System and Regenerative Braking Co-operative Control Algorithm for Automatic Transmission-based Hybrid Electric Vehicle,” *IEEE Trans. Veh. Technol.*, IEEE early access articles, 2014.

[19] M. J. Yang, H. L. Jhou, B. Y. Ma, and K. K. Shyu, “A cost-effective method of electric brake with energy regeneration for electric vehicles,” *IEEE Trans. Ind. Electron*., vol. 56, no. 6, pp. 2203–2212, Jun. 2009

[20] H. Yeo, and H. Kim, “Hardware-in-the-Loop Simulation of Regenerative Braking for a Hybrid Electric Vehicle”, *Journal of Automobile Engineering*, vol. 216, pp. 855-864, 2002.

[21] P. Fajri, R. Ahmadi, and M. Ferdowsi, “Control approach based on equivalent vehicle rotational inertia suitable for motor-dynamometer test bench emulation of electric vehicles,” in *Proc. IEEE International Electric Machines and Drives Conference (IEMDC)*, Chicago, IL, May 12-15, 2013, pp. 1155-1159.

[22] P. Fajri, R. Ahmadi, and M. Ferdowsi, “Test Bench for Emulating Electric Drive Vehicle System Using Equivalent Vehicle Rotational Inertia,” in *Proc. IEEE Power and Energy Conference at Illinois (PECI)*, Champaign, IL, Feb. 22-23, 2013, pp. 83-87.

[23] M. Ehsani, Y. Gao, S. E. Gay, and A. Emadi, *Modern Electric, Hybrid Electric, and Fuel Cell Vehicles: Fundamentals, Theory, and Design*. Boca Raton, FL: CRC, Dec. 2004.

[24] Y. Gao, L. Chen, and M. Ehsani, "Investigation of the effectiveness of regenerative braking for EV and HEV," *SAE transactions* 108.6; PART 2 (2000): 3184-3190.

[25] C. Maron, T. Dieckmann, S. Hauck, and H. Prinzler, "Electromechanical brake system: Actuator control development system," *SAE Technical Paper* 970814, 1997, doi:10.4271/970814.

[26] W. Xiang, P. C. Richardson, C. Zhao, and S. Mohammad. "Automobile brake-by-wire control system design and analysis." *IEEE Trans. Veh. Technol., vol.* 57, no. 1, pp.138-145, Jan. 2008.

[27] J. Cheon, "Brake By Wire System Configuration and Functions using Front EWB (Electric Wedge Brake) and Rear EMB (Electric-Mechanical Brake) Actuators," *SAE Technical Paper* 2010-01-1708, 2010, doi:10.4271/2010-01-1708..

[28] J. Ahn, K. Jung, D. Kim, H. Jin, H. Kim, and S. Hwang, "Analysis of a regenerative braking system for hybrid electric vehicles using an electromechanical brake," *Int. J. Automotive Technol.*, vol. 10, no. 2, pp. 229-234, Apr. 2009.

[29] C. Jo, S. Hwang, and H. Kim, "Clamping-Force Control for Electromechanical Brake," *IEEE Trans. Veh. Technol.*, vol. 59, no. 7, pp. 3205-3212, 2010.

[30] S. Saric, A. Bab-Hadiasher, and R. Hoseinnezhad, "Clamp-force estimation for a brake-by-wire system: A sensor-fusion approach," *IEEE Trans. Veh. Technol.*, vol. 57, no. 2, pp. 778–786, Mar. 2008.

[31] N. Mutoh and Y. Nakano, "Dynamics of front-and-rear-wheel-independent-drive-type electric vehicles at the time of failure," *IEEE Trans. Ind. Electron.*, vol. 59, no. 3, pp. 1488–1499, Mar. 2012.

[32] N. Mutoh, "Driving and braking torque distribution methods for front and rear-wheel-independent drive-type electric vehicles on roads with low friction coefficient," *IEEE Trans. Ind. Electron.*, vol. 59, no. 10, pp. 3919-3933, Oct. 2012.

[33] N. Mutoh, Y. Hayano, H. Yahagi, and K. Takita, "Electric braking control methods for electric vehicles with independently driven front and rear wheels," *IEEE Trans. Ind. Electron*., vol. 54, no. 2, pp. 1168-1176, Apr. 2007

[34] P. Fajri, R. Ahmadi, and M. Ferdowsi, “Equivalent vehicle rotational inertia used for electric vehicle test bench dynamic studies,” in *Proc. 38th IEEE Industrial Electronics Society Annual Conference*, Montreal, Canada, Oct. 25-28, 2012, pp. 4115-4120.

[35] K. B. Wipke, M. R. Cuddy, and S. D. Burch, “ADVISOR 2.1: A user-friendly advanced powertrain simulation using a combined backward/forward approach,” *IEEE Trans. Veh. Technol.*, vol. 48, pp. 1751-1761, Nov. 1999

[36] T. Markel, A. Brooker, T. Hendricks, V. Johnson, K. Kelly, B. Kramer, M. O’Keefe, S. Sprik, and K. Wipke, “ADVISOR: A systems analysis tool for advanced vehicle modeling,” *J. Power Sources*, vol. 110, no. 2, pp. 255-266, Aug. 2002C. C. Chan and K. T. Chau, *Modern electric vehicle technology*. Vol. 47. Oxford University Press on Demand, 2001.

III Development of an Educational Small-Scale Hybrid Electric Vehicle (HEV) Setup

I. INTRODUCTION

Transportation electrification is gaining mainstream attention across several sectors, from academia and research laboratories to automotive industries and their suppliers. Its rapid growth in recent years has focused mainly on reducing the dependence of the transportation sector on fossil fuels. In addition to the economic and political complications that oil consumption poses, environmental concerns also have had a tremendous effect on the effort to transition to transportation electrification.

Electrification in the automotive industry appears in the form of electric vehicles (EVs) and hybrid electric vehicles (HEVs). Different configurations of HEVs, namely series, parallel, and series-parallel [1], [2], display different characteristics based on their powertrain architecture and the different components used within them. All-electric vehicles, on the other hand, completely eliminate the need for an internal combustion engine (ICE), and thus the dependence on oil.

With increasing investments in projects pertaining to transportation electrification, educating a new generation of engineers in this field is of great importance. Hybrid vehicles, often considered cyber-physical systems, span multi-disciplinary fields of engineering and science. Therefore, professionals in this field must be familiar with a variety of topics, including vehicle dynamics, electric machines, power electronics, energy storage systems, automotive engineering, and control engineering. In recent years, instructional efforts aiming to prepare individuals and professionals for the

HEV industry have come in the form of books and research articles describing these vehicles and their components [2], software packages that can perform advanced simulations of vehicle behaviors [3], hardware-in-the-loop (HIL) simulations on a test bench [4], and real vehicle tests. Of these methods, the first two fail to provide the practical aspects of transportation electrification education. On the other hand, real vehicle tests and HIL simulations for electric and hybrid vehicles facilitate a hands-on, intuitive, and interactive experience. However, both these methods often require a dedicated system that is usually expensive, rigid, and difficult to test and adjust. Also, due to restrictions on using ICEs in most indoor environments, typical HIL simulation platforms for HEVs emulate the ICE using an electric motor. Therefore, the ICE, one of the main HEV components, usually is absent from the test platform.

To provide a practical, hands-on experience that is safe, affordable, and inclusive of all of the major components of a real HEV powertrain, a small-scale HEV setup was developed. Special attention was given to the overall cost of developing this test bench and the first prototype was built with a budget of $2000. All of the components were selected from commercially available small-scale versions of their full-size counterparts, which then were assembled to form a small-scale HEV test bench. This test bench features the flexibility to switch between different HEV architectures. In addition to the all-electric configuration, the test bench can operate in series, parallel, or series-parallel configurations with only minor changes to the powertrain.

The developed test bench can be used in institutes of higher education to complement theoretical coursework and to serve as an HEV research platform. In addition to familiarizing learners with different HEV components, this platform also can

be used to elaborate on various HEV architectures and designs. Some of the research topics that can be studied on the test bench include HEV design optimization, implementation of different control methodologies on individual components of the system, energy distribution, fuel consumption minimization, and many other research challenges encountered in real-world HEVs. This setup not only serves as a laboratory test platform to study different aspects of electric and hybrid vehicles, but also is designed to address a variety of audiences. Its light-weight, mobile characteristics allow it to be taken to schools and community events as a demonstration and education unit, with the aim of generating interest among younger audiences and encouraging the development and use of HEVs.

II. VEHICLE COMPONENTS

The idea of a small-scale HEV arose from the fact that all of the components of a real HEV are available in a smaller scale. Figure 1 shows the main components used in an HEV and their small-scale equivalents used in the proposed small-scale vehicle setup. By properly combining the parts in the same configuration as a real HEV, a very close model of the actual vehicle can be achieved. However, the scaled versions of the engine, electric motor, and generator must be compatible with each other and in a similar range of power. This will make their properties match, more closely resembling those of an actual vehicle. Figure 2 shows the actual small-scale vehicle setup with the main components outlined; these components then are described briefly.

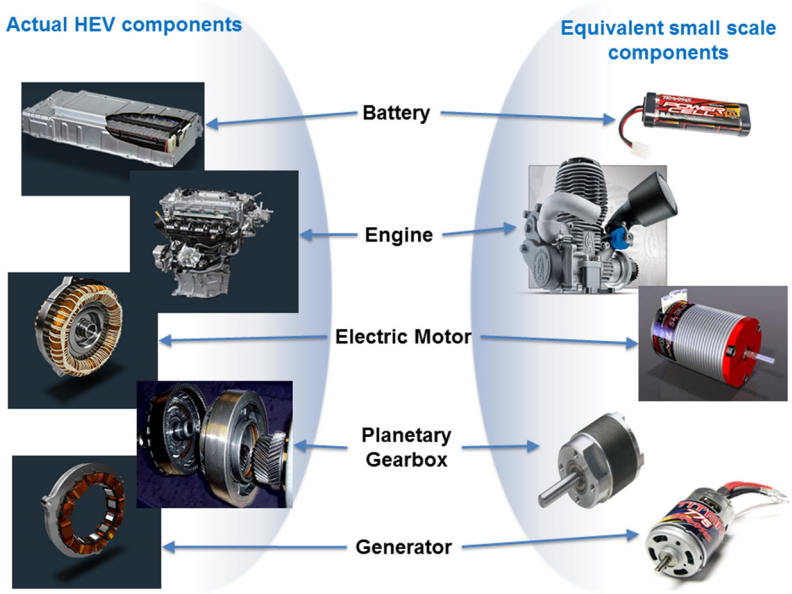

Figure 1. Actual and equivalent small-scale HEV components.

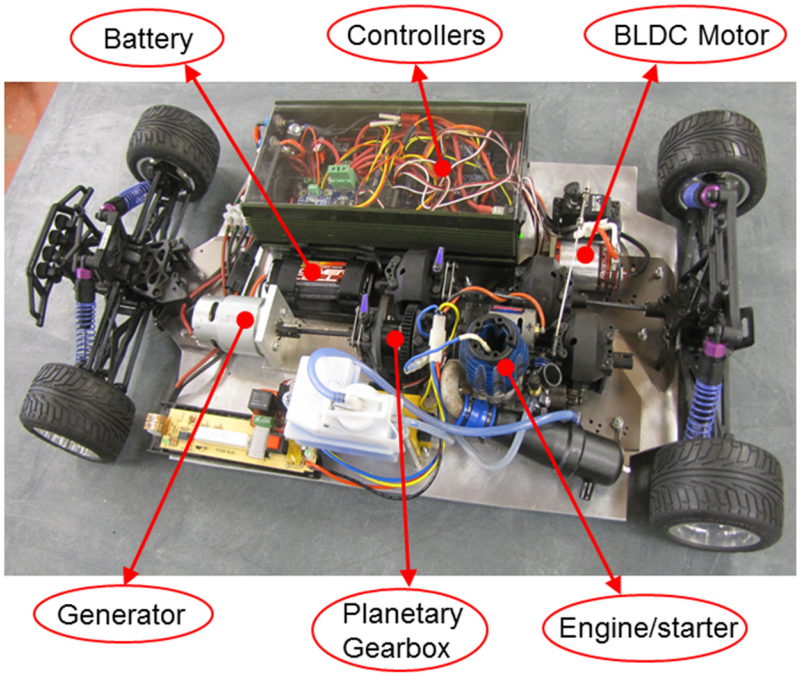

Figure 2. Small-scale HEV setup.

A. Engine/Starter

The vehicle platform engine is a 0.15 cubic inch displacement nitro engine capable of reaching a no-load top speed of 30,000 rpm, with an idling speed of approximately 8,000 rpm. The engine torque is controlled by a servo motor connected to its carburetor, which accurately controls the throttle response, allowing it to reach the desired operating points. There is also an onboard starter mounted on the engine which is used to crank the engine.

B. Electric motor

A small 131 W brushless DC motor capable of reaching 18,000 rpm serves as the electric propulsion unit for the vehicle. The motor is equipped with a dedicated motor drive that can be controlled externally. The motor drive uses three Hall effect sensors mounted inside the motor to estimate the rotor position. The controller also uses one Hall effect sensor to calculate the speed of the motor at each operating point.

C. Generator and DC/DC converter

The generator is a normal brushed DC motor that is operated as a generator to provide a varying DC voltage. The generator is connected to a DC/DC converter used to control the power flow between the generator and the battery by varying its output voltage. The switching of the converter is controlled by pulse width modulation (PWM) signals with an ultra-sonic switching frequency of 32 kHz.

D. Planetary gearbox

A small-scale planetary gearbox with a 46-tooth ring gear and a 14-tooth sun gear distributes mechanical power between the engine, generator, and electric motor. When the ring gear is stationary, a 4.3:1 gear ratio between the sun gear and the carrier allows an increase in speed from the engine to the generator.

E. Battery and battery management

The battery used as the main energy source is a 7.2 V NiMH battery with a capacity of 1200 mAh. One important state of the battery is its state of charge (SOC). The SOC shows the amount of charge remaining in the battery compared to a fully charged battery. In other words, it indicates the scope of operation of the battery-powered device. In HEVs, the battery SOC indicates how much longer the battery will be able to power the vehicle. For the test bench, the SOC of the battery is calculated at each instance by continuously measuring the current based on:

$$SOC = SOC_0 - \frac{1}{Q_T}\int_0^t i(\tau)d\tau$$

where Q_T is the total capacity of the battery, SOC_o is the initial SOC of the battery, and i is the output current of the battery, which is continuously measured using a current sensor. The parameter SOC_o can be found from the relationship between the battery SOC and its open-circuit voltage. For the battery used in this setup, this relationship was obtained using open-circuit voltage tests [5]. The experimental voltage measurements and fitted polynomial for this battery appear in Figure 3.

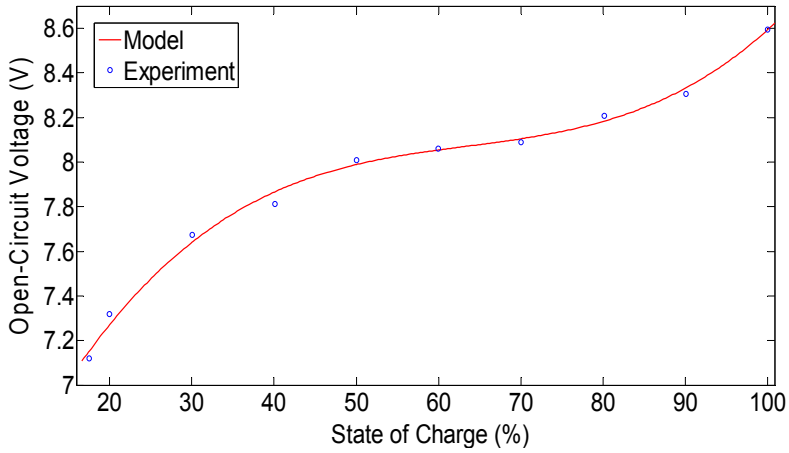

Figure 3. Experimental voltage measurements and fitted polynomial of the battery used in the small-scale HEV.

F. Controllers

Arduino boards [6] are used as controllers to execute control signals and monitor all of the components of the test bench. The Arduino Uno board used in this test bench is a microcontroller board based on the ATmega328 with 14 digital input/output pins (6 of which can be used as PWM outputs) and 6 analog inputs. These boards have the flexibility to be operated either by a program uploaded to the Arduino's memory or using the LabVIEW software [7]. In the latter case, the Arduino is used as a data acquisition (DAQ) device, and LabVIEW executes all of the control decisions. The test bench uses two Arduino boards, one responsible for calculating both the electric motor and the engine speeds, and the other connected to the PC through a USB cable and used as a DAQ device to interact with LabVIEW. The data are passed between two boards using a two-wire serial interface (I^2C), which is well suited for low/medium speed data transfer between integrated circuits.

III. VEHICLE CONFIGURATIONS

One of the main objectives of this setup was to develop a flexible test platform so that all different HEV configurations could be simulated with minimal hardware modifications. Figure 4 illustrates a block diagram of the overall configuration of the test bench, with the planetary gearbox or the power split device serving as the main component for splitting the power between the engine, motor, and generator.

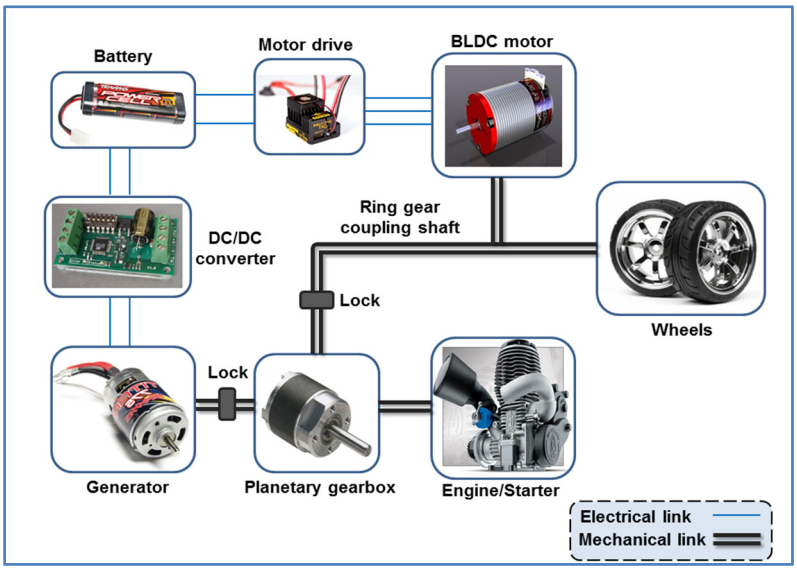

Figure 4. Overall configuration of the small-scale HEV.

This configuration is based on the Toyota Prius powertrain arrangement and allows the test bench to operate as a series, parallel, or series-parallel HEV, as well as an all-electric vehicle with minor modifications to the powertrain. In this configuration, the electric motor is connected to the ring gear of the planetary gear set. It is also directly connected to the differential, which drives the wheels. Therefore, the speed of the electric motor is always proportional to the speed of the vehicle. The generator is connected to

the sun gear of the gear set, and the engine is connected to the planet carrier. A locking mechanism allows each of the sun and ring gears of the planetary gearbox to be locked independently to provide different power flow paths and hence achieve different powertrain configurations. When none of the gears are locked, the output power of the ring gear can be controlled by the engine and generator.

A. All-electric configuration

The simplest configuration of the small-scale vehicle is the all-electric configuration, shown in Figure 5(a), in which the electric motor is the only propulsion unit and the rest of the components are decoupled from the powertrain. This can be achieved by removing the ring gear coupling shaft, thus breaking the mechanical link between the electric motor and the rest of the components.

B. Series configuration

In a series hybrid vehicle, there is a single path to power the wheels of the vehicle, but two energy sources; the speed of the engine is independent of that of the vehicle. In general, in this configuration, the engine is coupled to the generator to produce the power needed to charge the batteries. The electric power can either charge the battery or bypass the battery and be used to propel the wheels via the electric motor. In the proposed test setup, a series configuration can be achieved by removing the ring gear coupling shaft and locking the ring gear of the planetary gear set, as shown in Figure 5(b). This allows a fixed gear ratio between the engine and the generator and decouples the engine from the drive wheels, allowing the vehicle to be the propelled only by the electric motor.

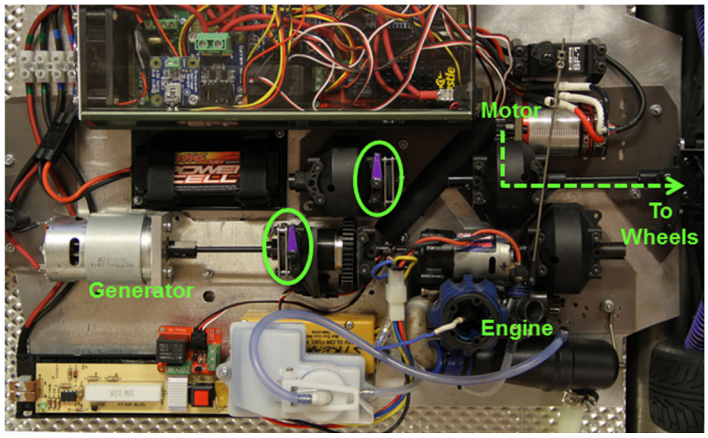

(a)

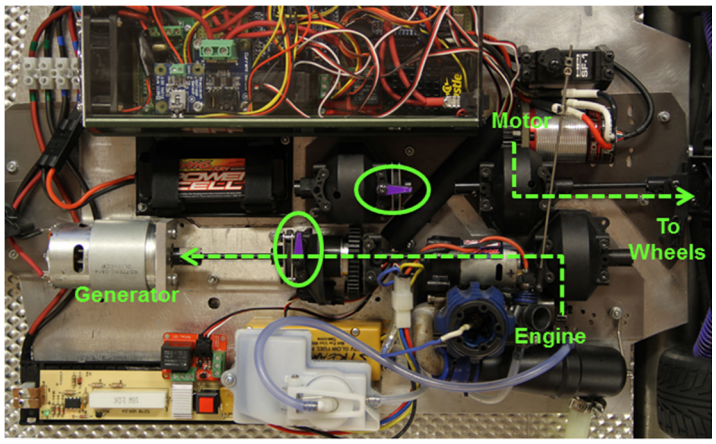

(b)

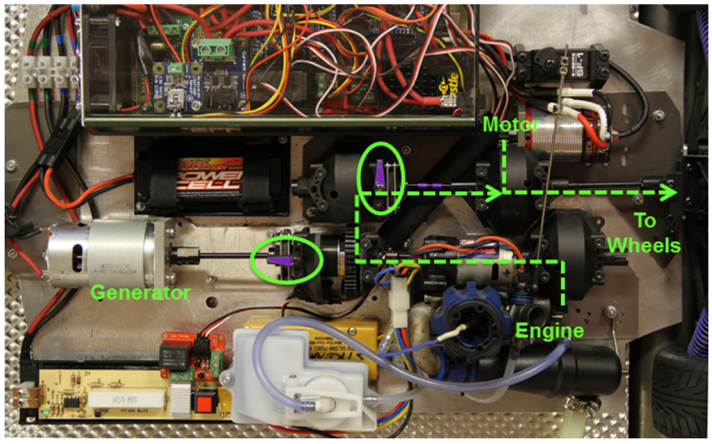

(c)

Figure 5. Different configurations of the small-scale HEV setup: (a) all-electric, (b) series, (c) parallel, and (d) series-parallel.

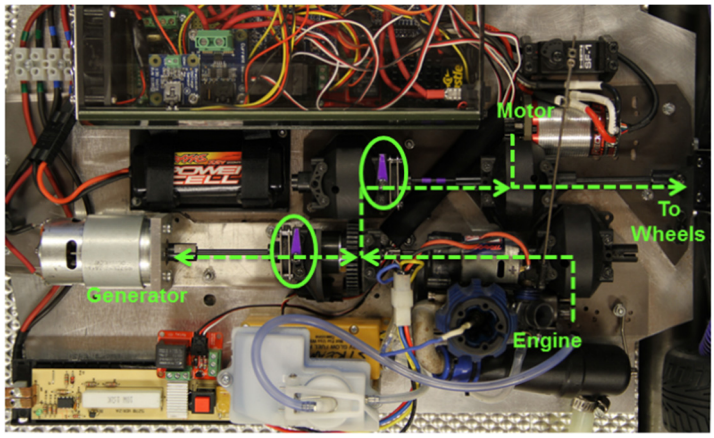

(d)

Figure 5. Different configurations of the small-scale HEV setup: (a) all-electric, (b) series, (c) parallel, and (d) series-parallel. (cont.)

C. Parallel configuration

In a parallel HEV, two parallel paths, an engine path and an electrical path, are used to power the wheels of the vehicle. Both the engine and the electric motor are coupled to the drive shaft, so the propulsion power may be supplied by the engine, by the electric motor, or by both. In the test bench, this configuration can be achieved by locking only the sun gear and permitting a fixed gear ratio between the engine and the electric motor drive shaft, allowing either or both to power the wheels. Figure 5(c) depicts this configuration.

D. Series-parallel configuration

The series-parallel configuration incorporates both series and parallel energy paths. As shown in Figure 5(d), this is the only configuration that utilizes all of the components of the test bench without the need to lock any of the gears of the planetary

gearbox. However, it is relatively complicated and more difficult to control compared to the other two configurations.

IV. CONTROL STRATEGIES

A critical consideration when designing a small-scale hybrid vehicle setup is energy management control for each configuration. In a real HEV, the vehicle control unit (VCU) is responsible for energy management control. It generates the control signals to the engine, traction motor, and generator based on the driver's command and other operating parameters, such as vehicle speed, engine speed, and battery SOC.

Generally, most HEV control strategies are based primarily on improving fuel economy, reducing emissions, and optimizing efficiency while simultaneously meeting performance demands. However, the main objective of this setup was to demonstrate the working principles of different hybrid vehicle structures and to provide a scaled model of an actual hybrid powertrain. Consequently, efficiency optimization was not the main design consideration for the VCU. Developing control logics to resemble real vehicle control strategies as closely as possible while maintaining a stable operation of each component was considered as the primary design goal.

One of the most common energy management strategies used in HEVs is rule-based energy management. In this strategy, predefined rules initially are set based on desirable outputs without any prior knowledge of the drive cycle. Predefined criteria, such as the engine or motor speed, vehicle speed, or the SOC of the battery, dictate transitions from one mode to another [8].

Rule-based strategies commonly are based on the concept of "load-leveling," in which the main objective is to shift the actual ICE operating point as close as possible to its optimal point. Furthermore, for configurations in which the engine and electric motor both can provide mechanical power to the drive shaft, using the electric motor alone is preferable at low vehicle speeds due to poor engine performance at such speeds.

The control strategies developed for different hybrid configurations of the small-scale module all were designed using rule-based energy management. For each configuration, a different LabVIEW code was executed, and vehicle operation was based on a different set of criteria. However, the overall control objectives for all configurations were the same and based on the following rules: 1) design the controller without prior knowledge of a predefined driving cycle, 2) always meet the reference speed command, 3) always maintain the battery SOC at a desirable level, and 4) operate the engine in its optimal region as much as possible.

A. Series hybrid energy management

In practice, a number of rule-based control strategies exist that can be used for hybrid vehicles with a series configuration based on different requirements [1]. In some control strategies developed for series configuration, the engine/generator operation is controlled only by the SOC of the battery, while in others, this operation is influenced by both the battery SOC and the load demand. In the latter case, the engine/generator unit either helps the batteries to power the electric motor when the load power demand is large or charges the batteries when the load power demand is small and the battery SOC is below its upper limit [1]. In all cases, the electric motor is responsible for producing the mechanical power required by the vehicle.

The control decision utilized for the small-scale test bench was based on the engine ON/OFF or thermostat control of the engine/generator strategy [9]. In this method, the battery SOC is always maintained between its preset upper and lower limits by turning the engine on and off, while the electric motor is controlled to produce the desired power request to meet driving demands. Figure 6 depicts the overall control rule for this configuration.

In this control strategy, the electric motor is always speed controlled; its controller receives the difference between the reference and actual speed and passes it through a PI controller that ensures accurate speed tracking. When the battery SOC reaches its preset lower limit, the engine/generator is turned on. On the other hand, when the battery SOC reaches its upper limit, the engine/generator is turned off, and the vehicle is propelled only by battery power.

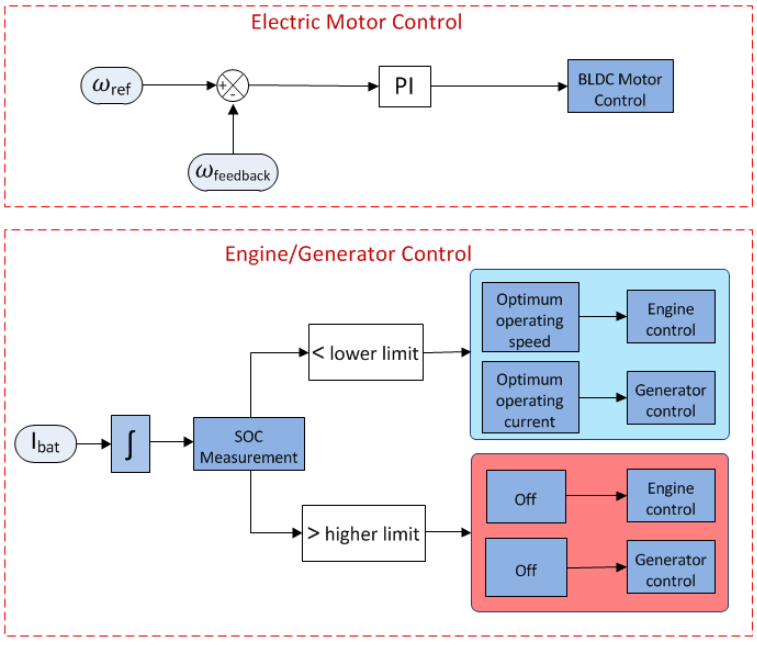

Figure 6. Controller block diagram for the series configuration.

Generally, with this control rule, the engine is controlled such that it always operates in its optimal operating region and the battery SOC is maintained in a preset window. This strategy allows the user to set the SOC bandwidth limits and explore the effect of different bandwidth limits on the overall performance of the vehicle.

B. Parallel hybrid energy management

The control of the parallel hybrid drive train is more complex than that of the series hybrid drive train because of the mechanical coupling between the engine and the electric motor [2]. The basic idea behind parallel control is to operate the engine within its optimal operating region with a constant average power and to control the electric motor to supply its power equal to the remaining load power.

Different operating modes and control strategies have been proposed for parallel hybrid vehicles [10]. Among these strategies, the power follower (baseline) control strategy is popular for energy management in parallel hybrid drive trains [9]. In this rule-based strategy, the engine supplies its power to meet the base load, and the electric motor supplies additional power when needed to meet the load requirement.

Consequently, the overall control scheme designed for the parallel configuration of the small-scale test bench also was based on the power follower control strategy. The only difference is that the power distribution between the engine and motor is controlled such that the engine provides power with regard to vehicle speed. In this case, the electric motor is controlled to supply the remaining load power. However, below a certain minimum vehicle speed, which is considered the base speed for engine operation, only the electric motor is used. The motor-only operating mode is used when the vehicle speed is so low that the engine cannot operate steadily. Also, if the battery SOC is lower than its

minimum allowable value, then the engine will provide additional power to constantly charge the battery. In such a case, the difference between the power generated by the ICE and the load power will be compensated by the motor in replenishing the battery. Figure 7 shows a block diagram sketch of the entire power management process for this configuration.

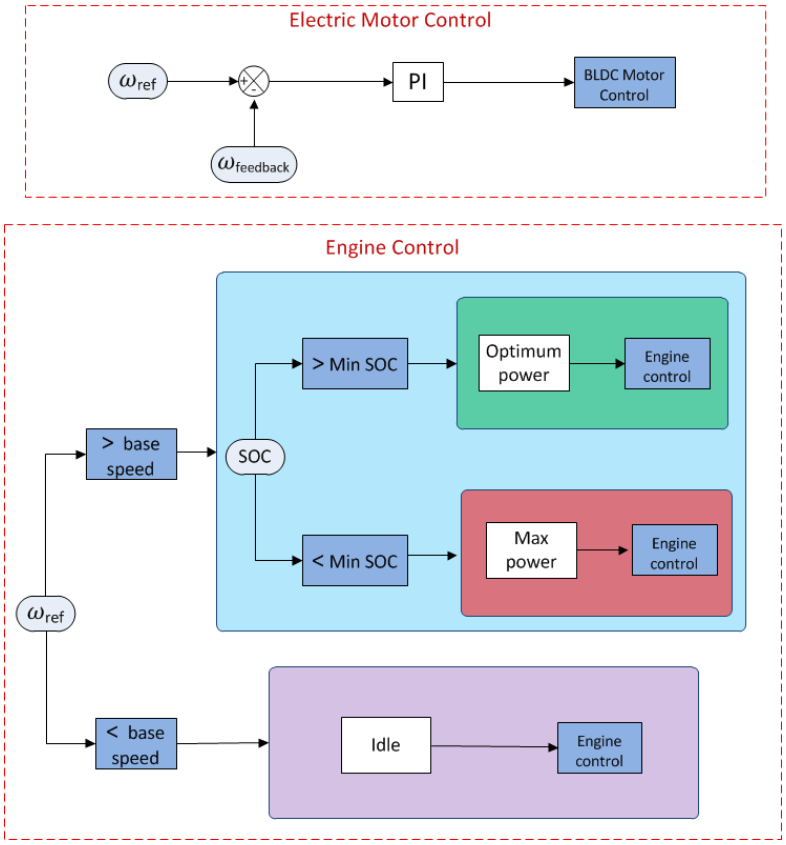

Figure 7. Controller block diagram for the parallel configuration.

In this strategy, the electric motor is always controlled to follow the commanded speed. At speeds lower than the base speed, the engine idles, and the electric motor is the only source that provides mechanical power to the wheels. At speeds higher than the base

speed, both the engine and the electric motor power the wheels. In this case, the commanded engine power varies depending on the vehicle speed and the battery SOC. When the SOC is above a predetermined minimum, the engine operates close to its optimal operating point. As soon as the SOC decreases to its minimum, the engine is forced to operate at a higher power, which exceeds the average required load power demand. Consequently, because the load power demand is less than the engine power, the electric motor is forced by its controller to function as a generator, using the remaining power of the engine to charge the battery.

C. Series-parallel hybrid energy management

For the series-parallel configuration, the engine speed is decoupled from the vehicle speed due to the kinematic properties of the planetary gear set [11]. This provides more flexibility and degrees of freedom in designing the control strategy compared to the other two configurations. However, it adds a great deal of complexity to the controller design. Therefore, it is necessary to impose more constraints on each component to ensure a stable operation of the vehicle platform.

The main ideas and control solutions for the parallel hybrid configuration can be extended to the series-parallel architecture [9]. For the small-scale vehicle, the control strategy designed for this configuration was based on a combination of the all-electric and parallel control strategies, with the exception that the generator is controlled to absorb excess engine power. The vehicle is operated in electric-only mode using only the electric motor until the SOC of the battery reaches a predefined value. From this point onward, the vehicle continues to operate as an HEV by switching to charge-sustaining (CS) mode [12], in which the vehicle is powered by the electric motor, the engine, or

both, with the constraint of maintaining a constant battery SOC [8]. In this mode, the decoupled engine speed and the amount of generator torque are the two degrees of freedom that the controller uses to maintain a constant SOC. Figure 8 illustrates the control principle for the series-parallel configuration for the CS mode. In the all-electric mode, only the electric motor is utilized and the engine and generator are off.

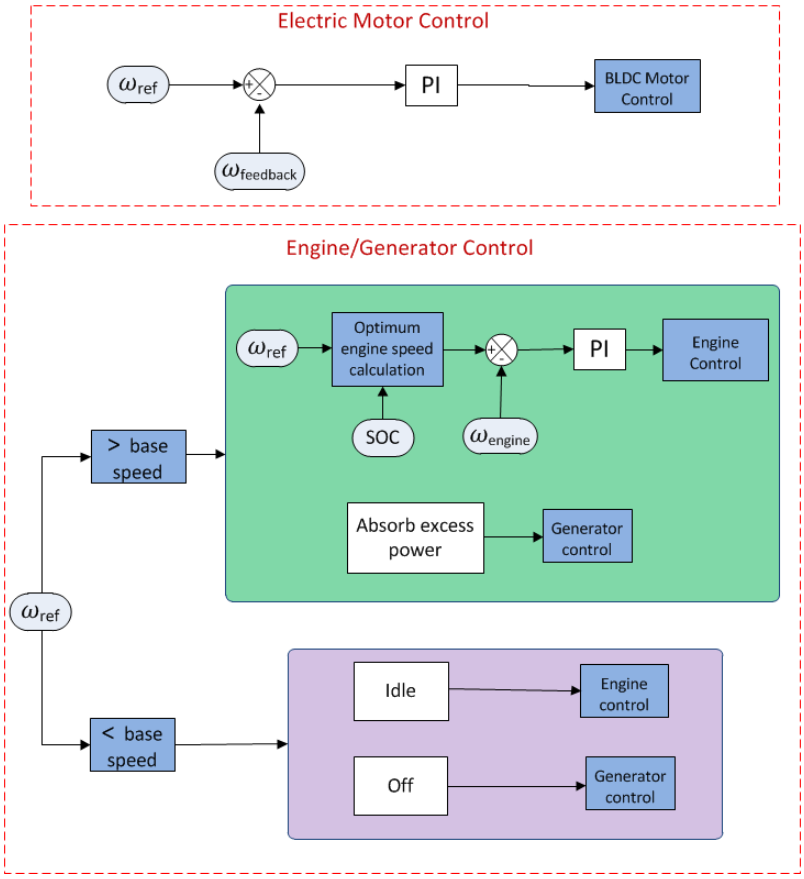

Figure 8. Controller block diagram of the CS mode for the series-parallel configuration.

In the CS mode, the optimal engine speed command is calculated based on the commanded reference speed, planetary gearbox gear ratios, and SOC of the battery at each instance. The engine operating point is maintained within a stable region by

controlling the engine throttle and generator torque. Due to the ability of the planetary gearbox to split power, a part of the power from the engine is transferred to the final drive shaft, and the remaining part is absorbed by the generator and used to charge the battery.

In this configuration, because the engine speed is decoupled from the vehicle speed, the base speed for engine operation is reduced, allowing engine assistance at lower speeds compared to the parallel configuration. This results in better use of the engine at lower vehicle speeds without compromising engine performance at low speeds.

V. MODES OF OPERATION

Each configuration of the test bench has two different modes of operation, which are based on a predefined drive-cycle simulation or user-defined driving behavior.

A. Drive-cycle mode

This mode of operation is used for simulating a predetermined drive cycle where the speed at each instance is known and given as a driving profile. The user only selects the desired drive cycle to be simulated and can only control the start and end time of the simulation. In this case, the vehicle speed reference is obtained from the drive cycle, and the LabVIEW program is responsible for controlling each component depending on the selected vehicle configuration.

B. Driver mode

This mode is used to analyze the vehicle operation directly from the command given by the user. In this case, the input reference signal is a varying speed signal commanded by the user through the LabVIEW interface panel which directly controls the

electric motor speed. The control of all other components, including decisions regarding how to control the engine and generator and when to charge the battery, are made within the LabVIEW program.

VI. LabVIEW Interface

The LabVIEW front panel interface designed for this setup is shown in Figures 9 and 10 for each mode of operation. For each mode, the interface allows the user to control the start and end time of the experiment while graphically indicating the actual speed of each component and the battery SOC at each instance. For the drive-cycle mode, the front panel window allows the user to select the desired drive cycle to be implemented, while for the driver mode, the user can continuously control the speed of the vehicle through a dial.

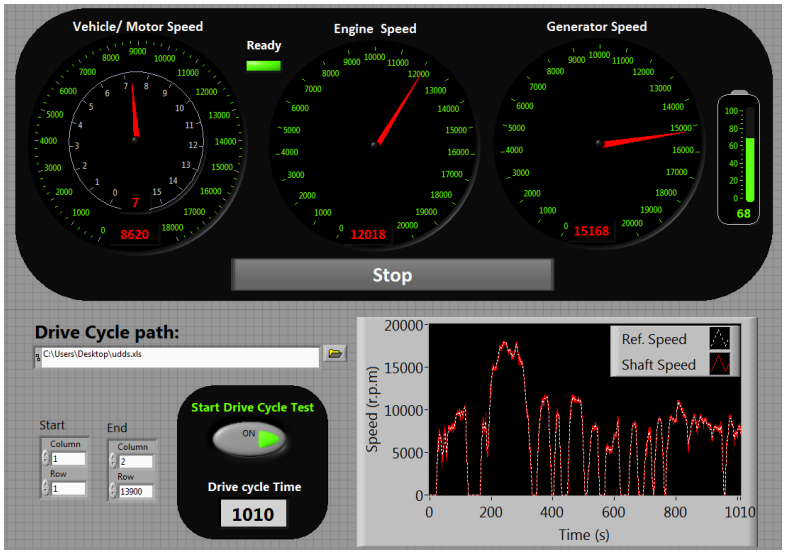

Figure 9. LabVIEW interface for the drive-cycle mode.

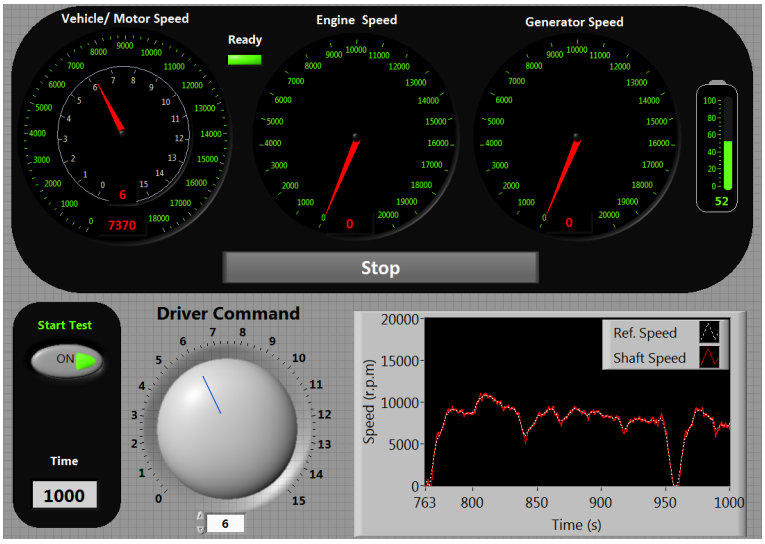

Figure 10. LabVIEW interface for the driver mode.

There is also a power management window designed in LabVIEW that indicates both mechanical and electrical power flow between components while the simulation is running. This allows a better understanding of electrical and mechanical power flow for each configuration. The power management window is shown in Figure 11. As soon as the simulation stops, a data log file containing real time data of the battery SOC and the speeds and currents of all components, is created and stored in an Excel file for future analysis.

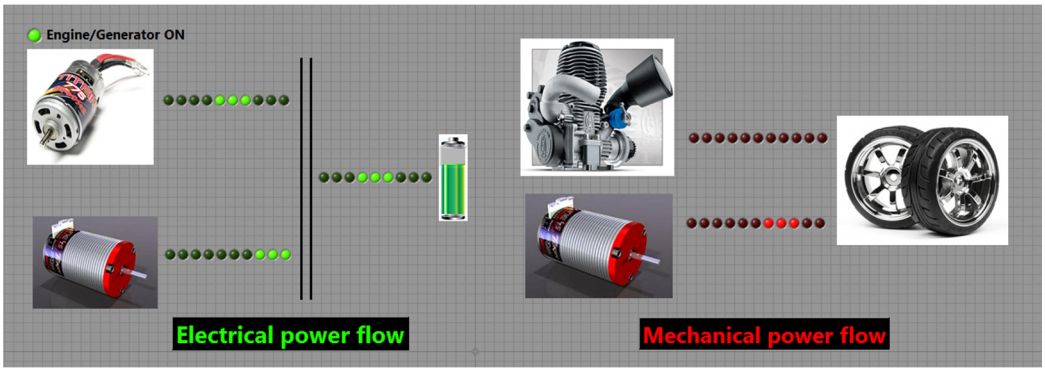

Figure 11. LabVIEW power management window.

VII. EXPERIMENTAL RESULTS

To illustrate the utilization of the small-scale vehicle setup in demonstrating the operation of an electric vehicle, as well as different configurations of HEVs, four experiments were performed. All of the tests were performed in drive-cycle mode, with the chosen drive cycle being a scaled version of the Urban Dynamometer Driving Schedule (UDDS) with a maximum speed of 10 mph. The tests were performed on a custom-made, small-scale chassis dynamometer, shown in Figure 12. The dynamometer consisted of two stainless steel roller bars, the mass and dimensions of which were chosen to have the same inertia effect of a moving vehicle, as calculated from [13] based on the vehicle weight and specifications. Furthermore, the rollers were mechanically connected to a DC motor with a fixed resistive load to account for all of the resistive forces applied to an actual moving vehicle of this scale.

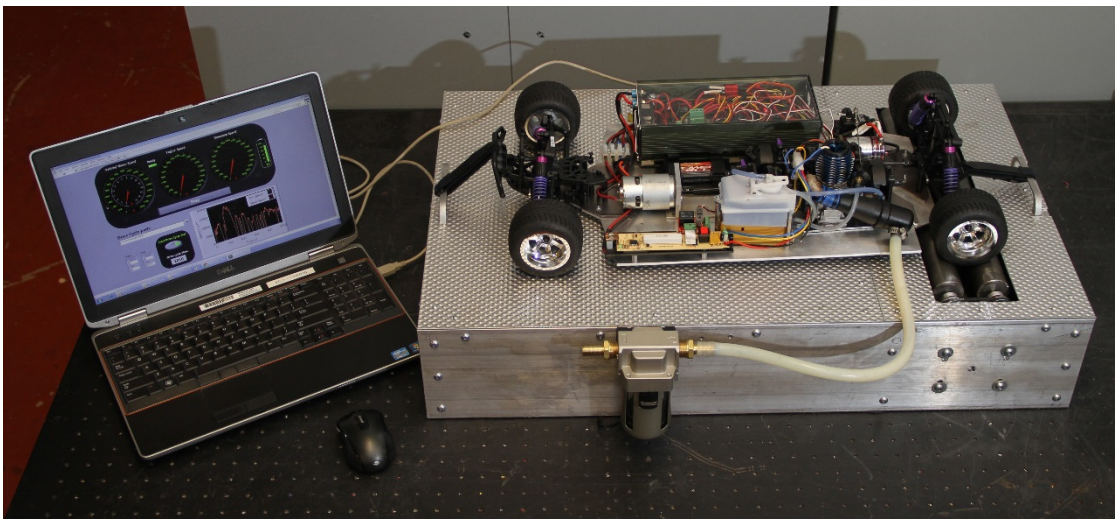

Figure 12. Experimental setup of the small-scale hybrid vehicle on a chassis dynamometer.

The goal of these simulations was to show that the developed model can indeed meet the design requirements of following a given drive cycle while simultaneously emulating the operation of an actual vehicle for each configuration. The experimental data regarding the battery SOC and the speed and current of the main component used for each configuration were recorded and appear in Figures 13-16.

Plots (a) of Figures 13–16 show the comparison between the commanded and actual vehicle speed in mph for different configurations of the test bench, illustrating that the vehicle responded appropriately in following the commanded speed profile for each case.

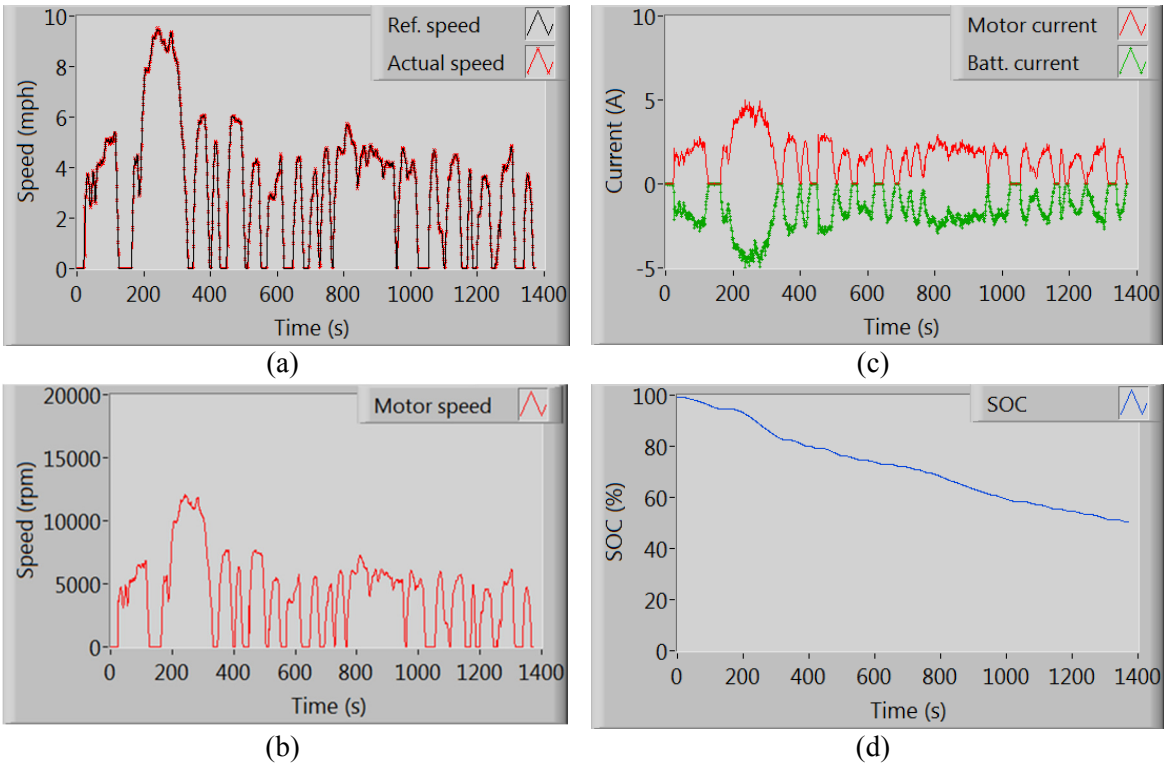

Figure 13. Experimental results for all-electric configuration: (a) vehicle translational speed, (b) electric motor speed, (c) electric motor and battery currents, and (d) battery SOC.

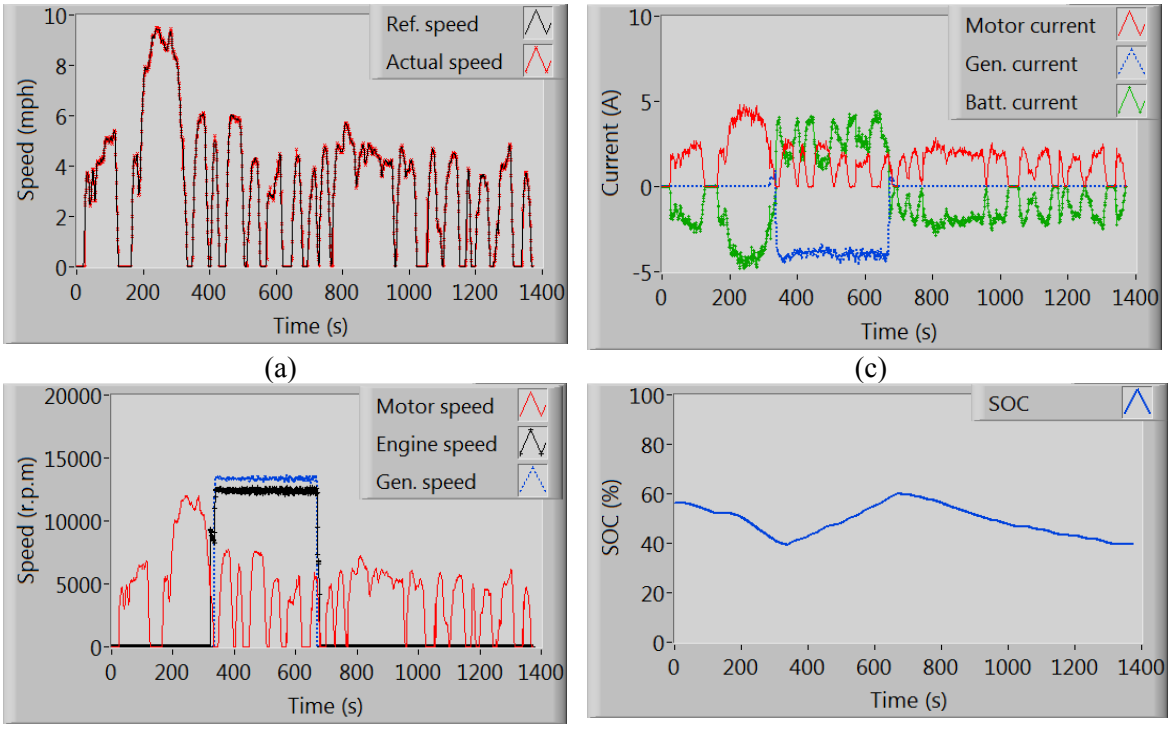

Figure 14. Experimental results for series configuration: (a) vehicle translational speed, (b) electric motor, engine and generator speeds, (c) electric motor, generator and battery currents, and (d) battery SOC.

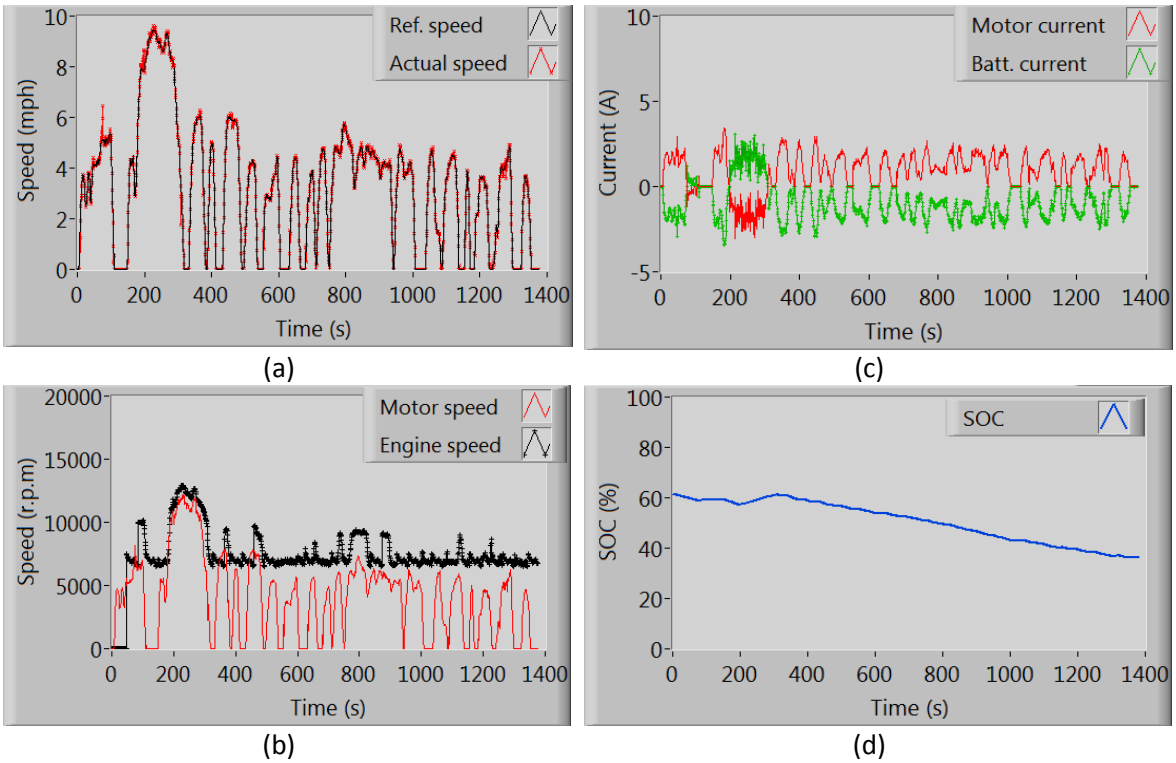

Figure 15. Experimental results for parallel configuration: (a) vehicle translational speed, (b) electric motor and engine speeds, (c) electric motor and battery currents, and (d) battery SOC.

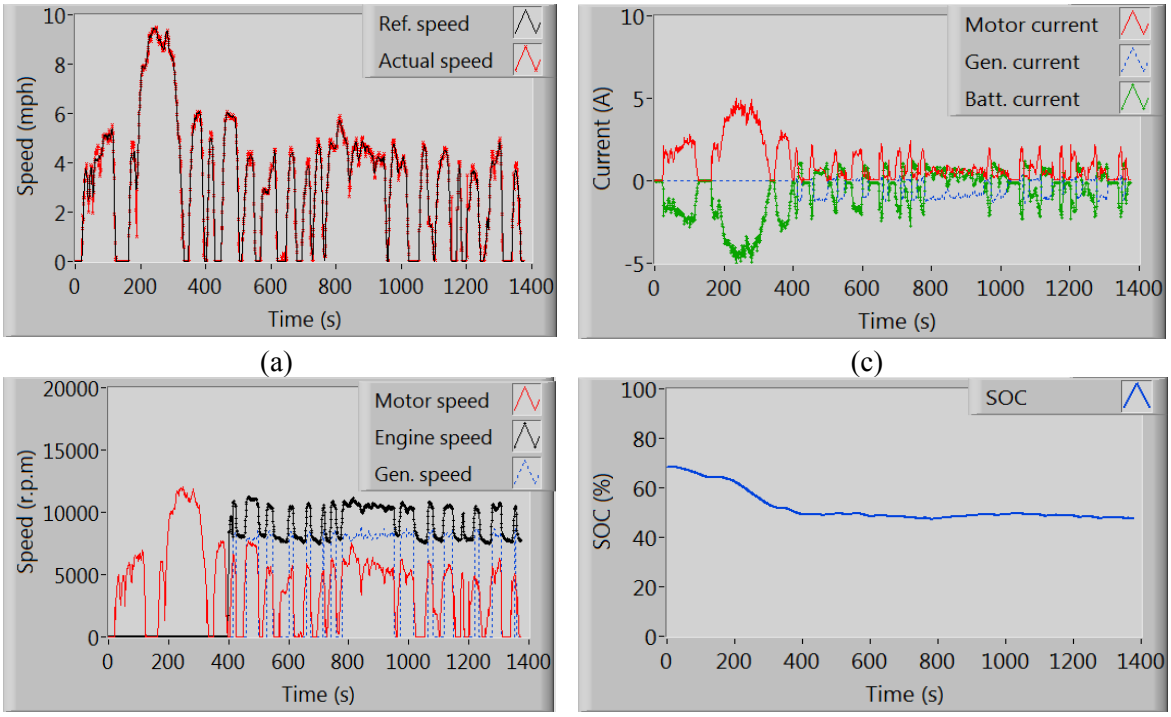

Figure 16. Experimental results for series-parallel configuration: (a) vehicle translational speed, (b) electric motor, engine and generator speeds, (c) electric motor, generator and battery currents, and (d) battery SOC.

A more detailed analysis of these results revealed that for the all-electric and series configurations, the actual recorded vehicle speeds very closely matched the desired speed profile, whereas for the parallel and series-parallel configurations, very small deviations from the desired speed profile occurred occasionally throughout the drive cycle. This behavior was due primarily to the fact that in the latter two configurations, the engine and electric motor both provided mechanical power to the drive shaft. As a result, the controller was responsible for controlling both power sources, and the smallest power mismatch between these components was reflected on the vehicle speed.

Plots (b) of Figures 13–16 illustrate the measured speed of each component that was utilized throughout the drive cycle for each configuration. For the all-electric configuration, the engine and generator speeds were not given, and for the parallel

configuration, the generator speed was not given, as these components were not utilized in their respective configurations. The role of each component becomes clear through a comparison of these plots from each configuration. These results clearly indicate that because the electric motor was connected directly to the final drive, its speed was proportional to the vehicle speed for each case. Furthermore, one may conclude that for the series configuration, the engine and generator speeds were related directly to each other. On the other hand, for the parallel configuration, at any speed exceeding the base speed, which was equal to a motor speed of 5000 rpm, the change in engine speed was almost proportional to the electric motor speed. However, for motor speeds below the base speed, the engine idled. In the series-parallel hybrid mode, the generator speed was always maintained around 7000-8000 rpm while the engine and motor both provided power. Also, the engine idling time for the series-parallel configuration was significantly less than for the parallel configuration. This is due to the decoupling nature of the planetary gearbox that allowed the engine speed to be decoupled from the electric motor speed.

The measured currents of the battery, motor, and generator (depending on the configuration) appear in plots (c) of Figures 13–16. In these plots, a positive motor and generator current indicates power consumption, whereas a negative current indicates power generation. Similarly, a negative battery current can be interpreted as a battery discharge, while a positive current means that the battery was charging.

Plots (d) of Figures 13–16 reveal the SOC variation of the battery over a complete drive cycle. The initial starting SOC and the change in SOC differed for each configuration. One obvious difference across configurations is the pattern of SOC

change. For the all-electric configuration shown in Figure 13 (d), the overall SOC pattern shows a negative slope. The SOC decreased from its initial value of 100% to almost 52% at the end of the cycle, indicating a change of 48% to accomplish the drive cycle. However, for the series configuration shown in Figure 14 (d), the battery SOC had both positive and negative slopes and was limited to preset values of 40% and 60%. As soon as the SOC reached its lower bound of 40%, the engine/generator set began to charge the battery, resulting in an increase in the SOC value. The engine/generator shut off when the SOC reached its upper bound of 60%. For the parallel configuration shown in Figure 15 (d), a small increase in the SOC was detected between 200-350 seconds. During this time period, the motor speed was at its highest, allowing it to be efficiently controlled as a load to the engine and charge the battery. The net change in the SOC for this configuration was approximately 22%, almost half of the SOC change for the all-electric configuration. This difference was due to the fact that in this configuration, above the base speed, the engine provides assistance to the electric motor, so the battery is not the only source of energy to propel the vehicle. For the series-parallel configuration shown in Figure 16 (d), the SOC decreased during the first part of the drive cycle as the vehicle drove electrically without assistance from the engine. Once reaching the CS SOC level, the SOC remained roughly steady as the engine and motor worked together to satisfy the vehicle power demand.

VIII. CONCLUSION

This paper provides insight into the design and development of a small-scale HEV learning module. The module consists of all of the key components of an actual HEV

scaled down to provide an ideal test platform to evaluate and study hybrid powertrains and to simulate both EV and HEV systems. The overall configuration was designed to allow the scaled vehicle to emulate the behavior of a series, parallel, or series-parallel HEV, as well as all-electric operation with minor modifications to the powertrain and a change over time of few minutes. One of the most important and challenging tasks in developing this test bench was designing the controller for each configuration. A control logic based on a rule-based energy management strategy was developed and implemented in LabVIEW software for each configuration. The different modes of operation of the test platform were discussed briefly, and the LabVIEW front panel interface designed for each mode was presented. The experimental results from tests performed on a custom-made, small-scale chassis dynamometer showed the overall operation of the vehicle platform for each configuration and validated its use in emulating real vehicle behavior. The small-scale HEV test bench not only facilitates hand-on experience but can be considered a safe, affordable solution to providing practical aspects of education in the field of electric and hybrid vehicle technology.

REFERENCES

[1] C. C. Chan and K. T. Chau, *Modern electric vehicle technology*. Vol. 47. Oxford University Press on Demand, 2001.

[2] M. Ehsani, Y. Gao, S. E. Gay, and A. Emadi, *Modern Electric, Hybrid Electric, and Fuel Cell Vehicles: Fundamentals, Theory, and Design*. Boca Raton, FL: CRC, Dec. 2004.

[3] K. B. Wipke, M. R. Cuddy, and S. D. Burch, "ADVISOR 2.1: A user-friendly advanced powertrain simulation using a combined backward/forward approach," *IEEE Trans. Veh. Technol.*, vol. 48, no. 6, pp. 1751-1761, Nov. 1999.

[4] J. M. Timmermans, J. Van Mierlo, P. Lataire, F. Van Mulders, and Z. McCaffree, "Test platform for hybrid electric power systems: Development of a HIL test platform," in *Proc. Eur. Conf. Power Electron. Appl.*, Aalborg, Denmark, Sep. 2-5, 2007, pp. 1-7.

[5] N. Lotfi, P. Fajri, S. Novosad, J. Savage, R. G. Landers, and M. Ferdowsi "Development of an Experimental Testbed for Research in Li-Ion Battery Management Systems," *Energies*, vol. 6, no. 10, pp. 5231-5258, Oct. 2013.

[6] J.D. Brock, R. F. Bruce, and S. L. Reiser, "Using Arduino for introductory programming courses," *Journal of Computing Sciences in Colleges*, vol. 25, no. 2, pp. 129-130, 2009.

[7] *LabVIEW User Manual*, National Instruments, Austin, TX, 1998.

[8] S. G. Wirasingha and Ali Emadi, "Classification and review of control strategies for plug-in hybrid electric vehicles," *IEEE Trans. Veh. Technol.*, vol. 60, no. 1, pp. 111-122, 2011.

[9] F. R. Salmasi, "Control strategies for hybrid electric vehicles: Evolution, classification, comparison, and future trends," *IEEE Trans. Veh. Technol.*, vol. 56, no. 5, pp. 2393-2404, 2007.

[10] S. Delprat, J. Lauber, T. M. Guerra, and J. Rimaux, "Control of a parallel hybrid powertrain: optimal control," *IEEE Trans. Veh. Technol.*, vol. 53, no. 3, pp. 872-881, 2004.

[11] F. U. Syed, M. L. Kuang, J. Czubay, and H. Ying, "Derivation and experimental validation of a power-split hybrid electric vehicle model," *IEEE Trans. Veh. Technol.*, vol. 55, no. 6, pp. 1731–1747, Nov. 2006.

[12] P. Fajri, B. Asaei, "Plug-in Hybrid Conversion of A Series Hybrid Electric Vehicle and Simulation Comparison," in *Proc. IEEE/OPTIM 11th International Conference on Optimization of Electrical and Electronic Equipment*, Brasov, Romania, May 22-24 , 2008, pp. 287-292.

[13] P. Fajri, R. Ahmadi, and M. Ferdowsi, "Equivalent Vehicle Rotational Inertia Used for Electric Vehicle Test Bench Dynamic Studies," in *Proc. 38th IEEE Industrial Electronics Society Annual Conference*, Montreal, Canada, Oct. 25-28, 2012, pp. 4115-4120.

SECTION

2. CONCLUSION

In this dissertation, two different modes of emulating the behavior of EDVs on a test bench comprising of a motor/dynamometer set were investigated. It was concluded that the effect of vehicle inertia for test bench studies should be considered carefully. An expression for estimating vehicle inertia was derived analytically by calculating the kinetic energy of a moving mass in the linear and rotational context and mapping the vehicle's linear inertia to an equivalent rotational inertia. This method not only takes into account all the stress imposed on the DM due to vehicle inertia effect, but also allows EDV emulation for any standard drive cycle as well as an undefined driving scenario. The results obtained from the simulation showed accurate calculation of vehicle resistive forces for both cases. Additionally the experimental results validated this method of EDV emulation on a motor/dynamometer setup.

Moreover, the integration of a brake model suitable for motor/dynamometer emulation of EDVs was discussed. The brake dynamic emulation was realized by taking into account both regenerative and friction braking limitations and controlling the dynamometer motor to emulate friction braking effect as well as vehicle inertia and resistive forces. It was concluded that by considering the proposed braking model a more realistic approach towards emulating EDV performance on a motor/dynamometer test bench is achieved. The comprehensive model allows for a more accurate assessment of

EDV performance and can further be used in efficiency and energy consumption analysis studies related to these vehicles.

The design and development of a small scale HEV learning module was also presented in the last section of this dissertation. The module uses small scale components of an actual vehicle to satisfy the need to evaluate and study different hybrid powertrains. A block diagram view of the overall configuration of the test module was explained which allows the scaled vehicle to emulate the behavior of a series, parallel or a series-parallel HEV as well as an all-electric operation with minor modification to the powertrain. The different modes of operation of the test platform were discussed briefly, and the LabVIEW front panel interface designed for each mode was presented. The experimental results from tests performed on a custom-made, small scale chassis dynamometer showed the overall operation of the vehicle platform and validated its use in emulating different hybrid configurations.

VITA

Poria Fajri received his B.Sc. degree in Electrical Engineering majoring Electronics from Urmia University, in 2005. He received the M.Sc. degree in Electrical Engineering majoring Power Electronics from the University of Tehran, in 2008, with honor. He joined the Missouri University of Science and Technology in 2011 and completed his Ph.D. in October 2014 in Electrical Engineering with an emphasis in Power Electronics and Motor Drives.